UNIVERSITY OF TWENTE.

Faculty of Engineering Technology
Maintenance Engineering / Fluid Dynamics

Dynamic Pipe Expansion in a Radial Confined Cemented Oil Well Foundation

MARCEL W VAN DEN BERG

June 2019

GRADUATION COMMITTEE:
Supervisor
prof. dr. ir. CH Venner
University of Twente

Chairman and Program Director of PDEng
prof. dr. ir. D.J. Schipper
University of Twente

Members
dr. ir. J.B.W. Kok
University of Twente

dr. MSc. A Martinetti
University of Twente

M.W. van den Berg:
Dynamic Pipe Expansion in a Radial Confined Cemented Foundation,
PDEng Dissertation, University of Twente, Enschede, The Netherlands
Report final version March 2018, Edited Titlepage version May 2019, Edited Titleback-page version June 2019,

Dynamic Pipe Expansion in a Radial Confined Cemented Oil Well Foundation

;

PDEng Dissertation

to obtain the degree of
Professional Doctorate in Engineering (PDEng) at the University of Twente,
on the authority of the rector magnificus,
prof. dr. T.T.M. Palstra,
on account of the decision of the graduation committee,
to be defended,
on Day the XXth of Month 2019 at XX:XX
by
Marcel W van den Berg
born on 6th of January 1988
in Rossum, The Netherlands.

;

This PDEng Dissertation has been approved by:
Supervisor: prof. dr. ir. CH Venner

ABSTRACT

In the last couple of decades a new design for an oil well emerged, known as the monobore or mono-diameter oil well. The oil well design is made possible due to a recent developed technology, the downhole expansion process. The technology opened up a pathway for the oil well to have from earth-surface all the way down to the reservoir, an approximate uniform inner diameter. In the design, in a repetitive procedure, expandable pipes are positioned in a borehole and expanded to allow another prior-to-expansion sized expandable pipe to be positioned further downhole. Expansion of the pipes occurs in a borehole with in-between the pipe and the soil borehole fluid saturated cement. The expansion of the pipe will compress the saturated cement, that will result in free fluid separation. The degree to which this separation of fluid will occur will depend upon a set of system variables, such as cement porosity or expansion speed and will lead to a potential failure behavior where the oil well would no longer be operational. In this project the consequential behavior of the expansion process with respect to the cement sheath is investigated.

To advance the development of the oil well and establish a failsafe design, the problem is dismantled in three relevant experiments for which individual designs are developed. Prior to the development of each experimental design, a theoretical and numerical analysis is performed that are utilized as a tool to establish the framework for each design. It is demonstrated in a simple one-dimensional model that throughout expansion of the pipe and compression of the cement sheath, the free fluid that emerged from the saturated cement has a preferential flow direction. Due to the former finding a more extensive model was developed to investigate the effect of fluid accumulation at the interface of the expandable pipe and cement sheath. The annulus model granted a parametric study of the expansion process and the cement sheath and established the foundation and framework for three distinct designs of experiments, the hydraulic bond strength test, the cement radial deformation test and the small-scale expansion test.

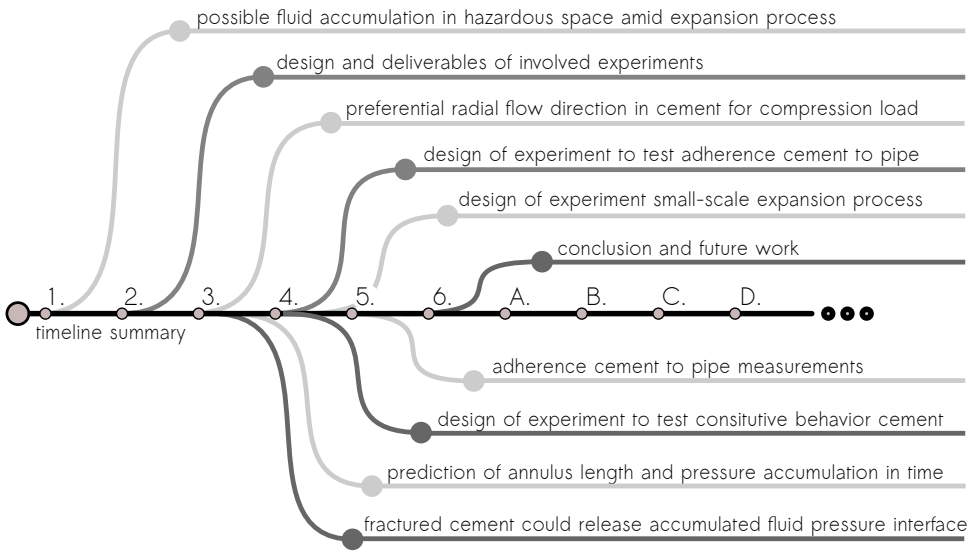

ACKNOWLEDGEMENTS

In fulfillment of my PDEng between May 2016 up to April 2018 I have had the great pleasure and opportunity to participate in a collaboration project between the University of Twente and Oil and Gas Company Shell.

I would like to thank prof. dr. ir. Kees Venner with the continuous support and guidance throughout the project, and even the continuous support and follow-ups after the official deadline of the project that was beyond doubt valuable. I greatly appreciate the granted freedom and opportunity to develop myself further in the field of my interest.

I would like to thank dr. ir. Wissam Assaad for the invested time in the project, and the constructive discussions.

I would like to thank ing. Erik Cornelissen for the kind and pragmatic involvement in the hydraulic bond strength test experiments.

I would like to thank prof. dr. ir. Dik Schippers for the opportunity of a PDEng position in the Maintenance program.

I would like to thank dr. ir. Rob Bosman for the constructive feedback in the Shell-UT meetings.

I would like to thank the students and colleagues of the Shell-UT project for the support in the project, and the enjoyable trips to the other side of the country.

A special and heartfelt appreciation to Sheila Rabanal, my beautiful wife, you encouraged me to keep up with this task and listened to me whenever I needed a listening ear, your unconditional support made this possible.

CONTENTS

LIST OF FIGURES

A_o	outer surface	$[m^2]$
A_i	inner surface	$[m^2]$
A_y	circumferential surface slice of length dy	$[m^2]$
a	crack length	$[m]$
E_{res}	residual stress energy	$[N \cdot m]$
E_b	elastic bond energy	$[N \cdot m]$
E_s	elastic strain energy	$[N \cdot m]$
E_f	elasticity modulus formation	$[N \cdot m^{-2}]$
E_c	elasticity modulus cement	$[N \cdot m^{-2}]$
F	force	$[N]$
F_{fo}	force active on formation	$[N]$
g	gravitational acceleration	$[m \cdot s^{-2}]$
H	total height in longitudinal direction	$[m]$
k	hydraulic conductivity	$[m \cdot s^{-1}]$
k_o	stiffness	$[N \cdot m^{-1}]$
k_{fo}	stiffness formation	$[N \cdot m^{-1}]$
L	total length in radial direction	$[m]$
L_c	length cone	$[m]$
l	increment crack length	$[m]$
m_v	confined compressibility	$[-]$
$\dot{m}_{tot}$	total massflow	$[kg \cdot (m \cdot s)^{-1}]$
$\dot{m}_c$	massflow towards cement sheath	$[kg \cdot (m \cdot s)^{-1}]$
$\dot{m}_a$	massflow towards annulus channel	$[kg \cdot (m \cdot s)^{-1}]$
N_r	number of elements in radial direction	$[-]$
N_θ	number of elements in tangential direction	$[-]$
n	fluid porosity	$[m^3 \cdot m^{-3}]$
p	fluid pore pressure	$[Pa]$
q	volumetric Darcy flux per unit area	$[m \cdot s^{-1}]$
R	radius	$[m]$
R_o	outer radius	$[m]$
R_i	inner radius	$[m]$
r_α	ratio of fluid towards annulus channel	$[-]$
S_o	uncompressed surface	$[m^2]$
S_c	compressed surface	$[m^2]$

S_p	storativity coefficient	$[-]$
s	solid averaged particle velocity	$[m \cdot s^{-1}]$
T	total simulation time	$[s]$
t	time	$[s]$
u	fluid velocity radial direction	$[m \cdot s^{-1}]$
u_b	velocity due to compliance expandable pipe	$[m \cdot s^{-1}]$
u_{fo}	radial solid displacement of formation	$[m]$
u_i	inner displacement	$[m]$
u_o	outer displacement	$[m]$
u_r	radial solid displacement	$[m]$
V	volume	$[m^3]$
v	fluid velocity longitudinal direction	$[m \cdot s^{-1}]$
v_b	velocity west due to cone migration speed	$[m \cdot s^{-1}]$
v_c	cone velocity	$[m \cdot s^{-2}]$
v_t	velocity east due to cone migration speed	$[m \cdot s^{-1}]$
W	work	$[N \cdot m]$
W_c	deformed cement sheath thickness	$[m]$
$W_{c,\infty}$	undeformed cement sheath thickness	$[m]$
w	local width annulus channel	$[m]$
w_o	width annulus channel at entrance channel	$[m]$
w_L	width annulus channel at exit channel	$[m]$
x	radial coordinate in cartesian system	$[m]$
y	longitudinal coordinate in cartesian system	$[m]$
α	Biot coefficient	$[-]$
ϵ	strain	$[-]$
ϕ	relative crack propagation angle	$[rad]$
γ_w	unit weight	$[kg \cdot m^{-3}]$
κ	permeability porous medium	$[m^2]$
ρ_f	fluid density	$[kg \cdot m^{-3}]$
ρ_s	solid density	$[kg \cdot m^{-3}]$
σ	total stress	$[N \cdot m^{-2}]$
σ'	effective stress	$[N \cdot m^{-2}]$
τ	turtuosity factor	$[-]$
μ	dynamic fluid viscosity	$[Pa \cdot s]$
σ_{vm}	Von Mises stress	$[N \cdot m^{-2}]$
σ_{uc}	ultimate compressive strength	$[N \cdot m^{-2}]$
σ_t	tensile strength	$[N \cdot m^{-2}]$
σ_θ	tangential stress	$[N \cdot m^{-2}]$
σ_R	radial stress	$[N \cdot m^{-2}]$

θ	tangential angle in cylindrical system	[rad]
ν	Poisson ratio	[–]

1 INTRODUCTION

1.1 BACKGROUND

A structural foundation is the most important part in construction building, whether it is a commercial or a residential structure [1]. The purpose of a foundation is to hold up or hold together a building structure. In- or external forces imposed on the foundation will damage the structure where the degree of damage that will occur depends on the size and quality of the foundation.

For an oil well in specific, the foundation can be up to several kilometers long, pointing out the paramount importance of the quality of the structural foundation. The foundation in an oil well - made of cement - will not only support the structure, it will also ensure a leak tight connection between the host pipe of the well and the surrounding earth layer. The quality of the cement job is therefore vital to the reliability and lifespan of the well and should be guaranteed at all time.

1.2 MOTIVATION

The global demand for oil - primarily due to emerging markets in the developing world - is in a state of incline. The Energy Information Administration of the USA predicted, with respect to the present day, about a 20% increase of global oil demand in the year 2030 [36]. The global oil demand prediction is in-line with what the International Energy Agency recorded the last 36 months [28], as is shown in figure 1. Due to a steady increase in the global oil demand the technological development related to oil field exploration, oil extraction and refinement since early 1980s has been intensified and has affected all regions around the world. The competitive petroleum industry promotes the technology transfer worldwide, that made the technology more accessible for competitive forces [35]. The exploration of *shallow* - and due to available technology worldwide - *accessible* oil fields therefore is a competitive business.

The *Expandables R&D* department of the petroleum company Royal Dutch Shell [49] is appointed with the task to develop an oil well that is to be operational on larger target depths, in contrast to the conventional oil well applicable for shallow oil fields. A potential new technology that can meet the requirement is the so-called *monobore oil well*, a well technology where the borehole diameter from the surface to the downhole oil field is approximately a constant. The monobore oil well technology is made possible by a *downhole expansion process* in which oil pipe segments are expanded into the surrounding cement layers. The expansion process will compress and shear the cement layer that at time of expansion is in an approximate fluid

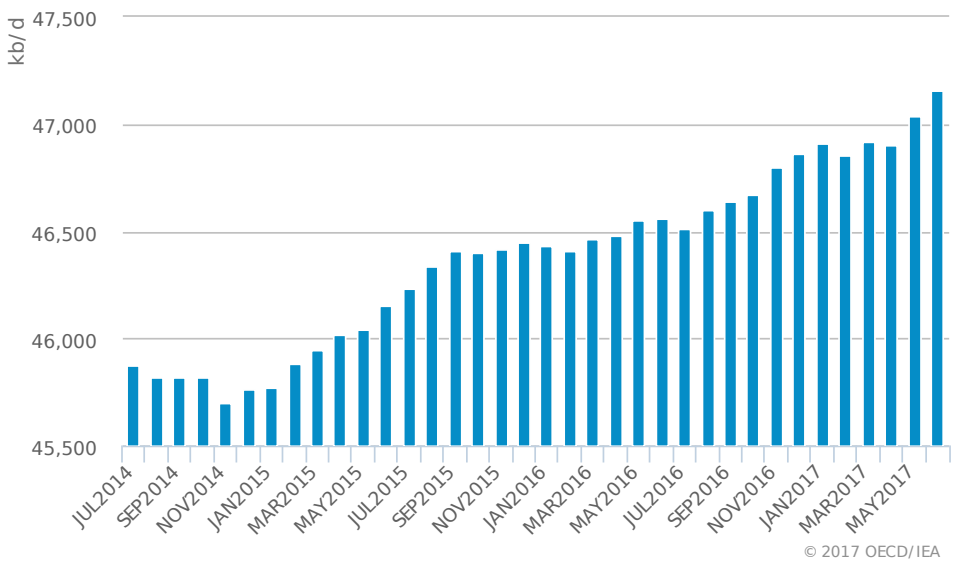

Figure 1: *The monthly averaged global total oil demand for a period of 36 months recorded by the International Energy Agency [28]. The vertical axis depicts the number of kilobarrels (x1000 barrels) per day.*

saturated state. The consequence is the formation of free fluid separation from the cement sheath. As the outside earth layer due to an excavation procedure is roughly impermeable the free fluid separation will occur in between the oil pipe and the cement layer. Accumulation of fluid will occur for an ongoing expansion process that will likewise increase the fluid pressure. The pressure will impose a radial inward strain on the pipe that may exceed the plastic deformation limit up to the point of a potential catastrophic pipe failure.

1.3 PROBLEM SCOPE OF THE PROJECT

In a conventional oil well design the cement job throughout the solidification phase is exposed to limited strain. After the borehole is established an oil pipe is placed in position and cement is pumped in between the pipe and the layer of earth or formation. Once solidified, the cement is able to hold up the construction and form a final sealant for the formation. Going downhole one-pipe-segment at a time, the pipe segments will narrow down in diameter to fit the previous pipe segment. After each of these pipe segments are placed in position, cement is pumped in between pipe and formation. Over the depth of the well a classic telescopic shape is obtained, see the left-side of figure 2. A benefit of this well design is the involved strain present in the cement that is limited to the natural shrinkage properties, up to 5% of the original size of the cement. However, as the pipe segments cannot narrow down in diameter infinitely often, a restraint in the telescopic well design is set on the target depth.

To go beyond the restraint of the target depth, a different approach than the telescopic well design is to be considered. The development of down-

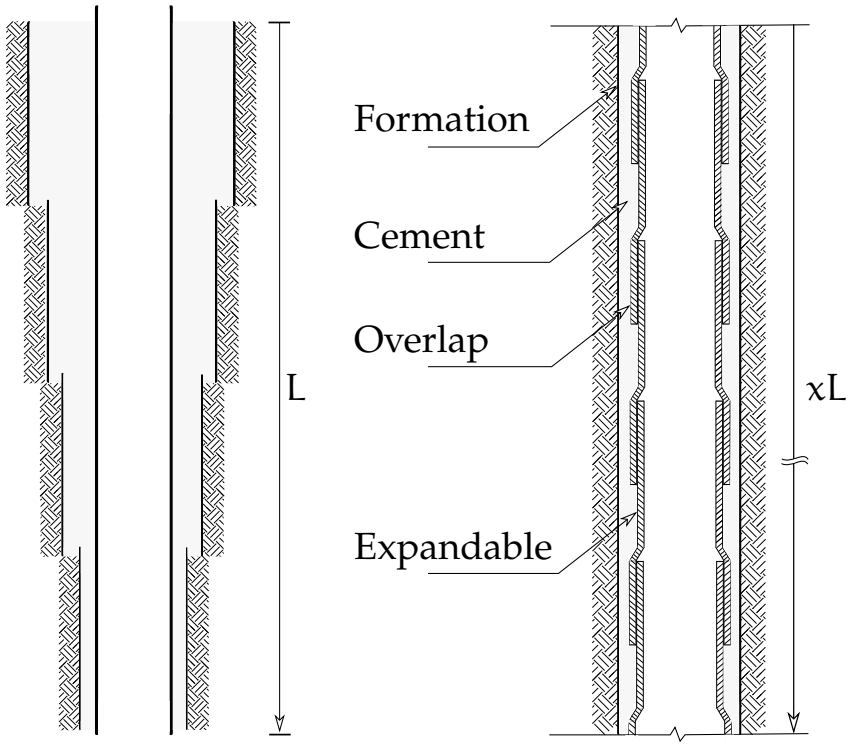

Figure 2: *Longitudinal schematic cross-section of the conventional (left) and mono-diameter (right) oil well design* ($x > 1$).

hole expansion technology has the potential to open up a pathway to the monobore well design. The latter technology can overcome the restriction on the pipe segment diameter, and can facilitate to greater target depths.

After cement is poured in between pipe and formation, a positioned cone at the bottom of the pipe is pulled upwards through the pipe to expand the inner diameter. This will allow the insertion of another pipe segment into a new excavated borehole such that a configuration is obtained that is depicted on the right of figure 2. A gradual expansion of the pipe segment from the bottom-up will exert shear and compression stresses upon the former poured saturated and partial-cured cement. The result is free fluid separation from the saturated cement sheath towards the path of least resistance. As the strength of a cement-aggregate bond is more vulnerable than the atomic bond strength of the cement paste [50], the path of least resistance will take the form of an annulus channel due to the weaker hydraulic bond strength of pipe and cement ahead of the cone, as depicted in subfigure (A) of figure 3. Due to the expansion process over time, free fluid will continue to accumulate in the annulus channel ahead of the cone at the interface of pipe and cement. Fluid volume formation is progressing over time that will invoke an increasing stress on the pipe in the radial inward direction, shown in subfigure (B). Without sufficient drainage of the accumulated fluid, the expansion process will cause accumulation of fluid into the created annulus channel up to a potential pipe failure, given in subfigure (C). Previous research observed this phenomena and named

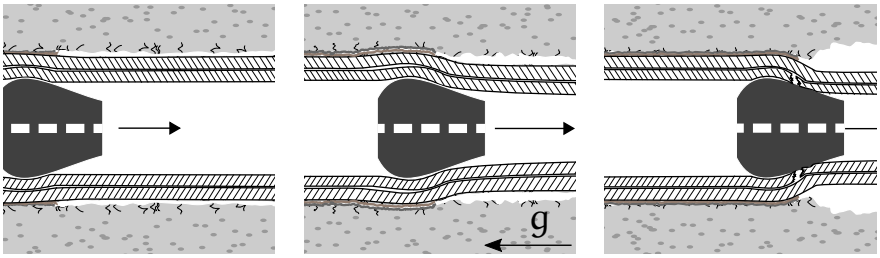

(A) Annulus formation (B) Local accumulation (C) Severe radial stress

Figure 3: *Possible failure modes due to cone migration that have been observed in experimental work [24][57], from left to right there is observed* `debonding`*,* `flattening` *and* `pipe collapse`*.*

the behavior of these failure modes from l-r the debonding mode, the pipe flattening mode and the potential pipe collapse [24][57].

The free fluid separation from the cement sheath due to compression and the accumulation of fluid pressure at the interface of the oil pipe and cement layer - as a consequence of the expansion process - is thus far troubled with uncertainties that require definite answers. Acquired certainties will aid in the control of a failsafe design for an oil well. This report will illuminate the path taken to institute and develop experimental product design to define the conditions wherein potential failure behavior may occur through the course of the expansion process.

1.4 OUTLINE OF THE REPORT

The report can be divided in four sections, an initial part in chapter 2, where the objectives with the deliverables of the project are described. In preparation of and to determine the framework of the design architecture a theoretical and numerical analyses is presented in chapter 3, related to the expansion process and cement response. Chapter 4 describes the institution and development of the experimental design architecture. Chapter 5 is dedicated to performed measurements for a developed experimental design, the hydraulic bond strength test.

The theoretical and numerical analysis of the cement response in the expansion process is divided into three subsections. Subsection 3.1, is a one-dimensional dynamical saturated cement response analysis to explore the preferential flow direction along the radial axis of the monobore well due to the expansion load imposed on the expandable pipe segment. The analysis is continued, in subsection 3.2, by consideration of the cement integrity where a failure prediction is carried out by cause of cement deformation through the course of the expansion process. Subsection 3.3, is a numerical model to analyze the accumulative effect of fluid, and the resulting increase of pressure at the interface of the cement sheath and expandable pipe over the course of the expansion process. The model consists of building blocks, each simulate a specific physical phenomena and is constructed by interchangeable modules where potential more suitable

building blocks can be substituted. A parametric study is performed of the influence of the various parameters in the expansion process. The experimental architecture in chapter 4, will cover the design steps and development phase of three distinct experiments, required to be performed to investigate the expansion process in detail, and to validate the developed theoretical and numerical models. Section 4.1, will present a design for an experiment to measure the adhesive strength of cement to an expandable pipe. A second design for an experiment is described in section 4.2, a setup to determine constitutive behavior of a cement sheath prior- and post deformation in radial direction. The third design in section 4.3, is a small-scale expansion test that is geometrically downscaled to about 25 [%] of the in-field setup. The last section of the experimental architecture, section 4.4, is the prototype description, techno-economic feasibility and impact of the performed work in the project. The design of the hydraulic bond strength test is developed and constructed in the laboratory to perform measurements on the adhesive strength of cement for nine different cases. The results of the adhesive cement strength test are presented in chapter 5. On a final note, the most important findings of this PDEng project are presented in chapter 6, with the recommendations for future work.

2 OBJECTIVE OF THE PROJECT

Section 2.1 below is to provide a perspective of how the former mentioned project problem scope is interpreted and tackled. Each objective given in the gray area, will offer foregoing context. A pragmatic translation of that interpretation in the form of project deliverables is presented in the preceding section 2.2.

2.1 DESCRIPTION OF THE DESIGN ARCHITECTURE

The monobore oil well is a relative new design for an oil well where the inner diameter of the oil pipe segments from the surface of the earth down to the oil field is an approximate constant. The oil well design is facilitated by a downhole expansion process, performed to increase the inner diameter of the oil pipe segment. Throughout expansion, the oil pipe will exert a shear load, though predominantly a compression load on the fluid saturated cement. As the saturated cement sheath surrounding the pipe is confined in between pipe and near impermeable formation, the radial deformation of the cement will - due to the fluid saturated state - result in an expulsion of fluid from the internal pore structure of the cement sheath.

OBJECTIVE I: Design an experimental setup able to reproduce the down hole conditions where the saturated cement sheath is monitored through the course of the expansion process. Free fluid separation from the saturated cement sheath is to be recorded, both in location and magnitude. Particularly the location where fluid will accumulate and its affect on the adherence of the cement to the pipe - during the expansion process - is of great importance. The accumulation of fluid will enact a significant fluid pressure at the interface of pipe and cement that will bring about an increased strain on the pipe, that to identify the conditions of potential failure behavior is to be monitored.

Prior to the development of a design for an experimental setup in which the effect of the expansion process is analyzed, a theoretical and numerical parametric study is to be performed to estimate the existing operating conditions. The aim here is the identification of free fluid separation from the cement sheath under shear and compression load. The cement structure is a porous medium that at time of the expansion process is in an approximate fluid saturated state. The framework is to consider the elementary components involved in the expansion process i.e., a fluid saturated porous cement sheath, a time dependent expansion or compression load, an interface in between oil pipe and cement, and free fluid separation or accumulation of fluid at the considered interface.

OBJECTIVE II: Develop a theoretical and numerical prediction tool to identify the free fluid separation from the cement sheath. Here it is necessary to consider the accumulation of fluid in front of the cone, and the generation of fluid pressure as a result at the interface of pipe and cement throughout the expansion process. The model is to be utilized as a tool to provide a parametric operating window that will support the experimental product design phase.

The strength of a cement-aggregate bond is weaker than the atomic bond strength of consistent cement paste [50]. Due to the natural shrinkage property of cement through the cement setting time and solidification process [44], and the adhesive property of unsettled cement to the formation, a microscopical annulus channel adjacent to the pipe is expected to form already prior to the expansion process. If accumulation of fluid would occur at the interface of the cement sheath and oil pipe, the parameter that determines the rate of expulsion of fluid towards the interface is the hydraulic bond, or bonding strength of cement to the metal pipe. The hydraulic bond strength - at this point an unknown parameter - will allow expansion in longitudinal direction once the fluid pressure in the annulus channel will exceed a certain system threshold value, as a result of the accumulation of fluid in the annulus throughout the expansion process.

OBJECTIVE III: Design a test capable of measuring constitutive behavior of wet cement under high hydrostatic pressure such that the constitutive behavior of downhole situated cement can be determined. The aim is the determination of (i) the hydraulic bond strength parameter of cement that is attached to the metal pipe and (ii) the constitutive behavior of cement prior- and post compression and shear load deformation.

2.2 THE DELIVERABLES OF THE PROJECT

The deliverables related to theoretical and numerical work are the following;

- A dynamic linear-elastic deformable cement response model to simulate the direction of fluid displacement in the expansion process.
- A cement failure prediction model to investigate the accumulated fluid drainage potential from the considered interface for different types of formations.
- A model simulating the growth of an annulus channel due to the expansion process to characterize the influence of individual parameters involved and to set an operating window for laboratory conditions.

The deliverables related to design methodology and experimental work are the following;

- A design and test report of a hydraulic bond test in a uni-axial cement to metal oil pipe configuration to investigate and to determine the permeability of the cement and the hydraulic bond parameter.
- A design for a cement deformation test to perform a classification on the degree of cement deformation to map the effect of pressure or deformation on cement porosity, to visualize the cement structure before and after deformation and the visualize and quantify the amount of liquid originating from the interior of the annulus or the exterior.
- A design for a small-scale expansion test to investigate the formation and evolution of the annulus channel in between the cement sheath and the expandable pipe and to validate the developed annulus channel theoretical and numerical model.

3

THEORETICAL AND NUMERICAL APPLICATION

To investigate the various aspects that are encountered within the expansion process with regards to the cement response, three different types of analyses will be performed in this chapter. The cement sheath comprised of cement paste contains the natural characteristic of near impermeability. The cement paste constitutes fine granular matter and is considered to be a fluid saturated porous medium. Recent development in advanced micro- and poromechanical experimental testing methods have made it possible to evaluate the microstructure of hardened cement paste [10][16]. The development made it possible to validate the theory of the *mechanics of porous media*[1] to describe the macroscopic behavior of near impermeable cement paste [20]. This theory of porous mechanics on the cement paste - or simply the *cement sheath* - will allow a theoretical and numerical investigation which is in this chapter. The main assumption is that the stress in a porous structure is not only carried by the solid structure, instead carried by the solid structure and fluid present in that solid structure.
In analysis (1) a multiphase problem is considered where the dynamic response of a one-dimensional cement sheath is investigated. The dynamical load imposed on the sheath is similar to what is to be expected in the field situation due to cone movement. The details of this analysis can be found in section 3.1.

It will be shown in former analysis (1) that the fluid has a preferential flow direction to the undesirable position of the imposed dynamical load. Due to this direction of fluid displacement, an accumulation of fluid will occur at the interface of expandable pipe and cement. In analysis (2), section 3.2, it is investigated when the accumulated fluid will find a way to penetrate the near impermeable cement sheath through a relative permeable fractured structure.

In the final section analysis (3), the accumulation effect of fluid will be studied over time. In section 3.3 the concept of a formation of an annulus (narrow fluid channel) will be introduced that is observed in earlier performed experimental work [57]. The model that attempts to simulate this behavior will provide information on the pressure and stress imposed on the expandable pipe and cement sheath.

1 The theory to describe physical propagation of matter through porous media e.g., saturated porous rock, sandbeds, beaches and dikes. Biot [7] and Terzaghi [52] were the first that established the corner stones of the mechanics of porous media. Verruijt [54][56] compiled the theory and made it accessible with practical examples.

3.1 CEMENT RESPONSE IN POROELASTIC MATERIAL

The present section describes a numerical analysis that attempts to model a continuum two phase flow in a fully saturated linear elastic one-dimensional deformable and isotropic porous medium. A brief theoretical explanation of the dynamics of a porous medium that is implemented in the numerical model is given in section 3.1.1. The theory put together in an assembly of the governing equations is given in section 3.1.2. An application of the model is given in section 3.1.3. In the application, a one-dimensional (in radial-direction of the liner system) cement sheath is exposed to a solid deformation that aims to mimic the effect of cone migration. The primary conclusions of the analysis are presented in section 3.1.4. In-depth details related to the space and time discretization of the governing equations, boundary conditions and bottlenecks of the numerical model can be found in appendix D.1.

3.1.1 *Theory of dynamic poroelasticity*

The theory of poroelasticity is a continuum analysis where a porous medium constitutes an elastic matrix with interconnected fluid saturated pores. It postulates that a porous matrix subjected to stress will develop a volumetric change in the pore space. As pore space is saturated with liquid, the result is flow of pore fluid. Biot [7] did some groundbreaking work on wave propagation through saturated porous media, and in fact, the model that is adopted in this section will embody the so-called Biot's poroelastic wave equations. The derivation of each equation is given in Verruijt [54]. Here only the essential wave equations are presented.

A cement column is investigated that constitutes a solid matrix and is fully saturated with liquid. The porosity n is the fraction of pore liquid inside of the cement sheath. Fluid mass that crosses the interface of a infinitesimal element can be described by fluid mass conservation,

$$\frac{\partial n\rho_f}{\partial t} + \frac{\partial n\rho_f u}{\partial x} = 0, \tag{1}$$

where ρ_f is the fluid density and u is the fluid velocity that is an average of the fluid particles. The solid particles that crosses a boundary of an infinitesimal element is described likewise, by the solid mass conservation,

$$\frac{\partial (1-n)\rho_s}{\partial t} + \frac{\partial (1-n)\rho_s s}{\partial x} = 0, \tag{2}$$

where ρ_s is the solid density and s is the solid particle velocity. The fluid and solid mass conservation equations can be coupled by assuming the fluid density is a function of the fluid pore pressure. When the density of the solid particles is assumed to be a function of the isotropic total stress and the pore pressure one can combine the two mass conservation equations to obtain the so-called storage equation,

$$\alpha \frac{\partial s}{\partial x} + S_p \frac{\partial p}{\partial t} = -\frac{\partial [n(u-s)]}{\partial x}, \tag{3}$$

where S_p is the storativity coefficient and α is the coefficient of Biot. The storativity coefficient is the capacity of the liquid to occupy pore space. The storage equation is the first governing equation of the numerical model.

The storage equation describes interaction between three still unknown variables, the fluid velocity, solid particle velocity and the pore pressure. Momentum conservation will provide two more governing equations, however, will also introduce another variable i.e., the effective stress. The momentum conservation for both phases for the one-dimensional case can be written as,

$$-\frac{\partial \sigma'}{\partial x} - \alpha\frac{\partial p}{\partial x} = n\rho_f\frac{\partial u}{\partial t} + (1-n)\rho_s\frac{\partial s}{\partial t}, \tag{4}$$

where σ' is the effective stress. A non-zero effective stress will indicate a state of deformation. The conservation of fluid momentum can be written as,

$$-n\frac{\partial p}{\partial x} - \frac{n^2\mu}{\kappa}(u-s) = n\rho_f\frac{\partial u}{\partial t} + \tau n\rho_f\frac{\partial (u-s)}{\partial t}, \tag{5}$$

where τ is the turtuosity factor that describes the added mass due to the turtuosity of the flow path, μ is the viscosity of the fluid and κ is the permeability of the porous medium.

The final equation assumes, as a first approximation, that the effective stresses are related to the strains by a generalized form of Hook's law. The result is a constitutive relation for a linear elastic deformable solid that can be written as,

$$m_v\frac{\partial \sigma'}{\partial t} = -\frac{\partial s}{\partial x}, \tag{6}$$

where m_v is the confined compressibility that in an isotropic material can be determined by the compression and bulk modulus.

3.1.2 *Implementation details of the numerical dynamic poroelastic model*

In the previous section Biot's poroelastic wave equations have been introduced. In this section a numerical solution of these equations is addressed. Equations (3) - (6) form a coupled system and are rewritten into a form that will allow a finite difference discretization. It can be shown that the equations can be written in the following form,

$$\left[1+\tau\left\{1+\frac{n\rho_f}{(1-n)\rho_s}\right\}\right]\frac{\partial u}{\partial t} = \ldots$$
$$\ldots -\frac{1}{\rho_f}\frac{\partial p}{\partial x} - \frac{ng}{k}(u-s) - \frac{\tau}{(1-n)\rho_s}\left\{\frac{\partial \sigma'}{\partial x} + \alpha\frac{\partial p}{\partial x}\right\}, \tag{7}$$

$$\frac{\partial s}{\partial t} + \frac{n\rho_f}{(1-n)\rho_s}\frac{\partial u}{\partial t} = -\frac{1}{(1-n)\rho_s}\left\{\frac{\partial \sigma'}{\partial x} + \alpha\frac{\partial p}{\partial x}\right\}, \tag{8}$$

$$\frac{\partial p}{\partial t} = -\frac{n}{S_p}\frac{\partial u}{\partial x} - \frac{\alpha-n}{S_p}\frac{\partial s}{\partial x}, \tag{9}$$

$$\frac{\partial \sigma'}{\partial t} = -\frac{1}{m_v}\frac{\partial s}{\partial x}, \tag{10}$$

where the permeability κ is replaced with the hydraulic conductivity $k = \kappa\rho_f g/\mu$. A more detailed derivation as well as the space- and time discretization can be found in appendix D.1.1.

3.1.3 *Cement response analysis*

One-dimensional cement response is investigated along the radial line $y = y_{x-s}$ of the cement sheath throughout the expansion process, illustrated in figure 4. The domain at the interface $x = 0$ of the cement sheath and expandable pipe is deformed with a time dependent sine function according to the shape and propagation speed of the cone, the opposite side $x = L$ is non-deformable but fluid penetrable. The situation is set-up similar to the pipe expansion process.

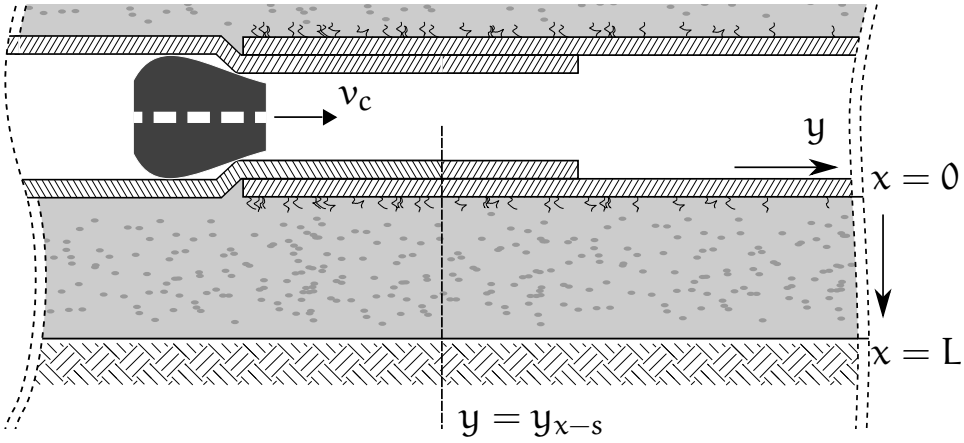

Figure 4: *Dynamic deformation model for the evolution of system variables along the radial cross-sectional line y_{x-s}. Cone displacement from left- to right through the linersystem will compress the cement sheath. As the cement sheath is saturated with liquid, deformation of the solid matrix will result in fluid transport.*

The cone will move with a migration speed v_c, whereas in the one-dimensional case, the expansion will impose deformation of the cement sheath in radial direction only. The solid deformation at the interface $f(t)$ imposed by the cone, is modeled by the following sine function,

$$f(0,t) = \frac{L}{2}\left(1 - \cos(\pi t/T)\right), \tag{11}$$

where $T = L_c/v_c$ and t is the time $t \in [0,T]$. Appendix D.1.2 gives an overview of the boundary conditions.

A typical situation is considered with a velocity $v_c = 500$ [mm/min] and length scale $L_c = 0.1$ [m] of the cone [25]. The material property and system values are summarized in appendix D.1, in table 16. Evolution of the variables in space due to deformation imposed by the cone is depicted in figure 5 for three different times $t = [0, T/2, T]$.

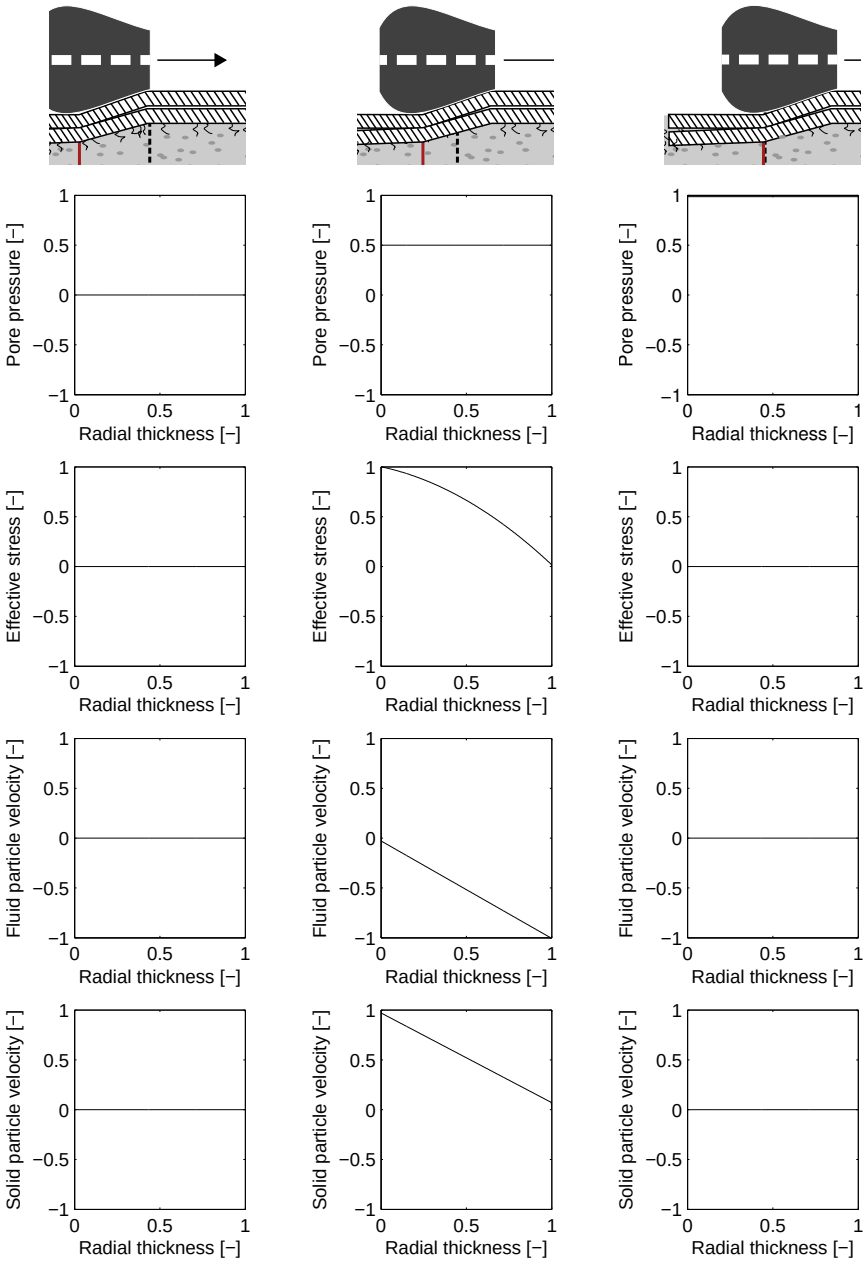

Figure 5: *The cement response along the radial thickness of the cement slab during the expansion process. Each column from l-r is the time* $t = 0$, $t = 1/2T$ *and* $t = T$, *and in each row from t-b is the fluid pore pressure, the effective stress, the cement particle velocity and the fluid particle velocity.*

These time intervals depict the initial condition, halfway situation and the end of the expansion process, respectively. An important observation is that the pore fluid pressure gradient along the radial path outward appears to be positive ($dp/dx > 0$) for the preset conditions, will also be shown in the next paragraph. As fluid will tend to move from a high pressure area to a lower pressure area, it will force an escape of liquid from the outside formation towards the interface of the cement sheath and expandable pipe. This observation is in qualitative agreement with the the

observations made in the Shell Expandables department [11][57], as depicted in figure 6. Here the liquid within the saturated cement sheath was squeezed out and started to accumulate at the interface of expandable pipe and cement. Accumulation of fluid broke the hydraulic bond strength of cement and carried an annulus channel ahead of the direction of cone migration. The annulus channel is visible in figure 6 by the *onset of annulus* comment.

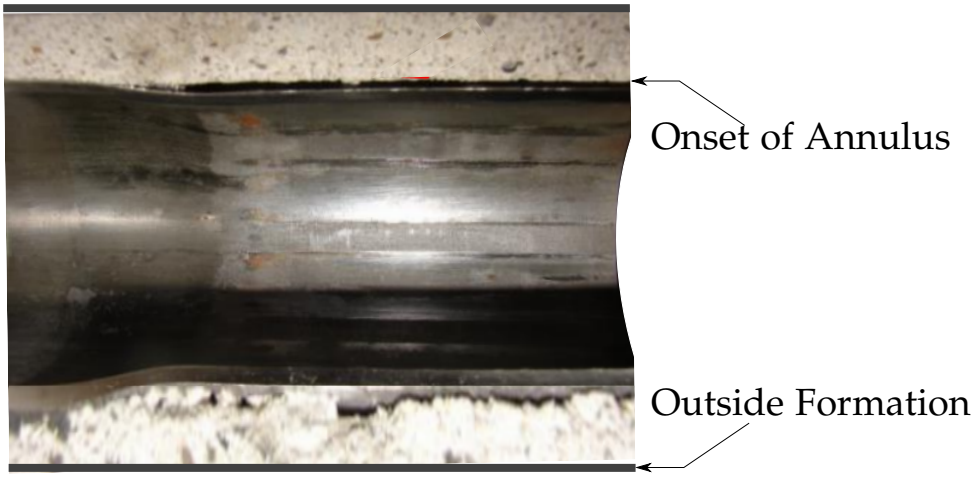

Figure 6: *Annulus formation ahead of the expansion process at interface of the expandable pipe and cement sheath [57]. Result from figure 5 (and figure 7) points out that fluid moves from the formation towards the interface expandable pipe, breaking the cement bond with the pipe and creating an annulus channel. Note that in the figure the expansion process occurred with a cone that moved to the right.*

Instead of an evolution of the variables along the cement thickness, a time response for three positions $x = [0, 1/2L, L]$ is given in figure 7. It can be seen that the liquid pore pressure takes the form of the implicit imposed solid deformation boundary condition given in (11). In the expansion process the cone will widen the expandable pipe that exerts a compression load on the cement sheath, the sheath is radially pushed outward illustrated by a positive defined solid cement particle velocity in figure 7, the right-bottom subfigure. While the solid cement sheath is compressed and pushed radially outward, a positive pressure gradient is formed shown in the left-top subfigure. It will break-apart the fluid pores and will force the dissolved fluid in the cement matrix to be expelled towards the interface of expandable pipe and cement, illustrated in the left-bottom subfigure by a negative fluid velocity.

3.1.4 *Conclusion*

To explore the evolution of the fluid pore pressure, effective stress, solid particle displacement and fluid particle displacement in the interior of a cement sheath a dynamic poroelastic model is developed that is able to analyze the cement response throughout the expansion process. The expansion process is an operation where a cone will move through a smaller

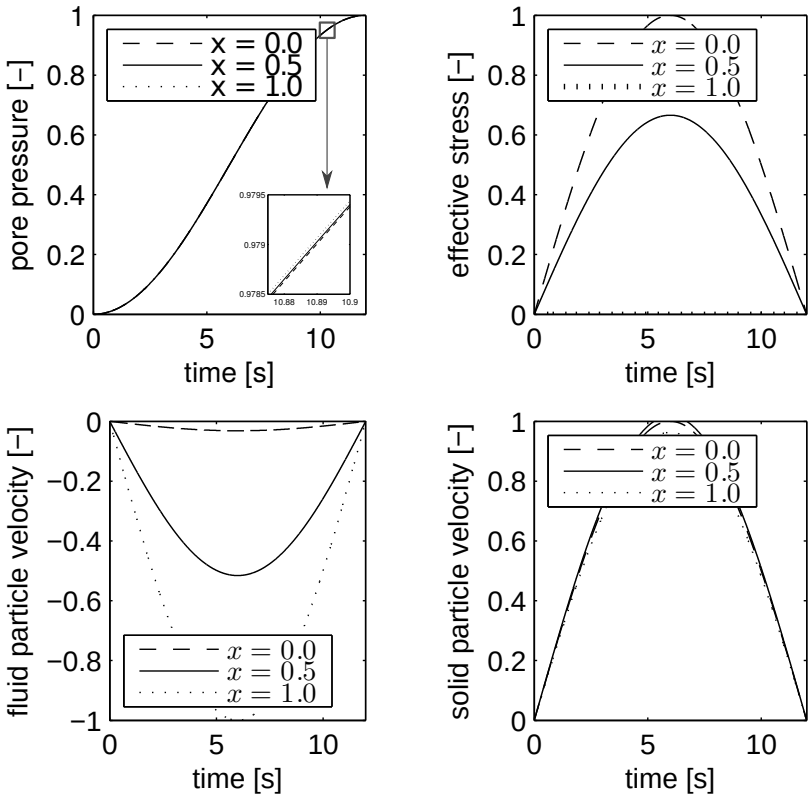

Figure 7: *Evolution of the system parameters in time up to* 12*[s] for three different spatial positions* $x = [0, 1/2L, L]$. *Note the pressure gradient that is emphasized in the additional inferior frame of the pore pressure.*

diameter expandable liner system. The cone will widen the expandable liner system, as a result the cement sheath will be compressed.

The assumptions made to construct the model are summarized as follows;

- A continuum two phase flow is assumed where the cement structure is completely saturated with fluid, this will assume an openfoam structure where the pore structure is interconnected to one another.
- A one-dimensional system is assumed to simulate the interaction of solid deformation, transport of fluid and pipe expansion. The implication is that compression of the cement sheath due to the expansion process will result in one dimensional deformation only.
- A linear elastic deformable isotropic porous medium is assumed, this will enable the application of, and couple the stress and strain by means of Hook's law.

It is found that the dynamic poroelastic model predicts a preferential flow direction from the interior of the cement matrix towards the interface of the expandable pipe and cement sheath. The fluid release is part of the expansion process and will force fluid to be accumulated at the interface of expandable pipe and cement, qualitatively confirming the observations

made in previous experimental work [11][57]. Accumulation of the fluid over time will eventually break the cement bond and will initiate an annulus channel, separating the cement and liner system as shown in figure 6. A return flow, from the fluid annulus back to the cement sheath is due to the close to impermeable layer of cement $\sim \mathcal{O}(\ 10e\text{-}15m^2\ )$ approximately non-existing. The implication is that without a pressure release the expansion process will constitute a continuous increase and accumulative effect of fluid pressure in the annulus channel, up to the point of a potential pipe failure.

3.2 CEMENT FAILURE PREDICTION

With the poroelastic cement response model it was demonstrated that the expansion process will discharge fluid from the fluid saturated cement sheath interior to the interface with the expandable pipe. The continuous migration of fluid will have an incompressible inflation effect at the interface. The manifested fluid will pressurize the interface which may threaten the integrity of the hydraulic cement bond, that holds the cement sheath and expandable pipe together. Eventually the hydraulic cement bond will break and the result is the onset of an annulus between the cement and expandable pipe. It was assumed that the cement sheath was near impermeable, which prevented migration of fluid towards the formation. However, due to the expansion process the cement may become fractured or crushed under the compression or shear load. A fracture or crack in the cement will substantially increase the permeability, and be a potential fluid pathway, that will allow depressurization of the annulus channel, by a release of fluid towards the formation. Depressurization of the annulus channel can prevent potential pipe failure, and is worth investigating.

The following section will investigate crack propagation through the cement layer by using an energy principle. The cement sheath will be confined between an expandable pipe and a stone formation. The pipe is expanded by the expansion process, which will compress the cement sheath, where interaction with the stone formation is permitted. Anisotropy of the material properties is incorporated by the assumption of a normally distributed porosity of the cement sheath, that is related by semi-empirical means to the permeability. The model is equipped with the energy principle of Griffith that will make it able to determine - for a given load - whether or not a crack will propagate.

The failure analysis of the cement sheath is given in section 3.2.1, that will illuminate the governing equations and the interaction with the stone formation. Section 3.2.2 will discuss the stress intensity factor imposed at the cracktip, and the energy propagation principle of Griffith. The analysis of crack growth for a degree of expansion, and an elastic moduli ratio will be assessed in section 3.2.3, the conclusions of this section will be given in section 3.2.4.

3.2.1 *The mechanism of crack formation and propagation*

A crack is the separation of a body into two or more pieces in response to an imposed stress. The applied stress may be tensile, compressive, shear, or torsional in nature and be a result from e.g., a mechanical- or thermal stress. In general, fracture development involves a two step procedure, a crack formation and a propagation in response to an imposed stress [14]. A brittle fracture, typical in cement material has little to no plastic deformation. Brittle material will require little energy to fracture and unstable crack propagation is in many cases unavoidable. Previous authors that modeled crack propagation of brittle material focused predominantly on a single

stand-alone brittle material [4][33][48][51]. Thus without consideration of the interaction of the brittle material with the environment, and neglecting the secondary present thermodynamic phase (e.g., gas or liquid) in the brittle material. Other authors that studied crack propagation of ductile material included entirely homogeneous material properties [40][45].

The cement sheath at the time of deformation is in a fully saturated state where a continuum two-phase system of a solid and fluid phase is considered. The consequence is that total stress equilibrium σ will be a superposition between an effective stress σ' and fluid pore pressure p, given by Verruijt [55],

$$\sigma_{r,\theta} = \sigma'_{r,\theta} + \alpha p, \tag{12}$$

where α is a Biot coefficient that is a measure of the compressibility of the solid and fluid phase.

A cement sheath confined between an expandable pipe at R_I (inner radius) and a stone formation at R_O (outer radius) is considered, see figure 8. When shear stress is neglected, an axi-symmetrical system can be as-

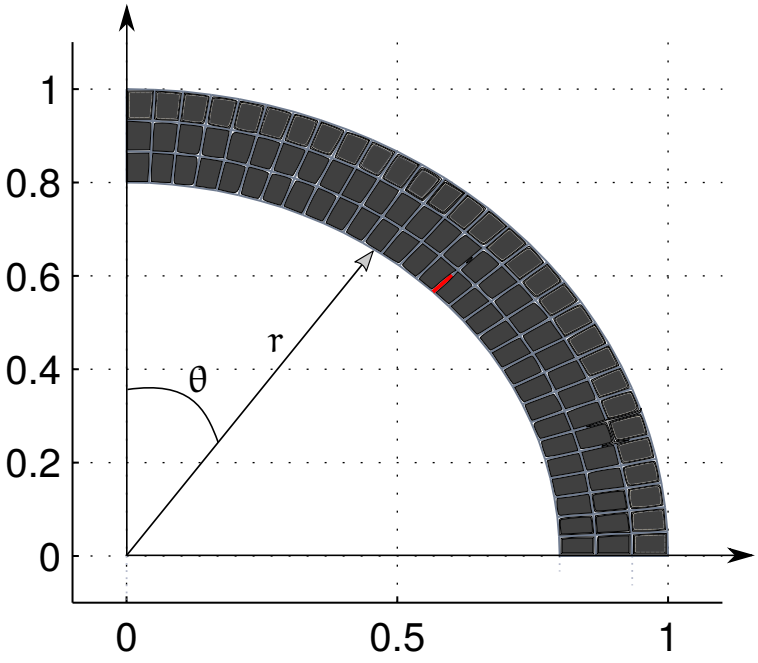

Figure 8: *A confined layer of cement (dark area) between an expandable pipe at* $r = R_I$ *and a stone formation at* $r = R_O$ *portrayed in a quarter circle with a preset crack at* $\theta = \pi/4$.

sumed. If moreover a plane strain analysis is assumed, then the governing equations can be expressed as,

$$\frac{\partial}{\partial r}\left(\frac{k}{\gamma}\frac{\partial p}{\partial r}\right) + \frac{1}{r}\frac{k}{\gamma}\frac{\partial p}{\partial r} + \frac{1}{r^2}\frac{\partial}{\partial \theta}\left(\frac{k}{\gamma}\frac{\partial p}{\partial \theta}\right) = 0, \tag{13}$$

$$\frac{\partial \sigma'_R}{\partial r} + \frac{\sigma'_R - \sigma'_\theta}{r} = 0, \tag{14}$$

$$\frac{1}{r}\frac{\partial \sigma'_\theta}{\partial \theta} = 0, \tag{15}$$

where k is the anisotropic permeability of the cement sheath and γ the volumetric weight of the fluid. A numerical solution is sought for the fluid pore pressure to incorporate the anisotropic permeability of the cement sheath. For the given assumptions, an analytical solution can be obtained for the effective stress equilibrium of the cement sheath.

Cone migration will determine the inner radial displacement u_i according to the geometry of the cone, whereas the outer radial displacement u_o is an unknown. If one considers linear-elastic interaction with the stone formation, one can determine the outer radial displacement. Consider u_o to be known (e.g., a guess value), than for a given u_i a radial stress σ_R can be calculated straightforwardly. The resulting force on the inner side of cement sheath given in figure 8 should be of the same order as the resulting force on the outside,

$$A_I \sigma_{R,I} \cong A_O \sigma_{R,O}. \tag{16}$$

For a linear elastic stone formation, the force is linearly proportional to the deformation at R_O. The force required to deform the formation by u_o is equal to,

$$F = k_O \cdot u_o, \tag{17}$$

where k_O is a spring constant that is characteristic for the formation. It is desired that the spring constant is expressed in terms of the elastic modulus of the formation E_f, and a characteristic length scale of the annulus. Taking into account the former premise, an expression for k_O is obtained,

$$k_O = E_s \left(\frac{A_O}{W_c}\right) = \frac{E_s}{2}\left(\frac{\pi R_O}{R_O - R_I}\right), \tag{18}$$

where W_c is a cement matrix thickness. Substitution of k_O (18) into (17) will lead to an expression for u_o. Now u_o can be obtained by combination of the solution for the radial stress component of the concrete and the resulting displacement of the formation, that in the present work is solved with a Picard iteration procedure [34].

3.2.2 *Griffith's energy principle*

A typical fracture in brittle material will contain little to no plastic deformation amid the crack formation process. The domain solution for elastic stress equilibrium will therefore not change with the propagation of a crack. However, the local stress distribution near the tip of a crack will change in the material. To determine whether or not a crack is to propagate, one will have to find a way to quantify the stress in the crack tip. Inglis *et al.* [29] in 1913 already showed that the stress at the tip of an infinitely sharp crack would reach an infinite value. In order to quantify the

stress in the vicinity of the crack tip a stress intensity factor K_I is imposed, given by Irwin [30],

$$K_I = f(l,\phi)\sigma_{VM}\sqrt{\pi a},$$
$$\textit{where} \quad f(l,\phi) = \frac{\cos(\phi/2)}{\sqrt{2\pi l}}\left[1 - \sin\left(\frac{\phi}{2}\right)\sin\left(\frac{3\phi}{2}\right)\right], \quad (19)$$

where a is the crack length from its origin and l is the increment of the crack length to its evaluation point. In the second part of (19) $f(l,\phi)$ is imposed to amplify and distribute the stress intensity factor in the vicinity of the crack tip over the surrounding elements of the crack tip. Moreover σ_{VM} is the Von Mises stress. Research do not agree whether to apply a Von Mises stress here, or a different stress component. In the present case the Von Mises stress is selected to deal with the fluid pore pressure in the cement matrix. The stress intensity factor is not part of the elastic stress equilibrium and will replace the stress in the vicinity of the crack tip. It is furthermore pointed out that K_I is proportional to the square-root of the length of the crack, which is relevant in the evaluation of the energy principle.

In terms of energy, crack growth occurs when the strain energy level due to elastic deformation will exceed the energy level required to maintain the atomic bond. The energy principle of Griffith originates in the mechanical form of energy, or work,

$$W = \int \vec{F} \cdot d\vec{x}, \quad (20)$$

where $\vec{F}$ is a force acting along the path $d\vec{x}$. One can transform (20) into an expression for the strain energy by multiplication with dV/AL. Doing so, the strain energy can be expressed as,

$$E_{st} = \frac{1}{2}\int_V (\vec{\sigma} \cdot \vec{\epsilon})\, dV, \quad (21)$$

where $dV = dr(rd\theta)dy$, $\sigma = [\sigma_r, \sigma_\theta]$ and $\epsilon = [\epsilon_r, \epsilon_\theta]$.
Atomic bonds that make up the solid matrix are in equilibrium in the absence of an external load. Considering a fracture, for an atomic bond to break, the strain energy E_{st} must exceed the energy level that makes up the bond between the atoms, i.e., the bond energy E_b. Considering the present situation, the failure mode most likely to occur is the *failure tensile mode*, where the brittle material is pulled apart due to the tangential stress component. If the tensile strength level of the cement matrix has been exceeded due to deformation, a crack will start to form. Consider (20), the atomic bond energy can be expressed in terms of the tensile strength σ_t of the cement,

$$E_b = \sigma_t dy \int_{a+l} \vec{x} d\vec{x} = \frac{\sigma_t dy}{2}[a+l]^2, \quad (22)$$

where a is the crack length from its origin, l the evaluated element length where the crack may propagate to, and dy is the crack thickness. In contrast to the stress intensity factor (19) the atomic bond energy (22) is proportional to the square of the length of the crack a.

3.2.3 *Crack propagation analysis*

The structural integrity of a cement sheath during the expansion process is evaluated. The cement sheath is confined between an expandable pipe and stone formation, where interaction with the stone formation is permitted. In the two-phase conditioned system the fluid pore pressure in the cement sheath is estimated with a finite difference solver to incorporate the anisotropic permeability. The discretization is given in appendix D.2.2. The analytic solution for the effective stress is obtained with a plane strain approximation and is given in appendix D.2.3. The tensile strength and the elasticity modulus are both unknown and are taken from empirical relations, given in section D.2.4. The algorithm for crack propagation is presented in section D.2.5, where it is explained how a crack propagates and until which point. Furthermore, in appendix section D.2.6 a grid convergence analysis is performed where it is shown that consistent results are obtained for a mesh of $\{NrxN_\theta\} = \{105x1007\}$.

The structural integrity of the cement sheath is evaluated for (i) the degree of expansion, and (ii) the elastic modulus cement/formation (E_c/E_s) ratio. For the numerical experiment the material property values summarized in table 18 have been used, that depict downhole well conditions.

Crack propagation is shown in figure 9 where six subfigures are shown. On the left- and right results for two different elastic moduli are depicted. From the top- down an increase in the degree of expansion for different stages of the expansion process. In relative terms, the left-side figures contain a flexible formation, whereas the right-side figures are for a stiff formation. Comparing the two top subfigures show little difference between cracking the two formations. However, an increase of the expansion rate, shown in the center and bottom two subfigures show that the cement sheath in fact has failed [2] for the flexible formation, whereas the cement matrix for the stiff formation is still in tact.

For a close to impermeable cement structure and accumulated fluid at R_I, the intact cement sheath would be unable to allow liquid to pass towards the formation, and no drainage would be possible. In contrast to the already failed cement sheath with an equal impermeable cement structure, where liquid would be able to flow through the cracks of the cement sheath towards the formation.

2 The cement sheath is failed when the following is true; $\textit{failure} = \left(\frac{a}{R_0 - R_I}\right) \geqslant 1$.

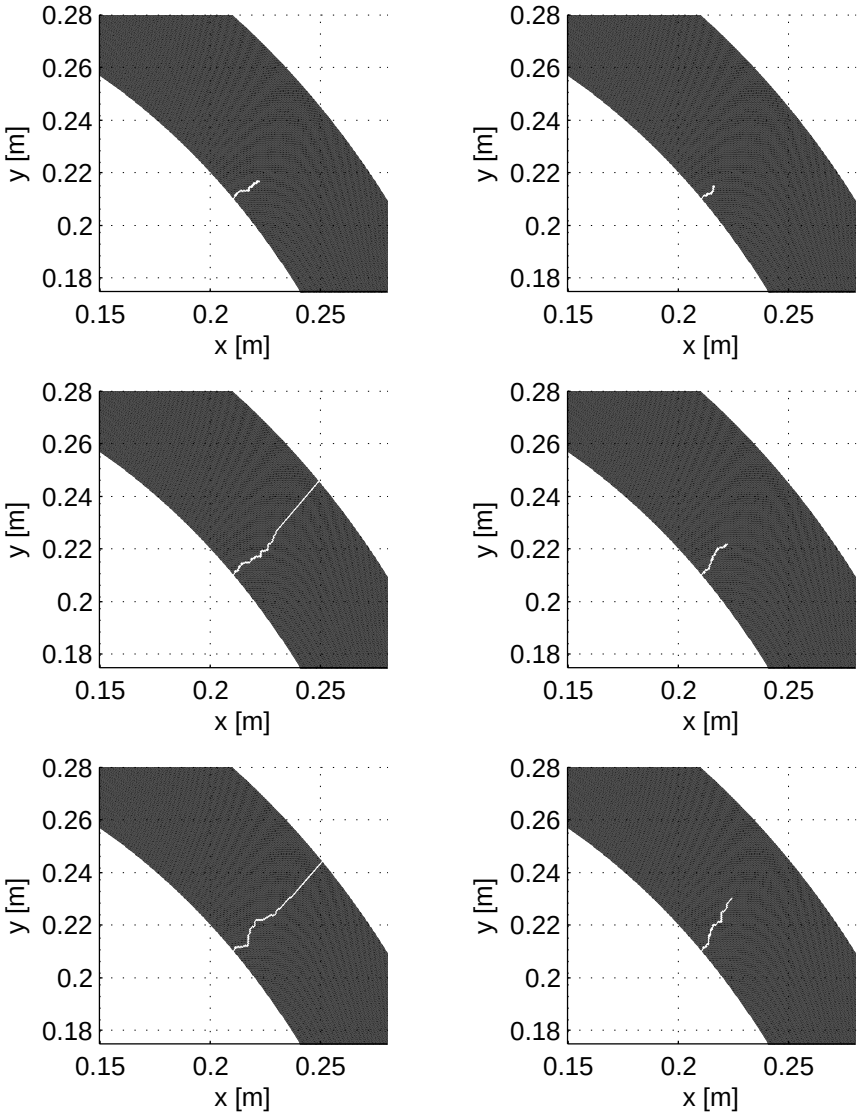

Figure 9: *Crack propagation for two different ratios of elastic moduli. From the top- to bottom there is a* $0.75[\mathrm{mm}]$*, a* $1.50[\mathrm{mm}]$ *and a* $2.25[\mathrm{mm}]$ *deformation imposed on the inner side of the cement sheath. The left side is an elastic modulus ratio of cement and formation* $E_c/E_s = 1/(4/3)[\mathrm{GPa}]$ *and on the right a* $E_c/E_s = 1/210[\mathrm{GPa}]$ *ratio. Porosity is normal distributed between* $n = \{0.15 - 0.35\}$ *with a mean set at* $\tilde{n} = \{0.25\}$*.*

Figure 10 presents results for four ratio of elastic moduli varying from flexible to stiff, it shows illuminates the failure rate against the degree of expansion imposed on the inner side of the cement sheath. Information given in figure 10 is the moment of instantaneous structural failure for different elastic moduli ratios. Furthermore, for the situation where the elastic modulus of the stone formation is much larger than the elastic modulus of cement $E_s >> E_c$ the differences in crack growth for the tested expansion ratios are diminished.

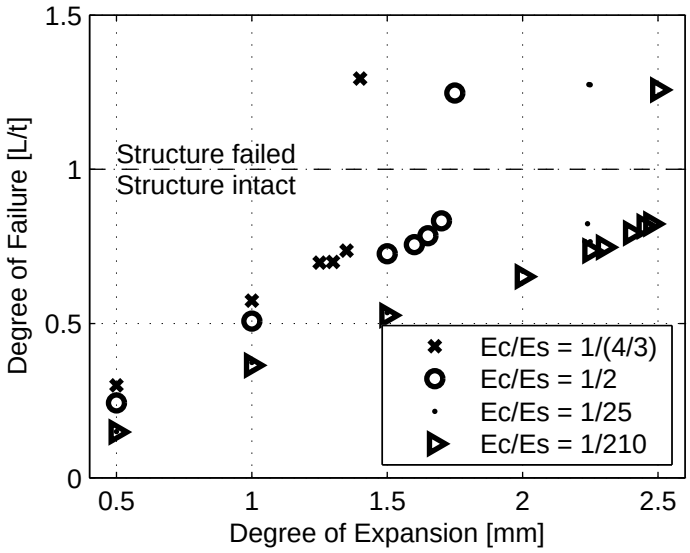

Figure 10: *Failure behavior for a set of different ratios of elastic moduli varying from an elastic formation to a stiff formation. The degree of expansion, or stage of expansion is given on the horizontal axis and a dimensionless measure of failure {Cracklength/Annulus thickness} on the vertical axis. Porosity is normal distributed between* $n = \{0.15 - 0.35\}$ *with a mean set at* $\tilde{n} = \{0.25\}$*. Note that unstable crack growth is present after a failure rate of approximately* $80[\%]$*. A degree of failure that surpassed a unity value, indicates a crack length larger than the cement sheath thickness.*

3.2.4 *Conclusion*

A failure prediction model is developed and implemented for crack growth in linear elastic brittle material. It is based on the energy principle of Griffith [22]. The model constitutes a fluid and a solid phase that is able to approximate the total-, effective stress and fluid pore pressure in a fluid saturated cement sheath. In a two-dimensional cylindrical coordinate system, the model - within its assumptions - is able to predict potential failure of the cement material. The assumptions made to construct the model are summarized as follows;

- A continuum two phase flow is assumed where the cement structure is completely saturated with fluid, this will assume an openfoam structure where the pore structure is interconnected to one another. The consequence is that the total stress is the summation of the effective stress and the pore pressure and that the permeability is a function of the porosity.
- A plane strain analysis is assumed. The implication is that the strains in longitudinal direction are disregarded which is similar to a hollow cylinder under internal pressure where the ends are fixed between immovable plates.

- A two-dimensional axi-symmetrical system is assumed, this will remove the $(\partial/\partial\theta)$ terms and will allow investigation of only a quarter circle.
- A linear elastic deformable isotropic porous medium is assumed, this will enable the application of- and couple the stress and strain by means of Hook's law.
- A brittle material is assumed, that will disregard plastic deformation and will allow the application of the linear elasticity equations.
- The semi-empirical energy principle of Griffith is adopted, this will provide a means to quantify the stress in the cracktip, and based on the quantified stress will determine whether or not a crack is to propagate or stagnate.

A simulation is performed where a cement matrix is confined in between an expandable pipe and a flexible formation, and an expandable pipe and a stiff formation. It was shown that for the case with a flexible formation, the cement sheath failed after an expansion rate of about 1.4[mm], while the stiff formation could resist almost double the expansion rate 2.5[mm] until failure. For a non- or low permeable cement structure an intact cement sheath would be unable to allow liquid to pass through towards the formation. This is an important finding when flow towards the formation is a beneficial factor for depressurization of the interface of the expandable pipe and the cement sheath.

3.3 EVOLUTION OF THE ANNULUS CHANNEL

In the section of the poroelastic cement response model it was demonstrated that a compression load performed on the cement sheath will separate the fluid and solid phase. A consequence was preferential fluid flow towards the interface of the pipe and cement sheath, that would course a fluid filled annulus channel at that interface. The analysis showed a qualitative agreement with former experimental work performed within Shell [11][57].

Encouraged by these findings, this section will exploit growth of a fluid annulus formation. A new model will be developed to capture the displacement of fluid in the cement sheath towards an assumed minor and prior-to-expansion defined fluid annulus. As a result of the accumulation of fluid near the interface, fluid pressure inside the annulus will rise. If the fluid pressure exceeds the cement adhesive strength to the expandable pipe, or the hydraulic bond strength of the cement, the annulus will grow in longitudinal direction along the pipe. However, when the pressure exceeds the collapse strength of the expandable liner, pipe failure will result. The evolution of the annulus channel will therefore determine the consequences of fluid accumulation, fluid pressure rise and the growth of the fluid filled annulus channel in the expansion process.

In consideration of the expansion process as a whole, the total problem is divided into a set of subproblems that will be explained in detail in section 3.3.1. The developed model is put-in-effect in section 3.3.2, where results will be shown according to an assumed model configuration. The conclusion is presented in section 3.3.3, which will present the parameters that are found to have a significant influence on the expansion process and that are modifiable in the laboratory.

3.3.1 *Coupled system*

The annulus model assumes presence of a fluid layer with a certain width $w = f(y)$ at the interface of the expandable pipe and cement. In the primary phase, three regions of different physical behavior will be considered separate. Once models and a solution are attainable for each respective section, the models are coupled. The first section, an area parallel to the progressing cone, will be the *compressed cement sheath*. Fluid from within the compressed cement sheath will be discharged to the second and third region, the *porous cement sheath* and *annulus channel*, which both are located upstream of the cone. As the cement is assumed to be fluid saturated with incompressible fluid, any compression of cement or influx of one fluid will result in a quantifiable amount of another discharged fluid. The three regions considered are depicted in figure 11 and are numbered, accordingly. Each region will require an individual approach to determine the coupled interaction in the expansion process and will be explained in a subsection.

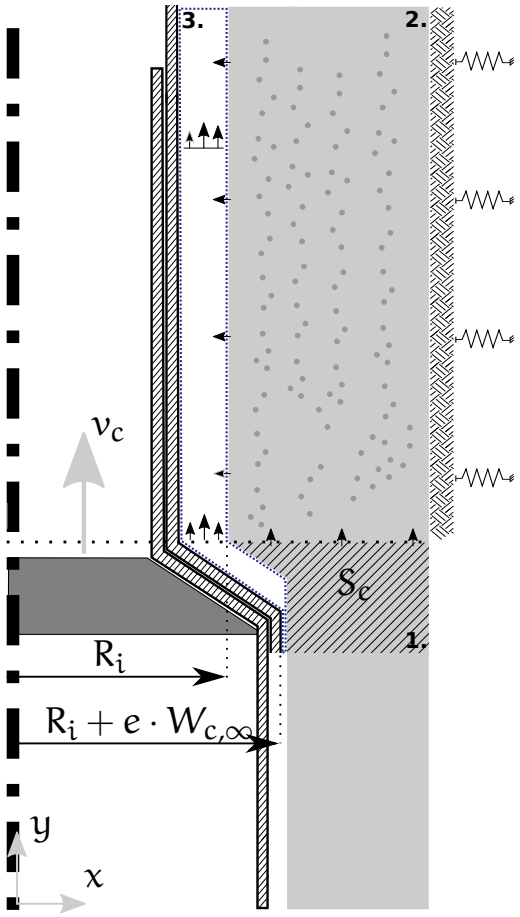

Figure 11: *The annulus model assumes a pre-existing annulus and constitutes three coupled physical domains. These are;* ***1:*** *the compressed cement sheath 3.3.1.1,* ***2:*** *the porous cement sheath 3.3.1.2 and* ***3:*** *the annulus channel 3.3.1.3.*

The compressed cement sheath

The compressed cement sheath (**1.**) is developed to quantify a fluid discharge from the domain due to the cone indentation. The compressed cement sheath is connected to the **2:** porous cement sheath and **3:** the annulus channel, that both will consume the discharged fluid. If the fluid in the domain is incompressible, the fluid porosity n is assumed, then according to the cone geometry one will be able to determine the quantity of discharged fluid, clarified in figure 12.

Examination of the involved geometry, fluid saturated state of the cement sheath and incompressibility of the fluid, the expression for the total discharged mass flow is derived, and is expressed as follows,

$$\dot{m}_{tot} = \rho_f S_c n \cdot \left(1 - \frac{S_o}{S_c}\right) \quad [kg/s/m]. \tag{23}$$

If it is assumed that the majority of the fluid will be expelled towards the path of least resistance than the massflow of fluid towards the annulus channel $\dot{m}_a$ and the porous cement sheath $\dot{m}_c$ is expressed by,

$$\dot{m}_a = r_\alpha \dot{m}_{tot}, \quad \dot{m}_c = (1 - r_\alpha)\dot{m}_{tot}, \tag{24}$$

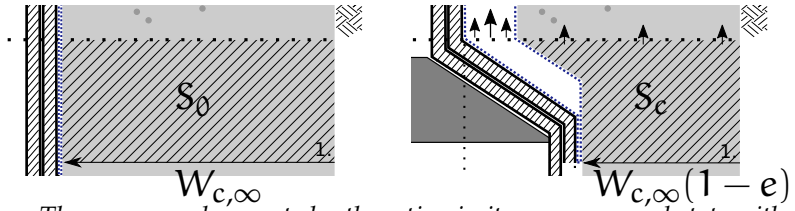

Figure 12: *The compressed cement sheath section in its uncompressed state with area S_0 (left) and compressed or deformed state with area S_c (right). As the cement sheath is considered saturated with fluid, compression of the sheath will discharge fluid from the interior domain.*

where $\varinjlim r_\alpha \to 1$ that is the percentage of fluid that is to proceed to the annulus channel. More detail with respect to the compressed cement sheath is given in appendix D.3.1.

The porous cement sheath

The porous cement sheath (**2.**) is positioned upstream of the cone, arranged parallel to the annulus channel. The porous sheath is to permit interaction from the annulus channel through the porous cement sheath towards the formation. As the porous cement sheath is fluid saturated, it will constitute a fluid and a solid phase. The significance is that the total stress in the sheath is associated with an effective stress in the solid phase, and a fluid pressure in the fluid pore space. The interaction that will take place in the porous cement sheath is appointed by the accumulated fluid pressure from the annulus channel, and the discharge of fluid from the compressed cement sheath, the situation is depicted in figure 13.

If deformation in the cement sheath upstream of the cone is expected to be minor, an analytical expression for the effective stress in the porous cement sheath could be obtained with a plane strain analysis similar to the one performed in section 3.2. To determine the total stress in the porous cement sheath, it is necessary to find an expression for the fluid pore pressure. For a strict incompressible and smooth inviscid fluid particle traveling from one point to another along a streamline in a porous medium, the energy conservation theorem of Bernoulli dictates,

$$\frac{1}{\rho_f}\left(p - \rho_f \vec{g} y + \frac{\rho_f V^2}{2}\right) = \texttt{constant}, \tag{25}$$

along a streamline. Here p/ρ_f is the enthalpy per unit mass, $\vec{g}y$ is the gravitational energy per unit mass, $V^2/2$ is the absolute kinetic energy $V = \sqrt{u^2 + v^2}$ and $\vec{g} = [0, -g]$. At this point it is desired to link this to describe viscous flow in a porous material. A way to achieve that is by application of a Darcy flux. Here it is recognized that the complexity of fluid flow through porous material and the former two assumptions of a Bernoulli flow and the combination with a Darcy flux may be considered rather bold. The application throughout the literature is therefore known

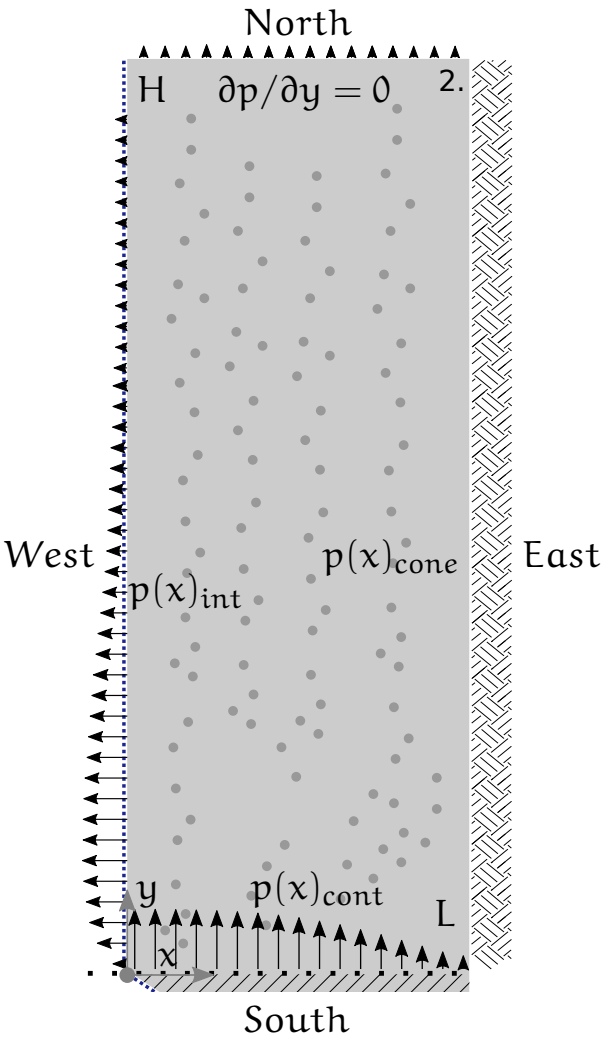

Figure 13: *Diffusion of fluid into the porous domain is done with a quadratic velocity inlet profile $V_c(x)$, a cubic velocity expulsion profile $U_w(y)$ and a zero outflow at the northern interface due to the impermeable nature of the porous medium.*

as an approximate justification of Darcy's law [32]. For a Darcy's flux the following Bernoulli relation is adopted [61],

$$q = -\frac{k}{\mu}\frac{d}{dn}\left(p - \rho_f \vec{g} y + \frac{\rho_f V^2}{2}\right), \tag{26}$$

where q is a volumetric flow per cross-sectional area $[m/s]$, k is a permeability $[m^2]$ and μ is a fluid viscosity $[Pa \cdot s]$. A fluid mass conservation principle across the circumference of figure 13 can be shown to yield,

$$-\left(\frac{\partial \rho_f q_x}{\partial x} + \frac{\partial \rho_f q_y}{\partial y}\right) = \frac{\partial \rho_f n}{\partial t}. \tag{27}$$

In recognition of the a horizontal, and vertical Darcy flux (26), one can derive with help of substitution and the chain rule for differentiation on

each term of (27) an differential equation for the fluid pore pressure. It can be shown that the former will yield an expression similar to the following,

$$\underbrace{\rho_f n\,(C_n + C_f)\,\frac{\partial p}{\partial t}}_{\texttt{Compressibility}} = \frac{\rho_f k}{\mu}\Bigg[C_f\Bigg\{\underbrace{\left(\frac{\partial p}{\partial x}\right)^2 + \left(\frac{\partial p}{\partial y}\right)^2}_{\texttt{Enthalpy energy}} \ldots$$

$$\ldots + \underbrace{\frac{\partial p}{\partial x}\frac{\partial k_E}{\partial x} + \frac{\partial p}{\partial y}\frac{\partial k_E}{\partial y}}_{\texttt{Kinetic energy}} + \underbrace{\frac{\partial p}{\partial y}\frac{\partial}{\partial y}(-\rho_f g y)}_{\texttt{Gravitational energy}}\Bigg\} \ldots$$

$$\ldots + \underbrace{\frac{\partial^2 p}{\partial x^2} + \frac{\partial^2 p}{\partial y^2}}_{\texttt{Enthalpy energy}} + \underbrace{\frac{\partial^2 k_E}{\partial x^2} + \frac{\partial^2 k_E}{\partial y^2}}_{\texttt{Kinetic energy}} + \underbrace{\frac{\partial^2}{\partial y^2}(-\rho_f g y)}_{\texttt{Gravitational energy}}\Bigg], \quad (28)$$

where $k_E = 1/2\rho_f V^2$. The factors C_n and C_f represent a compressibility of the solid and fluid, respectively and are defined by,

$$C_n = \frac{1}{n}\frac{\partial n}{\partial p}, \quad C_f = \frac{1}{\rho_f}\frac{\partial \rho_f}{\partial p}. \quad (29)$$

The expression given in (28) is the governing equation that describes transient physical flow of fluid through porous cement. There are two unknown variables in the equation, the fluid pore pressure p and the fluid velocity V. For a known velocity field, (28) can be adopted to compute the pressure field. The technical explanation of boundary conditions related to the fluid pore pressure distribution are given in section D.3.2, and an analytical solution is entailed for the fluid velocity distribution, that is given in appendix section D.3.3.

The fluid filled annulus channel

The fluid filled annulus channel (**3.**) is located upstream of the cone, between the porous cement sheath and the expandable pipe. Development of the annulus channel section will allow determination of the pressure state throughout the channel, hence assessment of the load imposed on the expandable pipe. The annulus channel will drain fluid from the **1:** compressed cement sheath, and a portion from the **2:** porous cement sheath, visualized in figure 14. The annulus channel will be able to expand in size in radial (x-coordinate) and longitudinal (y-coordinate) direction. Expansion in radial direction is determined by the fluid pressure in the annulus channel, while expansion in longitudinal direction is determined by the evaluation of the hydraulic bond strength and interface stress in the cement sheath, discussed in section 3.3.1.4.

For a given annulus geometry $\Omega \in \{0 < x < w(y)\}|\{0 < y < H(t, p_e)\}$ [3] a Reynolds equation can be derived to approximate the fluid pressure

3 The annulus height is determined by evaluation of p_e, a pressure evaluation point that will be covered below in section 3.3.1.5.

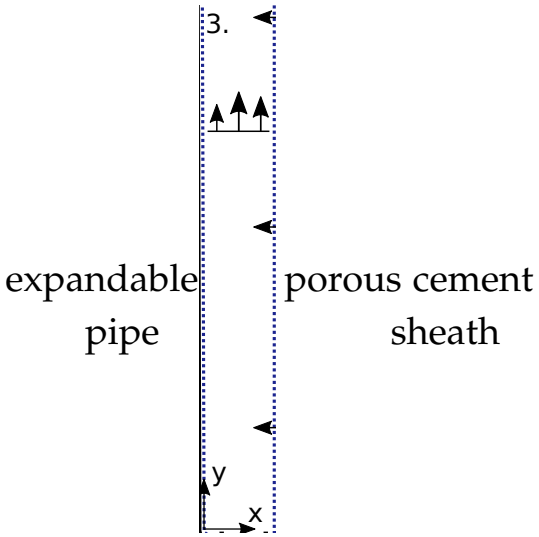

Figure 14: *A pre-existing fluid filled annulus channel between the interface of expandable pipe and* **2:** *porous cement sheath.*

in the channel. Here it is assumed that the initial width/height (w/H) of the channel is in a similar order $\sim O(1)$, and an additional creeping flow is considered $Re \sim O(1)$. The traditional Reynolds equation requires a solution for the velocity field $\vec{v} = \{u, v\}$, wherein the present case the flow direction is denoted by v (the longitudinal direction), whereas the velocity component perpendicular to the flow direction is denoted by u (the radial direction),

$$\frac{\partial u}{\partial x} + \frac{\partial v}{\partial y} = 0. \tag{30}$$

For the given assumptions it can be shown that the velocity field $\vec{v}$ can be approximated by Poisseulle flow approximations,

$$\frac{\partial p}{\partial x} = \mu \frac{\partial}{\partial x}\left(\frac{\partial u}{\partial x}\right), \quad \frac{\partial p}{\partial y} = \mu \frac{\partial}{\partial x}\left(\frac{\partial v}{\partial x}\right), \tag{31}$$

and is defined by,

$$\begin{aligned} &x = 0, && y: && u = u_b, && v = v_b, \\ &x = w(y), && y: && u = u_t(y), && v = v_t, \end{aligned} \tag{32}$$

where $u_t(y)$ is given in (122) and u_b, v_b and v_t are constants defined according to the compliance of the tube and migration speed of the cone, respectively. Solution of these velocity components for u and v, can be written as,

$$u(x,y) = \frac{1}{\mu}\left[\int_0^x p(x,y)dx - \left(\frac{x}{w}\right)\int_0^w p(x,y)dx\right] + \left[1 - \left(\frac{x}{w}\right)\right] u_b + \left(\frac{x}{w}\right) u_t(y), \tag{33}$$

$$v(x,y) = \frac{1}{\mu}\left[\int_0^x f_{p_y}(x,y)dx - \left(\frac{x}{w}\right)\int_0^w f^w_{p_y}(x,y)dx\right] + \left[1-\left(\frac{x}{w}\right)\right]v_b + \left(\frac{x}{w}\right)v_t, \quad (34)$$

where $f_{p_y}(x,y) = \int_0^x \left(\frac{\partial p}{\partial y}\right) dx$ and $f^w_{p_y}(x,y) = \int_0^w \left(\frac{\partial p}{\partial y}\right) dx$. Substitution of the velocity field into the continuity equation of (30) will lead to the Reynolds equation,

$$\begin{aligned} 0 = \frac{1}{\mu}\Bigg[& p(x,y) - \frac{1}{w}\int_0^w p(x,y)dx \\ & -\frac{1}{w}\int_0^w f^w_{p_y}(x,y)dx \cdot \frac{\partial x}{\partial y} - x\int_0^w f^w_{p_y}(x,y)dx \cdot \frac{\partial}{\partial y}\frac{1}{w} \\ & -\frac{x}{w}\frac{\partial}{\partial y}\int_0^w f^w_{p_y}(x,y)dx + \frac{\partial}{\partial y}\int_0^x f_{p_y}(x,y)dx\Bigg] \\ & + \left(\frac{1}{w}\frac{\partial x}{\partial y} + x\frac{\partial}{\partial y}\frac{1}{w}\right)(v_t - v_b) + \left(\frac{U_e(y) - u_b}{w}\right). \quad (35) \end{aligned}$$

The Reynolds equation describes the relation between the velocity field and the pressure distribution through a narrow channel. The Reynolds equation will be solved with a numerical solver to determine the approximate pressure field. This would allow a semi-analytical determination of the flow field with the equations (33) and (34). The technical details related to the boundary conditions are presented in appendix D.3.6.

Annulus width due to elastic formation

The Reynolds equation (35) will enable solution of the fluid pressure and the velocity field in the annulus channel for the conditions set in a specific time frame. However, evolution of radial expansion (x-coordinate) is not addressed thus far. In this section an approximation of the radial expansion of annulus width based on an elastic formation is given.

The fluid pressure $p(x,y)$ active in the annulus will exert a radial load on the (**2:**) porous cement sheath. The porous cement sheath will transmit the load in the form of an effective stress and fluid pore pressure towards the formation, pointed out in figure 15. The transmission of fluid pore pressure is referred to earlier in section 3.3.1.2, and the corresponding sections in the appendix. An effective stress for the solid phase in the cement sheath enclosed in between R_i and R_o is calculated with a plane strain analysis. The latter assumption will permit the effective radial- stress and displacement in the porous cement sheath to be expressed as follows,

$$\sigma_r = \frac{A}{R^2} + 2C, \quad u_r = \frac{1+\nu}{E_c}\left[-\frac{A}{R} + 2(1-2\nu)CR\right], \quad (36)$$

with the boundary conditions,

$$\sigma_r(R_i) = \sigma_{r,i}, \quad u_r(R_o) = u_{fo}, \quad (37)$$

where $\sigma_{r,i}$ is the imposed radial interface stress due to the fluid pressure active in the annulus. As the radial displacement at the outer interface u_{fo}

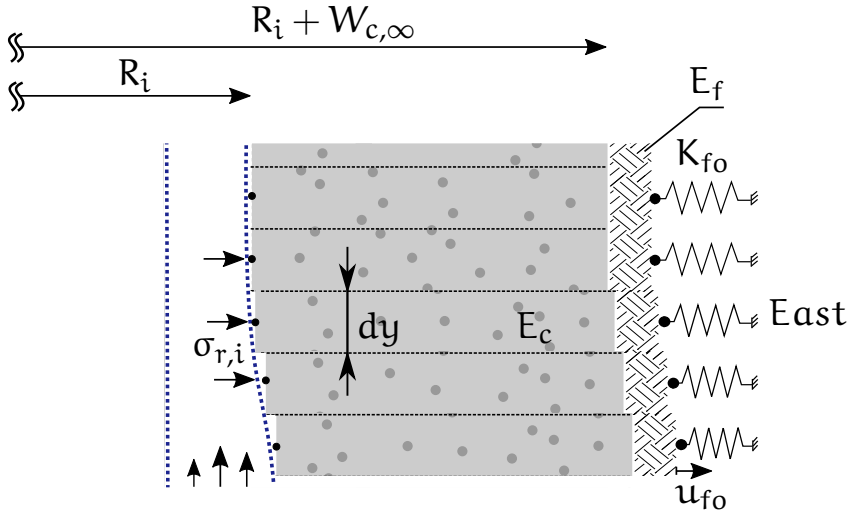

Figure 15: *The elastic formation will deform due to the fluid pressure within the annulus domain. The fluid pressure will impose a radial load on the cement sheath (E_c) that is transmitted with a stress equilibrium to the elastic formation (E_f). Deformation of the formation will result in an explicit expansion of the annulus domain.*

is an unknown, it is known that the cement sheath is in contact with the formation. There is a displacement continuity that will imply at the East interface $u_r(R_o) = u_{fo}$. To determine the solution an iterative picard solver is adopted similar to what is done in the earlier discussed section 3.2. The solution of equation (36) is presented in appendix D.3.7, where likewise the picard solution routine is given.

Radial and longitudinal expansion interaction

To complete the development of the annulus model, this section will treat the interaction of the individual discussed features. An overview of the individual discussed features is listed below;

- Compression of section **1:** the compressed cement sheath, positioned parallel to the cone, will result in fluid expulsion towards the porous cement sheath, and annulus channel.
- Ahead of the cone section **2:** the porous cement sheath, will utilize inflow of fluid from the compressed cement sheath to determine the fluid pore pressure, and will employ interaction of the parallel positioned formation and annulus channel to determine the total stress in the porous cement sheath.
- Parallel to the porous cement sheath is section **3:** the annulus channel, that will consume fluid from the compressed- and porous cement sheath to grow in radial- and longitudinal direction, interrelated to the fluid pressure throughout the channel.
- A linear elastic formation that is compliant due to the fluid pressure in the annulus channel, and interaction with the porous cement sheath.

The expansion routine of the annulus channel is performed in an algorithm, that will be explained in an example of three time steps in figure 16, and the developed algorithm given in 17. Incompressible fluid mass Δm is added to the annulus (step #1) each time step. For a known massflow Δm emanated from the compressed cement sheath, given in (23), the annulus will expand every second with,

$$\Delta V = \frac{\Delta m}{\rho_f} \quad [m^3/m]. \tag{38}$$

The quantity of mass that is added to the annulus channel (24), with a

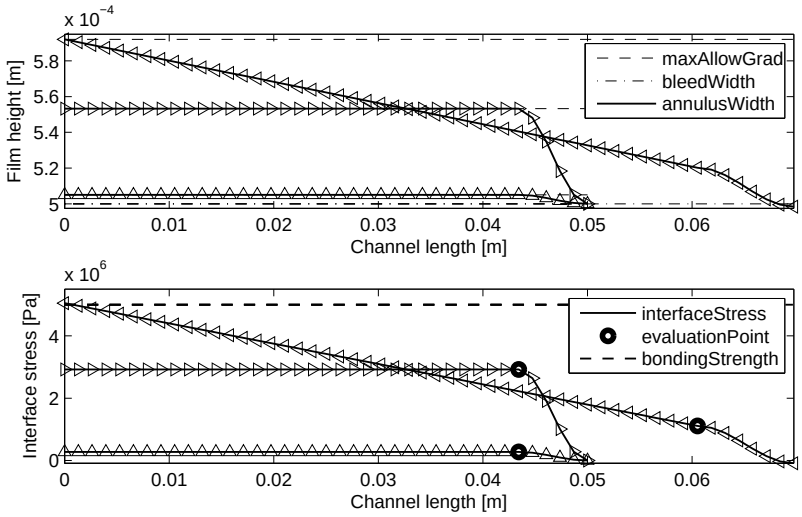

Figure 16: *The expansion routine of the annulus in radial and longitudinal direction for three different timesteps* $t = 1[\text{sec}]$, $t = 20[\text{sec}]$ *and* $t = 40[\text{sec}]$, *respectively denoted by* $\triangle$, $\triangleright$ *and* $\triangleleft$. *Note that initial time setting is* $t = 0[\text{sec}]$ *i.e., rectangular shaped channel. The dashed line in sub-figure (2,1) denotes a maximum allowable gradient determined by the initial pressure drop over the length of the channel. The dashed line in sub-figure (2,2) denotes the bonding strength* B_s, *that in this case is set to* $B_s = 5[\text{MPa}]$. *When the dot (•) exceeds the bonding strength, longitudinal expansion is consummated. The equivalent is said in the text when the evaluation pressure* (p_e) *surpasses the bonding strength.*

fluid bleed quantity, that is a percentage of the incoming mass set to leave the annulus, a necessary pressure drop (step #2) over the length of the channel is to be determined to enforce global fluid mass conservation. The difference of in- and outgoing mass will result in additional volume expansion, given in (38). The total mass present in the annulus constitutes the stored mass and the added mass each time(step), and will yield a corresponding volume. Throughout the sequence, the annulus width will attempt to adopt its shape according to the initial longitudinal pressure drop by means of a translation or inclination procedure (step #5a, b). The unknown annulus width is related to the volume with the following expression,

$$\Delta V = \int_0^H w(y)dy \quad [m^3/m], \tag{39}$$

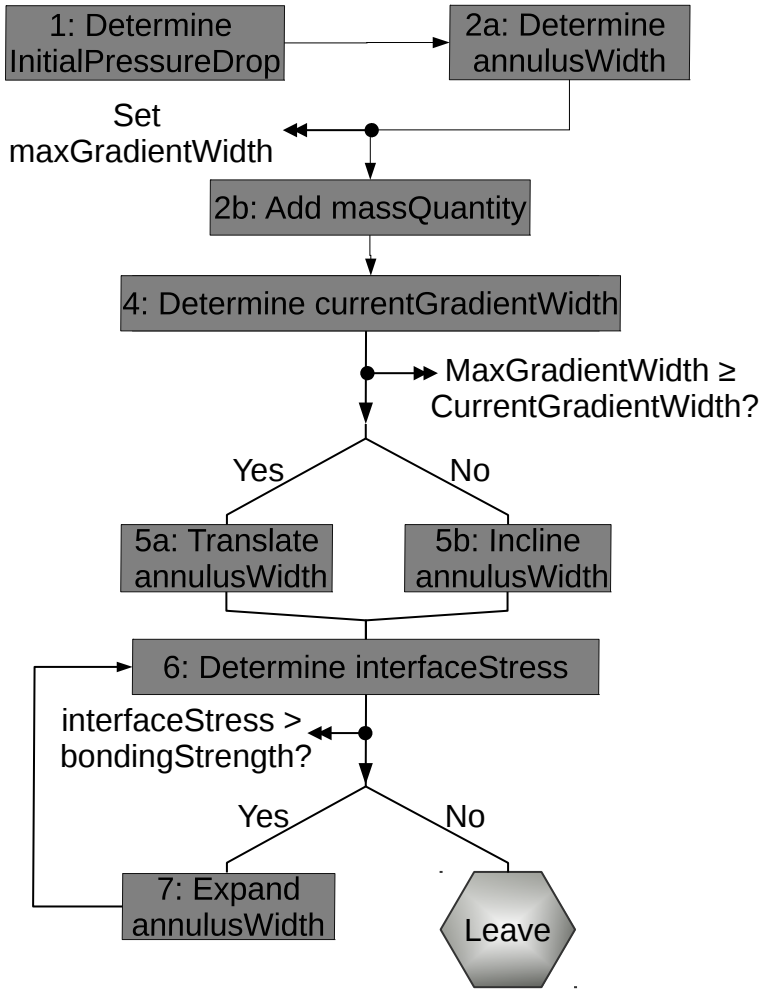

Figure 17: *The expansion routine of the annulus in radial (step #5) and longitudinal (step #7) direction for a single timestep. The routine is performed after the pressure distribution is computed in the annulus and cement domain.*

where $w(y)$ is the shape of the annulus width. At which point a *translation* procedure yields volume expansion with a constant annulus width gradient, and an *inclination* procedure yields volume expansion with a fixed inlet annulus width $w(y = 0) = const$. Once the interface stress at marked location (•) in figure 16, and determined earlier in (36), exceeded the hydraulic bond strength B_s, the annulus will be torn open and expand in longitudinal direction (step #7) until the added mass is accumulated and a new timestep is initiated.

3.3.2 *Annulus model analysis*

A numerical prediction model is developed and implemented to identify the effect of individual parameters that constitute and primarily determine the outcome of the expansion process. The model in the initial phase is

variable	name	unit	value
B_s	hydraulic bond strength	[Pa]	$5.0 \cdot 10^6$
E_c	elastic moduli cement	[Pa]	$1.0 \cdot 10^9$
E_f	elastic moduli formation	[Pa]	$210 \cdot 10^9$
e	compression ratio cement	[%]	30
H	height initial cement sheath	[m]	0.05
n	porosity cement sheath	[-]	0.2
p_o	reference pressure	[Pa]	$4.7 \cdot 10^7$
R_i	outer radius expandable pipe	[m]	0.2
v_c	velocity cone	[mm/min]	500
$W_{c,\infty}$	width cement sheath	[m]	0.02
w_o	width initial annulus	[m]	$5 \cdot 10^{-4}$
α_{ba}	liquid in annulus that bleeds off	[%]	10
α_{ca}	liquid through cement sheath	[%]	10
ρ_f	density fluid	[kg/m^3]	1000
μ_s	viscosity fluid	[Pa · s]	$8.9 \cdot 10^{-4}$
ν_c	poisson ratio cement	[-]	0.15

Table 2: *Standard operation conditions for the expansion process. The figures depicted in the section are obtained by means of these parameter settings, unless stated otherwise.*

split up in three branches; **1:** a compressed cement sheath part explained in section 3.3.1.1, a secondary **2:** porous cement sheath part explained in section 3.3.1.2, and a third part **3:** the fluid annulus channel 3.3.1.3. After a solution is attainable for each individual part, the respective branches are coupled and solved as an integral model. The integral model will interact linear elastic in time with the formation that surrounds the system, see section 3.3.1.4. The consequence of this interaction will result in radial and/or longitudinal expansion of the annulus channel, covered in section 3.3.1.5.

To identify the effect of individual parameters on the annulus growth over time, a basic configuration of the model is adopted from the literature and earlier performed experimental work that is shown in table 2. Simulations that are carried out use input values given in that table unless stated otherwise. For the given values, each time step, the flow- and pressure field is computed in both the fluid filled annulus channel, and porous cement sheath that got consummated due to the expelled fluid from the compressed cement sheath. A typical flow field in the annulus channel for the standard values of operation in the table, is elucidated in figure 18, for three time steps up to a simulation time of six minutes. Note that in that case the cone - with the defined cone movement speed - performed a total longitudinal displacement equal to 3.0[m] and where the tip of the

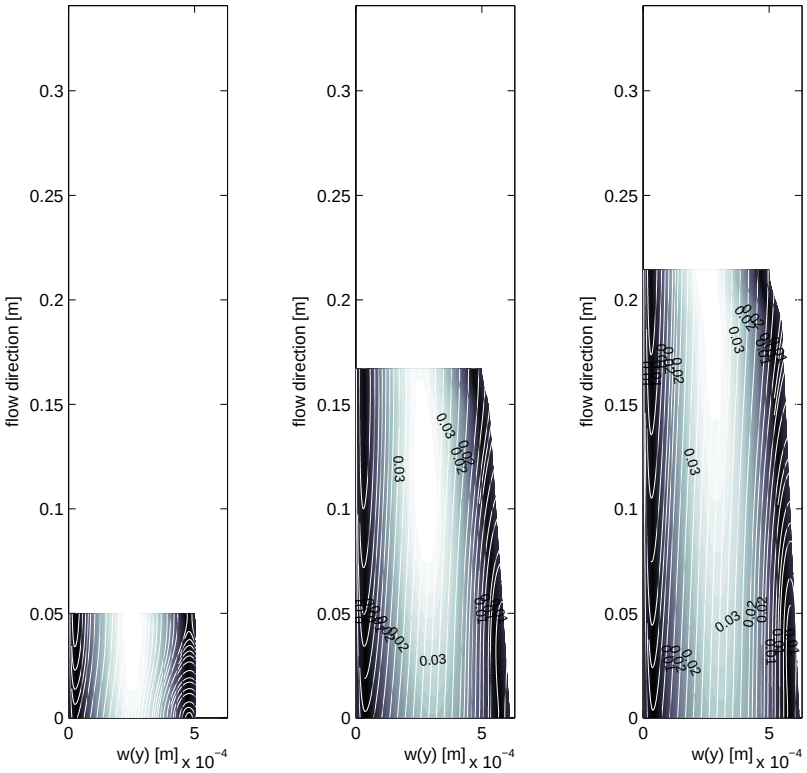

Figure 18: *An expansion flow field obtained with* (33), (34) *and* (35) *within the annulus domain depicted earlier in figure* 14. *Six different time steps have been shown, from l-r there is* $t = 1[sec]$, $t = 150[sec]$ *and* $t = 300[sec]$. *Parameter values adopted from table* 2.

annulus channel is approximately $22[cm]$ ahead of the cone. Inspection of the flow field in each subfigure will point out that backflow will occur at the East- and West boundaries. The backflow at these boundaries is the result of the collective unit (the three branched domains) to be synchronized with the movement of the cone, that will make the framework move as time evolves.

Modification of the standard values of operation for specific parameters will shed light on the effect of these parameters involved in the expansion process. The effect of the following parameters is studied; the hydraulic bond strength B_s, cone migration speed v_c, cement sheath thickness $W_{c,\infty}$, compression ratio cement e, and the elastic modulus of formation E_f, where the result is given in figure 19. Before evaluation of the parametric study, an additional quantifiable parameter is investigated, the amount of fluid mass that is expelled from the compressed cement sheath. The amount of fluid mass is a quantifiable parameter to be measured in the laboratory and is presented here for the performed numerical experiments of figure 19, and is given in table 3.

Parameter	Unit	serie 1	serie 2	serie 3
bonding strength	Pa	$5 \cdot 10^6$	$1 \cdot 10^7$	$5 \cdot 10^7$
mass expulsion	kg	6.3	16.6	16.5
cone migration speed	mm/min	250	500	750
mass expulsion	kg	3.7	6.9	10.1
cement thickness	m	0.01	0.02	0.03
mass expulsion	kg	6.9	7.0	7.0
cement sheath porosity	%	20	40	60
mass expulsion	kg	6.9	13.3	19.7
compression ratio	%	20	30	40
mass expulsion	kg	4.7	6.9	9.0
elastic moduli formation	Pa	$2 \cdot 10^9$	$25 \cdot 10^9$	$210 \cdot 10^9$
mass expulsion	kg	6.9	6.9	6.9

Table 3: *The amount of mass expulsion that originates from the compressed domain 3.3.1.1 for the numerical experiments performed in figure 19. This is a quantity that can be determined in the laboratory.*

Evaluation of the respective subfigures and the table will reveal that the hydraulic bond strength of the cement - shown in *subfigure A* - is for the performed numerical experiments the one property that potentially caused an expandable pipe failure. The interface stress in the cement layer for the case of $B_s = 5 \cdot 10^7 [Pa]$ exceeded the collapse strength of the expandable pipe. The accumulated fluid in the annulus channel could not have been sufficiently drained due to the hydraulic bond strength of the cement, that maintained a bond between the cement and the expandable pipe and thus suspended annulus expansion. The cement sheath porosity is investigated in *subfigure D* where it can be seen that a more porous structure will result in a more severe interface stress. The result came to be as a higher porous structure will contain more fluid per unit volume of cement that will issue more fluid per second to be expelled towards the annulus channel. Furthermore, *subfigure B* investigated the speed of cone migration, hence the expansion process and points out that a higher expansion speed will result in a higher interface stress.

The quantity of data provided in figure 19 and table 2 reveal that the numerical model is equipped with a versatile set of parameters that allow detailed investigation of the annulus growth and pressure generation. Moreover the data provided in figure 19 and table 3 permit the comparison with specific gathered experimental data as these variables are modifiable in the laboratory.

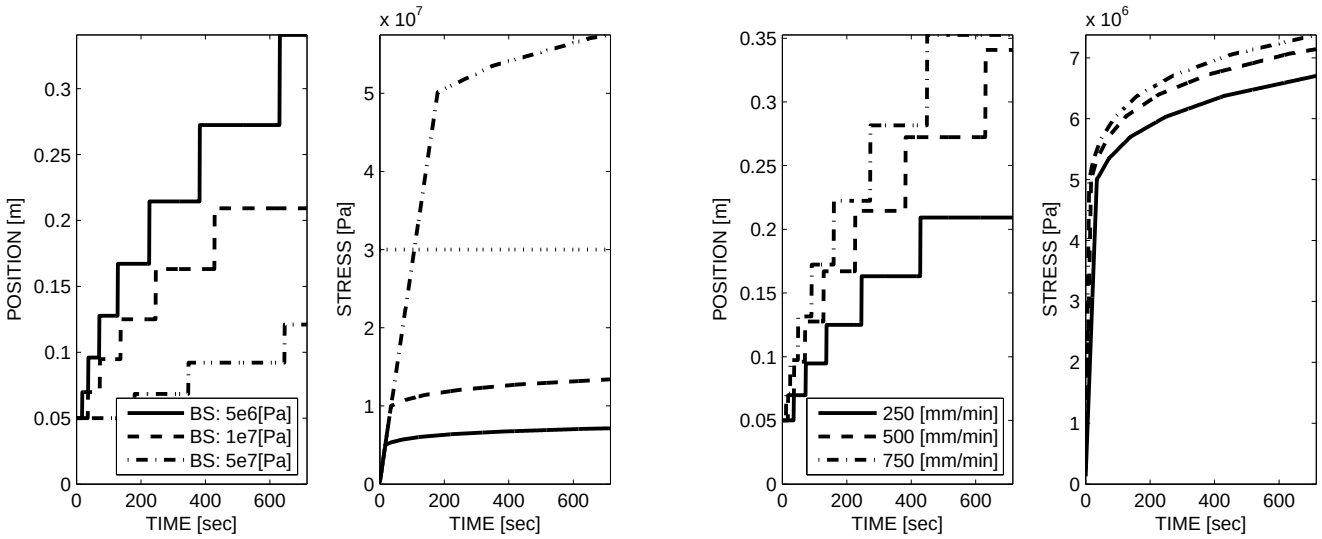

(A) Hydraulic bond strength (*w/* collapse strength VM50)

(B) Cone migration speed

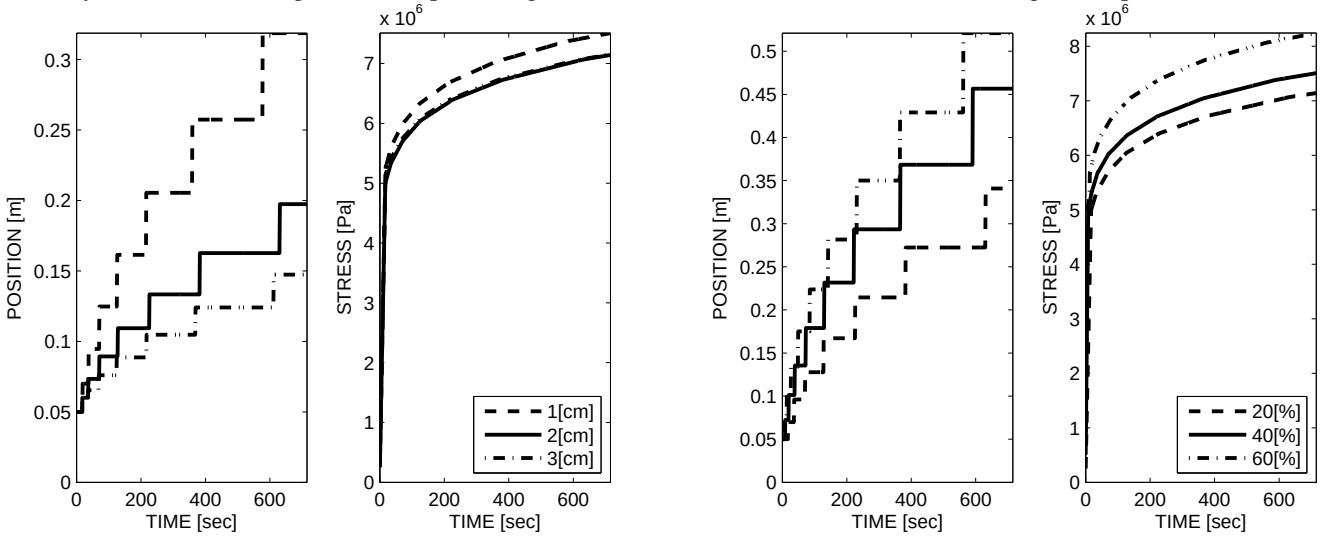

(C) Cement sheath thickness

(D) Cement sheath porosity

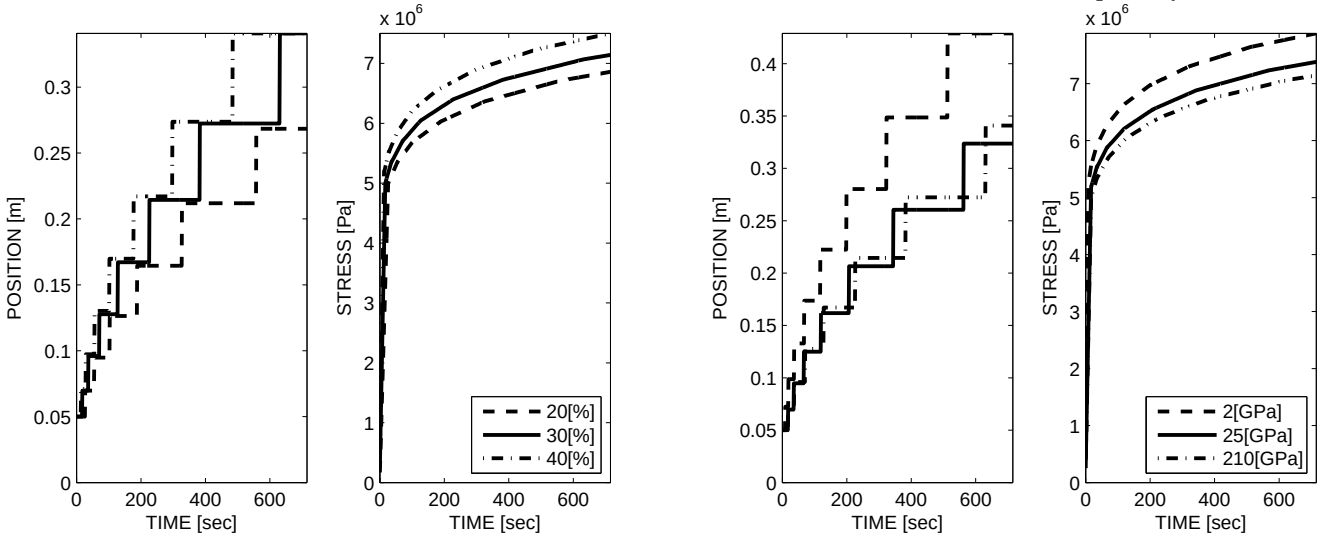

(E) Cement compression ratio

(F) Elastic moduli formation

Figure 19: *The identification of the effect for different parameter values involved in the expansion process. Shown is the wave tip length (left) and cement interface stress at* $y = 0$ *(right) of the annulus for three different values of the respective parameter, pointed out in the subcaption of the figure. The remainder of the parameter values are given in table 2.*

3.3.3 *Conclusion*

In this section a theoretical and numerical prediction tool was set up to investigate- and to identify the effect of individual parameters that are involved in the expansion process. The accumulation of fluid, in particular, is a time intensive feature embedded in the model that can unravel a potential pipe failure. The assumptions made to construct the model are summarized below;

- A two-dimensional axi-symmetrical system is assumed, this will allow evaluation of a radial slice in a Cartesian coordinate system.
- A continuum two phase flow is assumed where the cement structure is completely saturated with fluid, this will assume an openfoam structure where the pore structure is interconnected to one another.
- The fluid and solid phases both are incompressible, the implication is that compression of these phases result in a displacement of fluid.
- A two-dimensional plane strain analysis is assumed for the porous cement sheath. The implication is that the strain in longitudinal direction is disregarded that is similar to a hollow cylinder under internal pressure where the ends are fixed between immovable plates.
- Initial height/width ratio of the annulus channel is in the order of $\sim O(1)$, the implication is a pressure gradient in the flow direction and perpendicular to the flow direction.
- The flow in the annulus channel is assumed to be a creeping flow $Re \sim O(1)$, this will remove higher order velocity terms in the momentum conservation equation.
- An analytical velocity field is assumed within the cement sheath, this will result in a kinetic energy field that is to be used in the computation of the pore pressure in the cement sheath, although the contribution is only minor.
- An initial existing rectangular shaped fluid filled annulus channel is assumed, this will allow fluid from the compressed domain to be expelled towards an existing channel.
- The formation is assumed to be linear-elastic, this will couple linearly the stress and displacement that is to be used to expand the fluid filled annulus channel in radial direction.

In the numerical experiments performed it is found that the hydraulic bond strength of cement, that is confined in-between the expandable pipe and formation, is a decisive parameter in the expansion process. In regard to the given values of standard operation, a durable hydraulic bond strength is able to create a firm bond with the expandable pipe, that would suspend annulus expansion in longitudinal direction. It will force the accumulated fluid at the interface to inflate the annulus channel in radial

direction, that will invoke a growing radial inward strain on the pipe. The hydraulic bond strength of cement is influenced by the quality [4] and components in the mixture of cement. A second observation in the parametric study was related to the porosity of the cement, that is the quantity of fluid per unit volume in the porous cement. It was found that an increased fluid porosity would favor longitudinal annulus expansion. As each time step would carry additional fluid towards the annulus channel, while the fluid is assumed to be incompressible, the annulus channel would be forced to expand in size.

The purpose of the numerical model is to have a prediction tool that will aid in the design of an experimental setup. The parametric study in specific provided necessary information for the design of an experimental setup related to the hydraulic bond strength. Further assessment of the parametric study pointed out the relevance of the constitutive behavior of cement e.g., the porosity of the cement sheath, or capacity of the cement to withstand compression load. Information in regard to experimental design is introduced in more detail in the next chapter 4, where three different types of designs are discussed.

4 A high quality cement refers to the cement mixture that contains limited pollution of dirt and oil.

4

METHODOLOGY FOR EXPERIMENTAL DESIGN

In this chapter the methodology of the experimental design is discussed. Three experimental setups are initialized, developed and prepared. These are the hydraulic bond test, the cement deformation test and the small-scale expansion test. The hydraulic bond test is an experiment designed to quantify an essential system parameter involved in the expansion process. The cement deformation test is designed to determine constitutive behavior of cement paste and the small-scale expansion test is designed to investigate evolution of the fluid filled annulus channel in the expansion process.

Below each experiment is explained. The conceptual design will be presented where the required and paramount equipment is shown to perform the test. In the context of an individual experiment, tests have to be performed where a single parameter is changed with respect to the reference situation. Each section is completed with an overview of the total set of tests to be performed.

The hydraulic bond test is presented in section 4.1, the cement deformation test in section 4.2 and the small-scale expansion test in section 4.3. Moreover, at the end of the chapter, section 4.4, a summary is presented that considers the techno-economical feasibility and impact of the experimental design deliverables.

4.1 THE HYDRAULIC BOND TEST

The cone migration process in the monobore well will by expansion of the pipe compress the cement sheath. As the cement sheath at the time of expansion is in a fluid saturated state the compression of the cement will result in an escape of fluid from the porous matrix. In a close to impermeable cement sheath the vulnerable area where fluid might flow to is in an interface of expandable pipe and cement. The parameter that determines the growth of the annulus channel by fluid accumulation is the so-called hydraulic bond or *bond strength* between the expandable pipe and cement.

The hydraulic bond in question is a chemical bond between cement and the oil pipe. The bond is established after a chemical reaction between the dry additives of cement and water. Over time, the cement mixture will (1) settle, (2) solidify and (3) will adhere to the considered configuration i.e., formation and oil pipe. An established hydraulic bond will block the migration of fluids in a cemented area [9]. To the contrary, a broken bond - besides the natural characteristics of a porous medium - will allow an (un)desirable path of leakage for gases and liquids, see figure 20.

The hydraulic bond test, or bond strength test is necessary to investigate the adherence capacity of cement to an expandable pipe. In a concentric

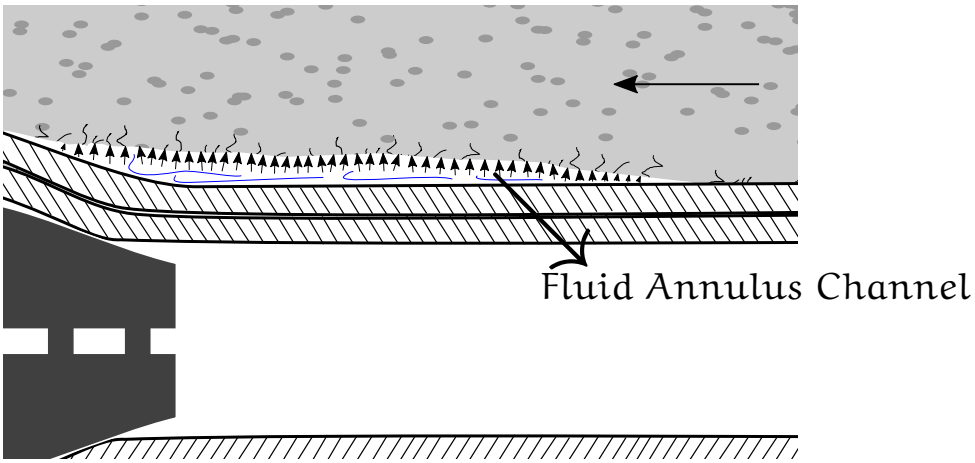

Figure 20: *The hydraulic bond strength is a parameter related to the adherence of cement to the oil pipe. The expansion process will add an additional strain to the existence of the hydraulic bond. In the present situation the hydraulic bond will break near the interface of the expandable pipe and the cement sheath. The result is a narrow opening where fluid will migrate to; the fluid filled annulus channel (↘).*

system that constitutes an expandable pipe, a formation or host pipe and a cement sheath in between, the cement adhesion is investigated in relation to the cement properties and pipe surface.

4.1.1 *Conceptual design*

Inspired by similar experiments from Carter *et al.* [9], this section will give a schematic overview of the hydraulic bond strength test. In addition, the framework for this experimental design is implemented with MSc. student Euving [17].

To evaluate the hydraulic bond the interface of the cement sheath and expandable pipe is put to the test. This is achieved by fluid pressurization of the cement sheath, whereas the position of the cement sheath with respect to the expandable- and host pipe is fixed. A schematic of the test setup is shown in figure 21. In clockwise motion, from the left bottom shown is, a fluid feed pump equipped with a return valve that will pressurize the cement sheath from the left. Along the length of the system strain gauges are attached to the inside of the expandable pipe. The left and right sides are closed of with flanges, while the flange on the right is opened up to ambient conditions. The pressure difference over the length of the cement sheath is the prescribed pressure on the left with the ambient pressure on the right.

A pressure difference over the length will result in fluid pushed out of the saturated cement sheath. At the stage where the hydraulic bond is in tact, one is able to couple the pressure drop to the outflow of fluid, which represents a system permeability. At some point when the pressure difference will become too severe for the system to withhold (depends on the configuration of the system), the hydraulic bond will be broken and a

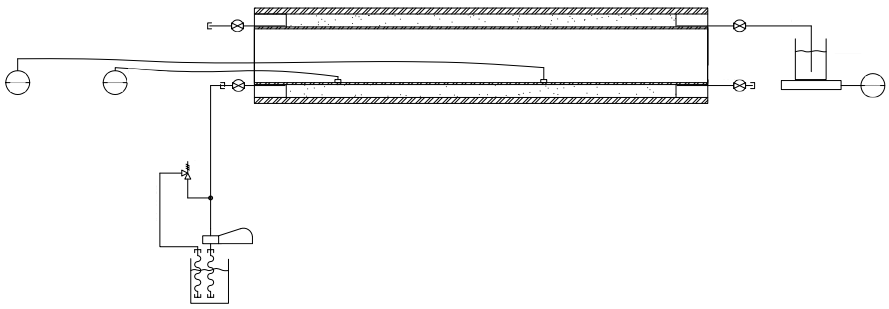

Figure 21: *A schematic of the hydraulic bond test. Shown is the core of the setup that constitutes an expandable pipe, host pipe and cement sheath in between. The cement sheath is pressurized by fluid with a pump from the left, and the emerged fluid is captured in a reservoir on the right.*

sudden increase of outflow of fluid will be measured. The crossing point of the two linear interpolations of the pre- and post permeability of the system will be the hydraulic bond, this will be illustrated in a later stage, chapter 5 figure 27.

The conceptual design consists of the following parts;

- An expandable pipe that is one of the test specimen, that is changed every experiment to investigate the effect of the compliance of the pipe on the bonding strength of the system.
- A host pipe for safety reasons is 15 [mm] thick that closes the complete tested system. It is expected that the over dimensionalization of the outer pipe will overestimate the bonding strength.
- A fluid feed pump that will pressurize the system with a liquid feed where the pressure is increased in intervals to increase the flow rate.
- Strain gauges along the length at the inside of the expandable pipe to map the effect of pressurization along longitudinal length of pipe and cement sheath.
- A cement layer between the inner and outer pipe that is 90 [mm] removed from either top-end of the respective pipes to limit boundary-effects of the both ends when the system is pressurized.
- A reservoir of fluid to squeeze through the cement sheath, and a collector vessel or leak tray to capture the outflow of fluid from the cement sheath.
- Top- and bottom flange to seal of the system, and rubber seal rings (o-ring) to block fluid flow in unwanted directions.

A workdrawing for the collective test unit, the expandable pipe, host pipe and the cement sheath in-between configuration with all required dimensions is presented in figure 33, in appendix A.

4.1.2 *Set-up*

In consideration of the conceptual design a total of 9 tests are formed that will allow determination of the hydraulic bond strength for different situations. Table 4 gives an overview of the scheduled experiments. Note that

test	inner pipe		outer pipe		expandable
	ID [mm]	WT [mm]	OD [mm]	WT [mm]	pipe
#1	112	2	188	15	water mud
#2	112	2	188	15	clean
#3	112	2	188	15	oil mud
#4	110	3	188	15	water mud
#5	110	3	188	15	clean
#6	110	3	188	15	oil mud
#7	108	4	188	15	water mud
#8	108	4	188	15	clean
#9	108	4	188	15	oil mud

Table 4: *Test overview of a total of 9 experiments. In test #2, #3, #8 and #9 strain gauges are present to estimate the deformation imposed on the inner pipe due to the presence of a fluid filled annulus in the cement layer. Variation in the different tests are related to the wall thickness of the expandable pipe, and the state of the cement where it is clean, polluted with water based mud, or polluted with oil based mud. The total length of the specimen is constant at* 480[mm] *and the length of the cement sheath is constant at* 300[mm].

in appendix A the test plan for the hydraulic bond is given as well as the technical drawings of the design and description of sample preparation. The appendix covers a description of the applicable cement, the cement additives and a specification of what is water/oil based mud or *polluted* cement.

4.2 THE CEMENT RADIAL DEFORMATION TEST

From the literature it appeared that the dynamic deformation or loading of cement paste is a topic still open to interpretation debate. The main differences occur in the type of load imposed, predominantly isotropic uniaxial, or triaxial load. The load rate imposed is for a certain duration of time in the range of the characteristic timescale of a Rayleigh wave through the specimen, or the duration of the hydration process of cement paste at room temperature.

Darwin *et al.* [12] investigated uniaxial compressed cement paste where the specimen prior to the test was fluid saturated, cubical and cuboid shaped and attained stress-strain curves for loads typically imposed in a timespan of two minutes. Similar to Darwin the research performed by Fischer *et al.* [18] investigated uniaxial compression of saturated cement paste, but for a cylindrical shaped specimen. High dynamic strain rates were imposed in the timescale order of Rayleigh waves through the cement paste specimen. The objective was to investigate the cement paste strength versus the imposed load rate. A conclusion of the research was that the increase of load duration would deteriorate the strength of the cement paste, that is to be considered for the cement deformation test. Ghabezloo *et al.* [20] performed triaxial compression tests on fluid saturated and cylindrical shaped cement paste specimens, where a typical test would take 40-50 hours. The intention of the investigation was to verify the validity of the theory of porous media. The conclusion was that the good compatibility and consistency of the obtained poromechanical parameters demonstrated that the behavior of the hardened cement paste can indeed be described within the framework of the theory of porous media, i.e., the theoretical foundation of the numerical analyses performed in section 3.1, 3.2 and 3.3. Zhang *et al.* [60] performed a numerical analysis of the dynamic cement paste deformation caused by hydration of a square shaped cube for the time duration of 1-7-28 days. The intention was to investigate the failure behavior due to fractures in the cement paste by cause of hydration and they adopted an energy propagation principle similar to the one described in section 3.2.

None of the investigations performed a dynamic deformation of cement paste in the context of the downhole expansion process; compression and shear load that result in double digits strain deformation (expansion ratio) appears to be thus far unexplored territory in the literature. It is desired to investigate a concentric fluid saturated cement sheath confined between an expandable and host pipe configuration that is radially expanded outward. Key points of interest for the investigation are;

1. the state of structural integrity of the cement sheath for different types of radial expansion,
2. the fluid porosity of the cement sheath before and after expansion,
3. the preferential flow direction of cement paste, fluid slurry or fluid expulsion and consequently quantify the expulsion.

4.2.1 *Conceptual design*

The following section will provide a conceptual design for the cement deformation test where the aim is to investigate the effect of the degree of cement sheath deformation while keeping in mind the key points of interest, mentioned in the previous paragraph. Furthermore, a more detailed overview is provided in appendix B with an additional scope of the test, material overview, vision and sample preparation.

In chapter 3, section 3.1 attention was given to investigate the radial direction of fluid transport across the cement sheath thickness in the expansion process. In section 3.2 the focus was on the failure behavior of the cement sheath and the study of the effect of explicit radial deformation of the confined cement sheath between expandable pipe and surrounding formation. The design for the cement deformation test must allow investigation of;

1. The state of structural integrity of the cement sheath for different types of radial expansion. Fischer *et al.* [18] concluded that the increase of the load rate duration would deteriorate the cement paste strength. The type of cement deformation is therefore dedicated to the degree of radial outward expansion, and the additional rate or speed of expansion. In the evaluation of micro-fractures in the cement structure, Darwin *et al.* [12] pointed out that these fractures have a typical surface density of 0.04 to 0.14 mm/mm^2 and can be observed with an optical microscope at magnifications below 50x, that is to be adopted for the present investigation.

2. The total fluid porosity of the cement sheath before and after expansion. One is able to determine the total fluid porosity by consideration of a fluid saturated, yet arbitrary volume chunk of the cement sheath, weigh it and vacuum oven dry the specimen in intervals until a constant weight is obtained [20]. This result will indicate that all fluid in the cement sheath internal structure has evaporated.

3. Determination of the preferential flow direction of cement paste, fluid slurry or fluid expulsion in expansion and consequently quantify the expulsion. In the numerical analysis performed in section 3.1 it was concluded that the fluid pressure gradient over the radial thickness of the cement sheath is defined positive. In consideration of Darcy's law (26), the consequence was for fluid to move towards the interior boundary of the domain, i.e., the expandable pipe which is to be confirmed in the cement deformation test and is to be quantified as a result.

These requirements have been assembled and are put together into a cement deformation test of which the conceptual design is shown in figure 22. Five major components of the test are shown, and numbered. The test specimen (1.) is a confined layer of cement paste between an expandable

and host pipe. The wedges (2.) are positioned on the bottom flange between test specimen and cone, and are sliced in vertical direction for a distributed radial uniform expansion of the test specimen. On the inside the wedges are oblique in the shape of the cone to make a fit, when the cone (5.) will move downwards. A thin top disc (3.) is shown to position the bolts together with drain/vent holes to determine the preferential direction of fluid (slurry) expulsion and to quantify the amount of expulsion. The last component, the thick bottom disc (4.), is required together with the top disc to position the test specimen, to absorb the exerted load from the cone, and to allow vertical displacement of the cone.

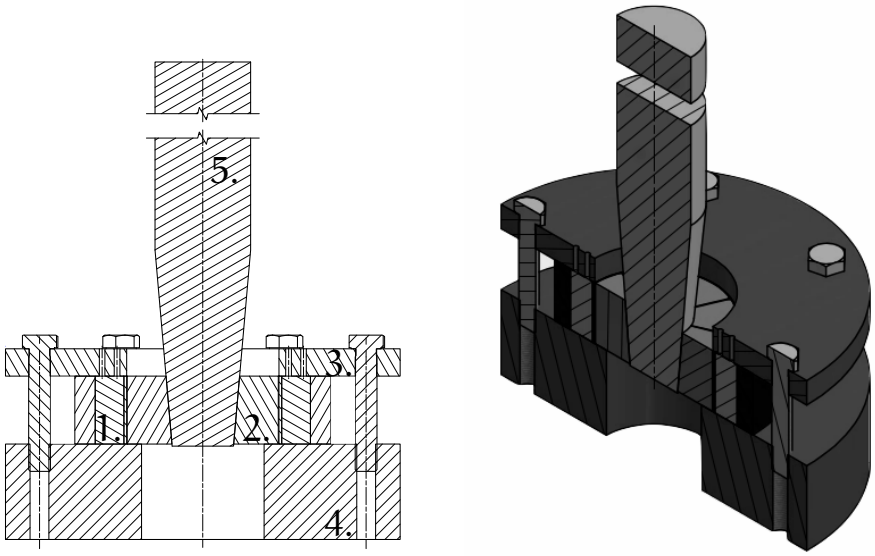

Figure 22: *An overview of the cement deformation test where l-r depicts a front view and an isometric view, respectively. Shown is a hardened cone (5.) with a degree of freedom in the vertical direction, a thinner- (3.) and thicker (4.) disc placed on the top and bottom, respectively. The test specimen (1.) is positioned in-between the top and bottom disc, and is expanded by the cone that is pushed downward towards the adjacent wedges (2.) that are radially pushed outward as a result.*

4.2.2 *Set-up*

A down-to-earth and feasible design approach is considered in the development of the conceptual design shown in figure 22. A ∅70 [mm] hardened cone is embedded in the design that is, at due time of this report, in the cement laboratory of Shell, Rijswijk and available for direct utilization. The test specimens are cut-up slices of length 50 [mm] from the aforementioned hydraulic bond strength test of section 4.1. Note that the test specimen are thus already present, that includes the expandable and host pipe, and the enclosed cured cement paste in-between, made according to

the cement manufacturers recipe. The test schedule overview is provided in table 5, where material dimensions are given, the estimated expansion force, the degree of expansion, the expansion ratio and the axial cone displacement speed per test are given.

test	inner pipe ID [mm]	cement sheath WT [mm]	outer pipe OD [mm]	WT [mm]	cone axial disp. [mm]	cone radial indent [mm]	expansion force [kN]	expansion ratio [%]	cone axial speed [mm/min]
#1	112	21	188	15	22.95	2	119	3.57	70
#2	112	21	188	15	45.90	4	170	7.14	70
#3	112	21	188	15	68.86	6	220	10.71	70
#4	112	21	188	15	22.95	2	119	3.57	140
#5	112	21	188	15	45.90	4	170	7.14	140
#6	112	21	188	15	22.95	2	119	3.57	70
#7	112	21	188	15	45.90	4	170	7.14	70
#8	112	21	188	15	22.95	2	119	3.57	140
#9	112	21	188	15	45.90	4	170	7.14	140
#10	112	21	188	15	68.86	6	220	10.71	140
#11	112	21	188	15	22.95	2	119	3.57	70
#12	112	21	188	15	45.90	4	170	7.14	70
#13	112	21	188	15	22.95	2	119	3.57	210
#14	112	21	188	15	45.90	4	170	7.14	210
#15	112	21	188	15	68.86	6	220	10.71	210

Table 5: *Test overview for the concentric cement deformation test. Three subdivisions are dedicated to clean cement, oil-mud polluted cement and water-mud polluted cement, respectively. Estimation of the expansion force is done by evaluation of section D.5. The test samples are manufactured from the aforementioned hydraulic bond strength test* #1, #2 *and* #3 *of table 4. System parameters; host pipe yield pressure* $= 58[\mathrm{MPa}]$*, host pipe diameter/WT ratio* $= 12.5[-]$*, cement paste compressive strength* $= 25[\mathrm{MPa}]$.

4.3 THE SMALL-SCALE EXPANSION TEST

The expansion process will result in a compression and shear load of the cement sheath. As the formation in the borehole is covered with a thin layer of near impermeable *mudcake*, similar to the near impermeable cement sheath, a complication will arise that is related to the expulsion of fluid due to the expansion process.

The cement sheath is a porous medium and compression load beyond the yield point will collapse the pore structure. For a saturated permeable porous matrix, collapse of the structure results in displacement of fluid. However, as the present cement sheath is near *im*permeable, compression of the porous structure would indeed collapse the pore structure but the fluid could still be entrapped. In that case with fluid and cement particles both incompressible, one may question the validity of the experimental observation in figure 6, where fluid did accumulate at the interface of cement sheath and expandable pipe. After all, in consideration of the analysis of section 3.1, the pressure gradient over the cement sheath thickness is defined positive outward, implying fluid to move inward towards the considered interface.

As mentioned above, in addition to the compression load imposed on the cement sheath, there will be an active shear load because of circumferential expansion. Shear load will establish a tension mode in the cement matrix. A cement matrix is to a high degree capable to withstand compression load [3], but has little shear load resistance against tension. As tension is most significant near the interface of the cement sheath and expandable pipe - contrary to cement sheath and formation - it is possible that the cement structure would fracture as a result near the interface. A fracture as discussed in section 3.2, is in terms of permeability an open channel that allows fluid to pass through significantly easier than the near impermeable porous structure. The situation is portrayed in figure 23.

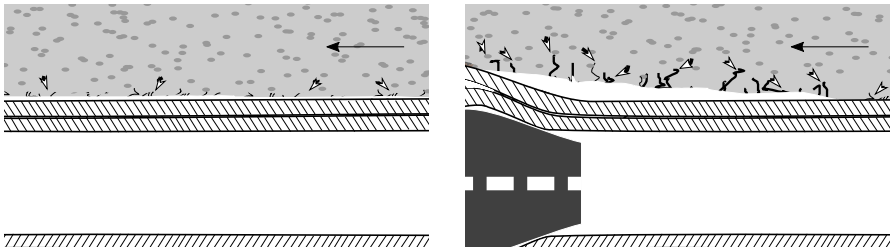

Figure 23: *An overview of the scenario that is regarded throughout the expansion process. Left: An undeformed cement sheath with the presence of an annulus gap at the interface due to natural shrinkage properties of cement [], the cement structure is intact with a limited amount of fractures. Right: Throughout the expansion process the cement sheath is compressed and sheared, that results in pore structure collapse and local near interface fracturing of the porous matrix, respectively. The consequence is that fluid is displaced from the interior of the cement to the interface with the pipe.*

To investigate if an annulus channel indeed manifest itself between the cement sheath and the expandable pipe, in the expansion process, the small-scale expansion test is commenced. Key here is to locate and quantify the amount of fluid accumulated throughout the process.

4.3.1 *Conceptual design*

The details of the small-scale expansion experiment and the test plan are in appendix C. The parametric study of section 3.3 pointed out the importance of five parameters in specific that require experimental investigation.

In view of the results of the parametric study the small-scale expansion test is to investigate the evolution of an annulus channel and map the influence of the following parameters,

a. a variation of yield pressure of the host pipe,

b. a variation of the expansion ratio of the expandable pipe,

c. a variation of the cement sheath thickness,

d. a variation of the cement mixture with respect to porosity,

e. a variation of artificial permeability in the top-flange.

These parameters are illustrated in figure 24. It is important to point out that when changes one parameter in the experimental setup an additional parameter unwillingly be affected too as a result. However, the design is set-up to minimize these effects, or when there is, a controlled one. Per parameter three variations are suggested.

The yield pressure of the host pipe (44) is set as a variable (a.) to evaluate the effect of the direction of cement displacement. The yield pressure of the host pipe is compared to the unconfined compression strength of cement. It is assumed that a yield pressure of the host pipe larger than the unconfined compression strength of cement will result in the cement to be crushed before the host pipe would start to yield. The consequence would be that the cement is pushed forward, in the length direction. A yield pressure lower than the unconfined compression strength that will push the cement radially outward, and is assumed not to happen in the downhole condition.

The size of the cone (b.) will determine the expansion ratio (43) of the expandable pipe. It will determine the degree of cement deformation, cement displacement and the amount of fluid to be expelled upwards for a given fluid porosity.

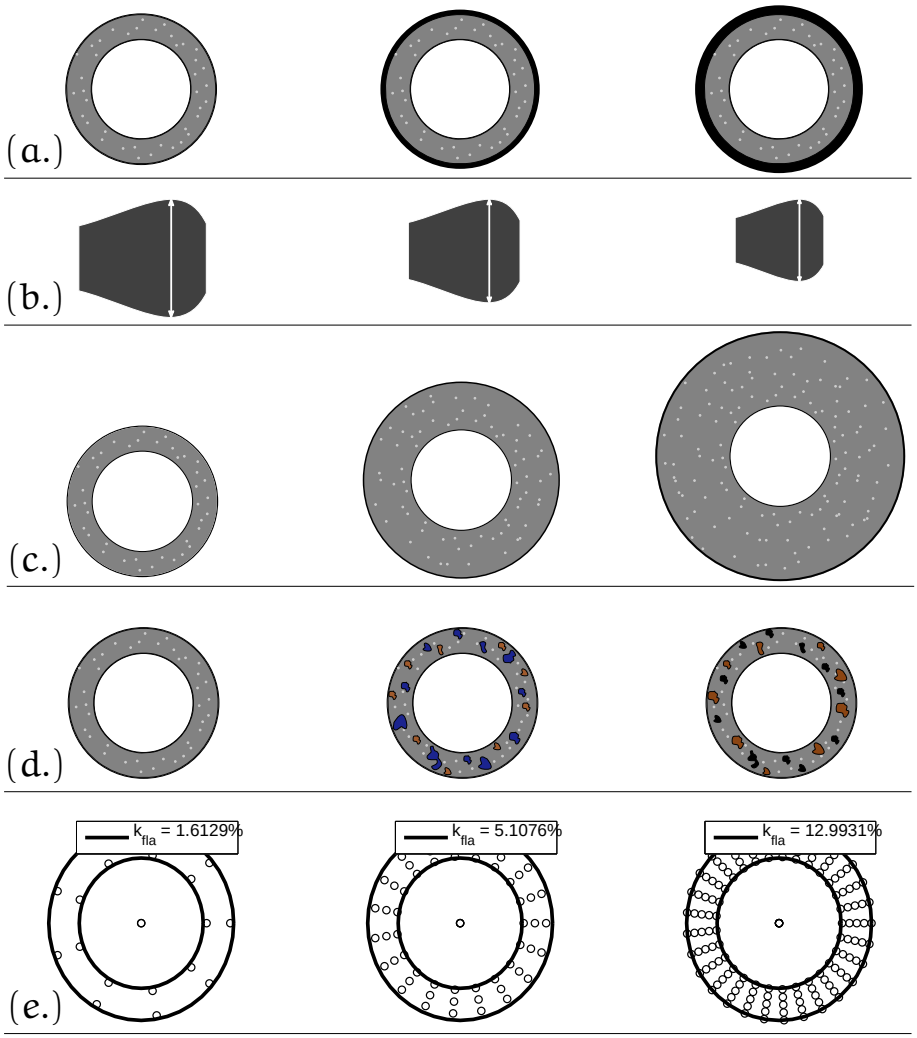

Figure 24: *An overview of the to be investigated parameters that follow from the parametric study of section 3.3 and showed to influence the imposed strain on the expandable pipe significantly. From top- to bottom there is (a.) variation of yield pressure for the host pipe or formation pipe, variation of (b.) the expansion ratio of expandable pipe, variation of (c.) the cement sheath thickness, variation of (d.) the cement mixture (clean/water-mud/oil-mud) and final (e.) the variation of artificial permeability of the top-flange.*

Variation of the cement sheath thickness (c.) will change the quantity of liquid present in the experiment. This will also effect the amount of fluid to be expelled upwards for a given porosity.

The cement mixture (d.) is varied to investigate the effect of porosity on the evolution of an annulus channel during the expansion process. However, as mentioned before, in this situation there will be a side-effect related to the bond strength of the cement to the expandable and to the host pipe. Therefore, the results of the bond strength experiment presented in section 5.1 are necessary to allow evaluation of the behavior for different cement mixtures.

The top-flange (e.) that will close of the system and confine the cement sheath, is perforated to simulate a limited amount of formation permeability. A permeability scales inversely proportional to the longitudinal pressure gradient (26). That is relevant for potential depressurization in the downhole oil well situation where cement permeability, formation permeability or required pressure gradient across the radial or longitudinal cement sheath can release accumulated fluid.

An assembly of the requirements for the design of a small-scale expansion test will result in the schematic overview shown in figure 25. Shown

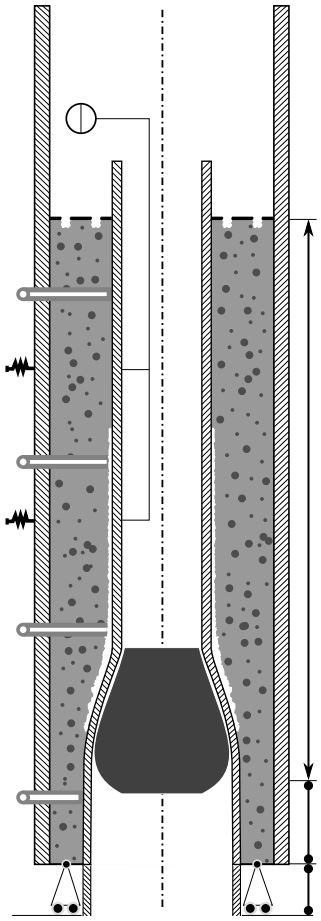

Figure 25: *A schematic of the small-scale expansion test. Shown is the core of the setup that constitutes an expandable pipe, host pipe and cement sheath in between. The cement sheath is pressurized by fluid with a pump from the left, and the emerged fluid is captured in a reservoir on the right.*

is a confined layer of cement between an expandable pipe and host pipe. The system, downscaled to 25% of the field trial is expanded with a cone. Through the host pipe holes are drilled that are equipped with fluid pressure sensors to measure the fluid stress in the cement sheath. On the inside, strain-gauges are attached to the expandable pipe to capture the position of the forming annulus channel. In addition, on the opposite side, in the host pipe and in between fluid pressure sensors, the radial displacement of the host pipe is measured. That will provide information about the stress state of the host pipe and an estimation of the cement stress state. The

system is equipped with a bottom- and a top-flange, where the bottom flange is only mounted and welded after an initial expansion to close of the system and obtain a fixed-fixed position from bottom and top. The latter will limit expandable or host pipe elongation similar to the field situation where a bottom and top hole anchors are employed prior to expansion and moreover will make it comparable to the former performed experimental work the *small-cab test* [24].

4.3.2 *Set-up*

For the design of the small-scale expansion test a standard 25% down-scaled hardened 63.5[mm] cone is considered [24]. Pipe dimensions that are selected are standard size expandables, available from a production line [46]. The host pipe diameter over thickness ratio (D/t) is mimicked and respected as much as possible from the full scale experimental setup [57]. As for the type of cement, additives and type of pollution/impure cement is defined and given in appendix A. Finally, table 6 gives the planned test overview where configuration #2 serves as a reference case.

test	ID_{hos}[mm]	OD_{hos}[mm]	wt_{hos} [mm]	$(D/t)_{hos}$	wt_{cem}[mm]	OD_{cone}[mm]	α_{cone} [%]	k_{fla} [%]	sample	F [kN]
#1	90	94.5	2.25	42.0	14.85	63.5	16.5	1.6	pure	135[kN]
#2	**90**	**99**	**4.5**	**22.0**	**14.85**	**63.5**	**16.5**	**1.6**	**pure**	**149**[kN]
#3	90	102.6	6.3	16.3	14.85	63.5	16.5	1.6	pure	162[kN]
#4	90	110.0	10	11.0	14.85	63.5	16.5	1.6	pure	188[kN]
#5	90	94.5	2.25	42.0	14.85	63.5	16.5	1.6	impure	122[kN]
#6	90	99.0	4.5	22.0	14.85	63.5	16.5	1.6	impure	135[kN]
#7	90	102.6	6.3	16.3	14.85	63.5	16.5	1.6	impure	147[kN]
#8	90	110.0	10	11.0	14.85	63.5	16.5	1.6	impure	171[kN]
#9	90	99.0	4.5	22.0	14.85	63.5	16.5	5.1	pure	NA
#10	90	99.0	4.5	22.0	14.85	63.5	16.5	13.0	pure	NA
#11	90	99.0	4.5	22.0	14.85	64.5	18.3	1.6	pure	157[kN]
#12	90	99.0	4.5	22.0	14.85	65.5	20.2	1.6	pure	164[kN]
#13	98	107	4.5	23.8	18.85	63.5	16.5	1.6	pure	126[kN]
#14	106	115	4.5	25.6	22.85	63.5	16.5	1.6	pure	108[kN]
#15	90	99	4.5	22.0	14.85	63.5	0	1.6	pre-perm	NA
#16	90	99	4.5	22.0	10.35	63.5	0	1.6	post-perm	NA
number	host pipe	host pipe	host pipe	ratio	cement layer	cone	cone	flange	cement	force (fig 36)

Table 6: *Test overview of the experiments. The diameter/thickness ratio (D/t) of the host pipe in the full scale setup is* 22.1*, the aim is to get similar conditions in the downscaled setup. Assumed is constant expandable pipe dimensions, given in appendix C. Presented in red is the variable that is to be investigated in the experiment. The expansion force is estimated with a numerical computation D.5. The experiment written in* ***bold*** *letters, experiment* #2*, is the reference case. Experiment* #15 *and* #16 *are no expansion tests, though permeability tests where one side is pressurized to consequentially measure leakage of fluid running through the cement specimen, see section 5.1 for more details on permeability measurements.*

4.4 DESIGN DELIVERABLES

4.4.1 *Prototype description*

1. HYDRAULIC BOND STRENGTH TEST:

   Design and realization of an experimental setup to investigate the adhesive strength of cement to metal in a concentric expandable and host pipe configuration with the confined cement in-between. The experiment is set-up for different expandable pipe wall thicknesses and clean cement, or water-mud or oil-mud cement.

2. CEMENT RADIAL DEFORMATION TEST:

   Design of an experimental setup to investigate the constitutive behavior of fluid saturated cement in between an expandable and host pipe configuration that is expanded in pure radial direction. A cut-up slab of confined cement from the hydraulic bond strength test is considered that is expanded to different- degrees and distinct cone displacement speeds.

3. SMALL-SCALE EXPANSION TEST:

   Design of an experimental setup to investigate the development and evolution of the annulus channel or formation of the traveled pressure wave that will manifest itself between the cement sheath and the expandable pipe, and the fluid (pressure) accumulation that will induce severe strain in radial inward direction of the expandable pipe. The experiment is designed for five different system parameters that originate from the parametric study performed in section 3.3.

4.4.2 *Techno-economic feasibility*

In this subsection the impact of the to be developed technology is considered and is related to the potential economic gain for the petroleum company. It is pointed out that this subsection is speculation, and the arguments or discussed outcomes are questionable.

The primary goal, or desire, of the petroleum company, is to secure the structural integrity of the foundation, that is the cement layer in between the expandable pipe and the formation. Attainment of the former will reduce the possibility of undesired external oil or gas leakage, and potential oilwell blowout due to accumulated leakage. The downhole expansion process will introduce additional compression and shear strain on the cement sheath, that may compared to established technology involve risk factors for the structural integrity of the cement sheath which need to be controlled.

The primary need of the petroleum company is to investigate the ramification effect of the downhole expansion process and the consequences for the cement sheath. The notion of the techno-economic feasibility of the

monobore well technology boils down to the competitiveness of the technology in terms of benefits. The notion is twofold where on the credit side are the expenses already made, and are going to be made by the research and development disciplinary field in the future to achieve the primary goal. While on the debit side that should exceed the made expenses on the credit side is the potential financial gain of the developed technology that will allow access to new oil fields that once were unreachable and now are open for exploration.

At this stage, and in sole consideration of the structural foundation, or cement sheath, the petroleum company can go into a multitude of directions to develop the monobore well technology further, though a single direction will be discussed below. Consider for the time being a general overview, of the downhole expansion process and the repercussions it holds for the cement sheath with in specific different type of parameters that are involved. A combined compression and shear load of the cement sheath with double digits expansion ratios will yield among others; (non-)linear elastic/plastic behavior, a potential fractured cement structure with non-continuum mechanics, and moreover solid and fluid particle interaction in a near impermeable porous medium where even the strain rate will affect the behavior of the cement sheath. To explain the behavior of a detailed appearance in the problem as a whole is an interconnected parametric problem, where a single system parameter is related to a potential second, third and ℕ'th parameter. Division of the expansion process as a whole is thus a prerequisite to tackle individual involved phenomena. The hydraulic bond strength test, the cement radial deformation test and the small-scale expansion test (downscaled geometric to 25% of in-field) emerged as a necessity to investigate the problem as a whole. To carry out the former individual experiments and fine-tune the numerical models developed in this report, sufficient knowledge is- and can be obtained to feed and contribute to- and improve the original design of the monobore well and the involved repercussions of the downhole expansion process.

4.4.3 *Impact*

In extension of the previous section the impact of successful techno-economic implementation and realization will introduce the next generation oilwells that can reach larger target depths with a smaller surface footprint. Thorough analyses of the repercussions in the cement sheath due to the downhole expansion process will provide a wide range of perspectives to consider, where one can limit the emergence of a potential blow out and other safety hazards. An important factor here is the hydraulic strength bond of cement. Determination of the adhesive strength of cement to the expandable pipe for different circumstances will contribute to an economical, safe and stable production of a reservoir [43]. Despite the fact that more information would be acquired with respect to the hydraulic bond strength of cement, leakage throughout some areas along the longitudinal length of the well is not uncommon and thus erosion would be a phenomena

that is to be considered too. Moreover, production of oil in the well will result in wear of the cement bond to expandable pipe over time. Hence to perform predictive and preventative maintenance on the oilwell is a necessity. For a typical oilwell in the Gulf of Mexico, US, the production is about 50.000 barrels of oil equivalent per day at peak production [53]. A typical maintenance procedure - sonic or ultrasonic probe logging - would require per probe per well about a day to extract the necessary data [39]. To stop production due to maintenance is thus a rigorous situation that is to be scheduled accurately according to preventative and predictive maintenance measures.

The theoretical and numerical models and the designs for experimental setups done in this project aim to provide tools that contribute to safety, and control.

5 EXPERIMENTS AND EVALUATION

In this section the results of the hydraulic bond strength test are presented and discussed. The experiment of the hydraulic bond strength, is a test where one pressurizes with fluid the cement sheath in between the expandable and host pipe up to an extent where the cement sheath concedes. At that point the cement sheath has failed, the fluid that surges through the pores of the cement sheath will now in addition allow fluid to flow through the fractures of the cement sheath. The result is a measurable increase in fluid flow and thus a identifiable hydraulic bond pressure.

Section 5.1 will present the observations made at hindsight. Extension to the general observations are made in section 5.1.1, where parameters are introduced that describe fundamental flow behavior through the confined cement sheath. A generic occurrence throughout the nine performed measurements was an unstable flow path, in section 5.1.2 a possible explanation will be projected.

5.1 OBSERVATIONS IN HYDRAULIC BOND TEST

Incremental increase of fluid pressure will result in an incremental increase of fluid to be squeezed through the cement sheath, a typical result for this development is shown in figure 26. The pressure profile in time will adopt stepwise the shape of a staircase due to the maintained stabilization sequence that will allow fluid to find a way through the porous medium. Due to the near impermeability of the cement, this is a slow process. An additional observation can be made in the figure, after a time-frame of about 4 hours. Though the pressure increment attained a stable value, the flow path is deemed to reveal unstable behavior. Despite a second pressure increment, after the former time-frame observation, the flow path cannot stabilize without support. A possible explanation for this behavior is bestowed in section 5.1.2, for now it appeared that a pressure reset to a null value would restabilize the flow path. Figure 27 shows the fluid pressure and the fluid flow through the cement sheath. The change of slope is the position of the hydraulic bond strength. Two asymptotes are visible in the figure at approximately a pressure drop of 45- and 115 [bar/m]. For a cement sheath with a length of 30 [cm] that will result in a bond strength of roughly 15- and 34 [bar]. To surpass the threshold value of the hydraulic bond, one will tear open a pathway for fluid to flow through, the potential annulus at the interface of expandable pipe and cement sheath.

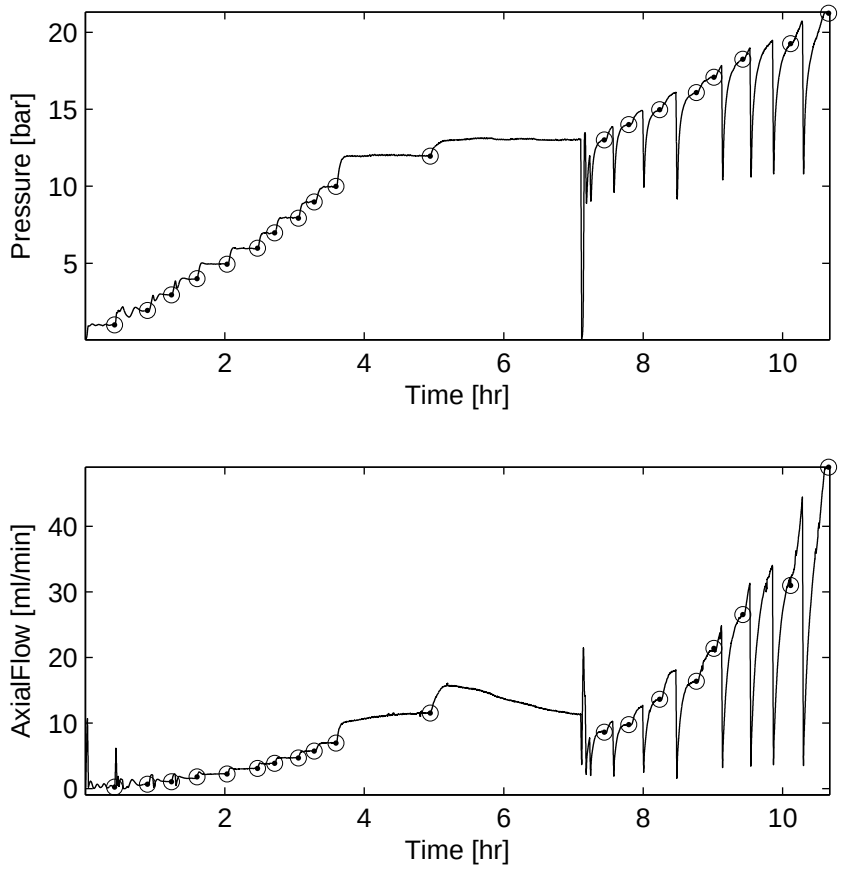

Figure 26: *An imposed incremental increase of fluid pressure to investigate the point where the bond between the cement sheath and expandable pipe initiates a failure, observed with a sudden increase in fluid flow through the cement sheath. Data points belong to test #2 from table 9.*

5.1.1 *Parameters in the bond strength test*

For a given fluid - in the present case water at room temperature - one is able to estimate the system permeability k that is related to the cement sheath. In consideration of the former mentioned Darcy flux q (26) the permeability is,

$$k = -\frac{q\mu}{dp/dn} \quad [m^2], \tag{40}$$

where q is the Darcy flux in [m/s], μ is the dynamic viscosity in [Pa·s] and dp/dn is the pressure drop over the longitudinal length of the cement sheath in [Pa/m].

With the estimated permeability the friction factor in a porous medium can be determined. It can be expressed in terms of the permeability and the pressure drop [5],

$$f = \frac{-\left(\frac{dp}{dn}\right) k^{1/2}}{\rho q^2} \quad [-]. \tag{41}$$

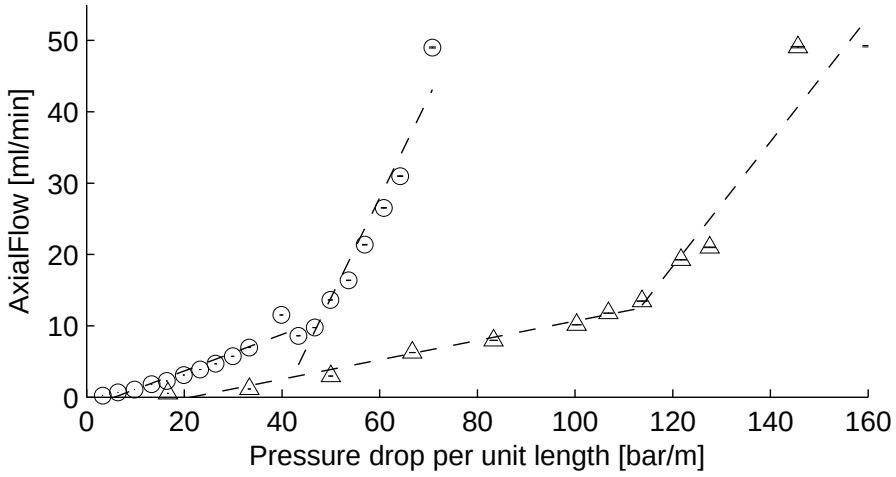

Figure 27: *Data points belong to test #2 marked by circles (⊙) and test #8 marked by triangles (△) from figure 9. The difference between the shown tests is the thickness of the expandable pipe, and is 2 and 4 [mm], respectively. The asymptote is approximately the hydraulic bond strength of the system [9].*

The friction factor can be expressed in terms of the dimensionless Reynolds number Re for a porous media, where $Re = \rho q k^{1/2}/\mu$, when the Darcy flux (40) is substituted in (41) to eliminate the pressure gradient. The result is a friction factor inversely proportional to the Reynolds number $f = 1/Re$.

An overview of the considered parameters, the hydraulic bond strength, the pre- and post; permeability, friction factor and porous Reynolds number for the nine performed tests is presented in table 7. The attained param-

test	B_s [bar]	k^{pre} [mD]	k^{post} [mD]	$(f^{pre}/f^{post}) \cdot 10^6$	$(Re^{pre}/Re^{post}) \cdot 10^{-9}$
#1	16.20	5.04	30.68	40/7	25/146
#2	11.96	3.36	27.91	118/7	8/139
#3	18.31	4.84	18.40	45/9	22/113
#4	28.10	3.74	48.83	43/6	23/183
#5	NA	NA	NA	NA	NA
#6	19.07	5.17	20.69	39/11	26/93
#7	28.03	1.74	NA	99/NA	10/NA
#8	32.05	2.17	16.46	94/9	11/107
#9	19.26	4.94	11.40	49/11	20/89

Table 7: *An overview of the extracted parameters of the hydraulic bond strength test results. From left- to right the following parameters are provided; bond strength B_s, the pre-permeability k^{pre}, the post-permeability k^{post}, the ratio of pre/post friction factor f and the ratio of the pre/post Reynolds number for porous media Re. Note that the permeability is given in mDarcy [mD] where $1D = 1 \cdot 10e-12[m^2]$. The cement sheath in test #7 collapsed such that pressurization was no longer possible, secondary parameters are therefor ignored.*

eters, and in specific the spread of the hydraulic bond strength parameter from the experiment, emphasize the predicament to model the present case study. A reference back to the numerical annulus model, the paramet-

ric analysis performed in section 3.3, figure 19(A) showed the effect of a variation in hydraulic bond strength. In table 7 it is apparent that addition of oil-mud to a clean cement sample for identical expandable pipe wall thickness can change the bond strength value up to 70[%]. This clearly shows the importance of knowing the cement composition downhole at the time of expansion.

5.1.2 *Analysis of the expandable pipe deformation*

In this section the unstable flow path observed in figure 26 is contemplated and an explanation is projected. To demonstrate the unstable scrutinized flow path, the data of the mounted strain gauges had to be utilized. Reason for that is the possibility of expandable pipe compliance to have an affect on the hydraulic bond strength test. The bond strength is an inherent property of cement if, and only if poured in an encapsulated and infinitely rigid system [9]. The expandable pipe, and even the over-dimensionalized wall of the host pipe both are still flexible. The consequence is an over-

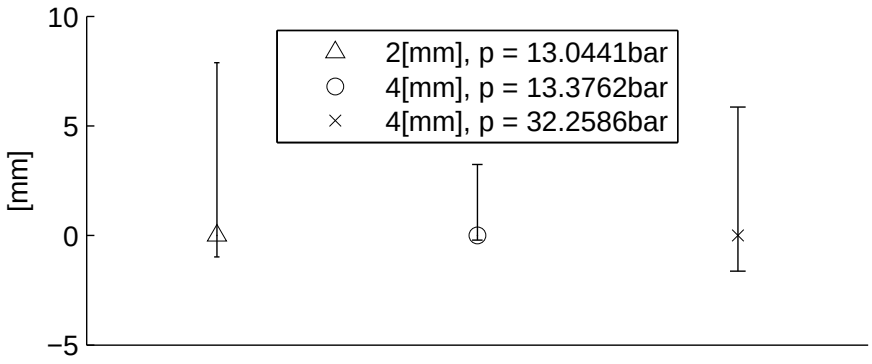

Figure 28: *The maximum and minimum radial displacement of the expandable pipe with clean cement under the assumption of an axisymmetrical system. Compression is positive, expansion negative, the symbols show the reference state. Shown from l-r is the 2[mm] pipe at its respective bond strength pressure rate* (△)*, the 4 [mm] pipe at the same pressure rate* (⊙) *and the 4 [mm] pipe at its respective bond strength pressure rate* (×)*.*

estimation of the hydraulic bond as the fluid pressure - imposed by the pump - in between the expandable and host pipe will expand the clearance area and create a flow path. In an attempt to correlate the compliance of the expandable pipe and the bond strength, strain measurements have been performed on the inside of the respective pipe. Figure 28 shows two successful strain measurements that are expressed in terms of radial displacement for an assumed axi-symmetrical deformation. The figure shows the minimum and maximum measured radial displacement, where compression is positive- and expansion is negative. The two measurements are the oil-mud covered 2[mm] and 4[mm] expandable pipe. Note that the figure gives three intervals, the left- (△) and right (×) give the state of radial displacement at the estimated hydraulic bond of the 2[mm] and

4[mm] oil-mud smeared expandable pipe, respectively. The central ($\odot$) interval represents the state of radial displacement for the 4[mm] oil-mud smeared expandable pipe at the hydraulic bond rate of the 2[mm] expandable pipe. The maximum compression (positive radial displacement) is observed near the entrance, whereas maximum expansion (negative radial displacement) is observed in the mid-section, see also figure 21 for the entrance and mid-section position of the strain gauges along the length of the expandable pipe. Figure 28 shows the observation of both pipe compression and non-intuitive pipe expansion for a compression load.

To display the former observation, the deformation of the pipe is visualized with a cross-sectional overview of the hydraulic bond test, in figure

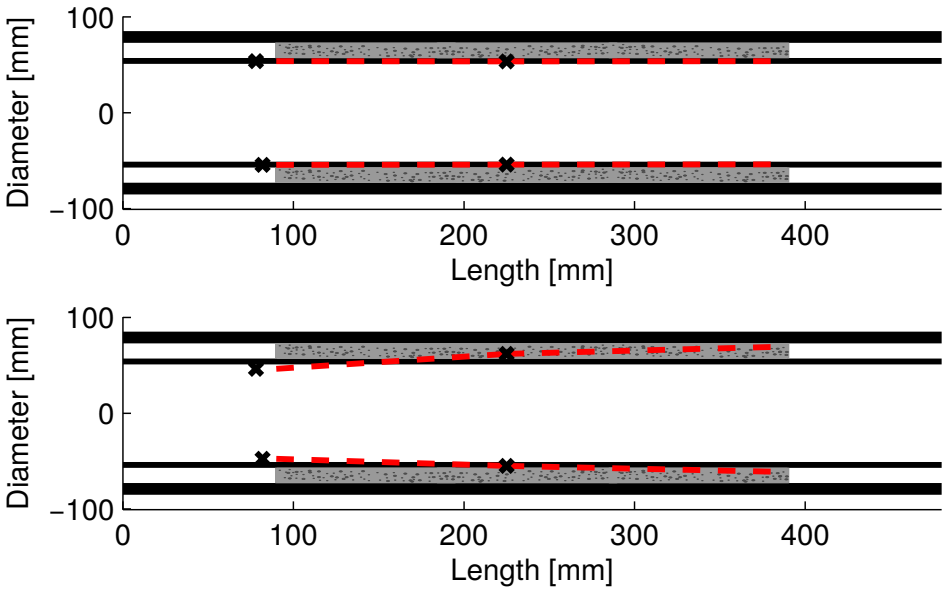

Figure 29: *A schematic view of the longitudinal cross-section of the hydraulic bond test with the additional result of the strain gauges. The radial deformation due to measured circumferential strain under the assumption of axi-symmetrical deformation. Top- and bottom are two time intervals at* $t = 0[hr]$ *and* $t = 7[hr]$ *time-frame interval. Position of strain gauges are depicted with* ($\times$) *symbols. The feed pump is to pressurize the left side, such that fluid will emerge on the right side. The dashed red-line is between the strain-gauges an interpolation, while from the middle strain gauge to the right-end is an illustrative extrapolation, provided for informative purposes only. Shown deformation path is for test #2 from table 7.*

29. Two time frames are given for $t = 0[hr]$ and $t = 7[hr]$ for top- and bottom, respectively. Shown is a thick host pipe with a thin expandable pipe and the gray cement layer in-between, the left and right white area is dedicated space for the flanges. At the inlet of pressurized fluid it is observed that compression of the expandable pipe will lead to radial inward displacement, whereas radial *out*ward expansion is observed at the midsection of the expandable pipe. The consequence is the fluid flow path to be obstructed at the midsection, also observed earlier in figure 26. The observed behavior is non-intuitive, possible and not excluded due to the

assumption of an axi-symmetrical system or faulty strain gauges. An inconclusive explanation is founded on the near impermeable cement sheath that will not allow fluid to pass through at the imposed rate of fluid flow. A consequence is fluid to accumulate at the pressure side, which will result in an unknown locally distributed compression of the expandable pipe. As pressurized fluid will flow through the cement sheath towards the atmospheric pressure side, a pressure transition is expected to take place. Given

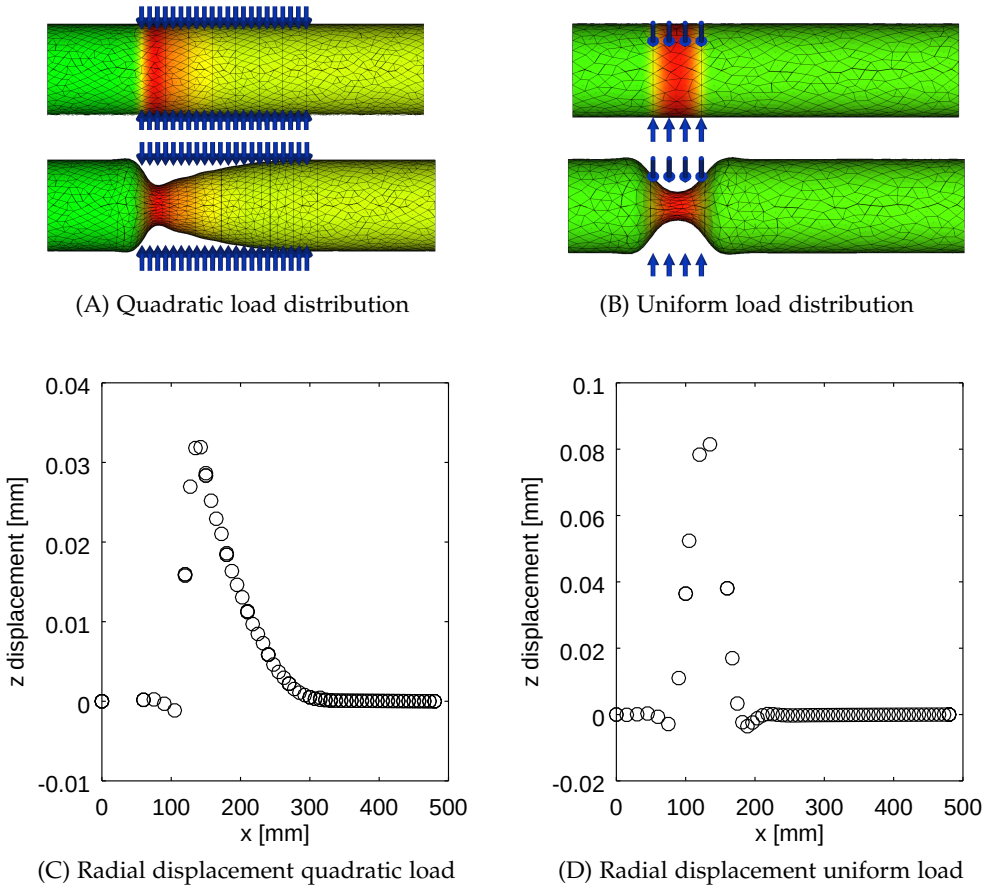

(A) Quadratic load distribution

(B) Uniform load distribution

(C) Radial displacement quadratic load

(D) Radial displacement uniform load

Figure 30: *Expandable pipe FEM deformation analysis for a 3D axisymmetrical quadratic and uniform load distribution. Peak value for the pressure is set at 40 [bar]. Radial deformation shown in subfigure (C) and (D) is the displacement observed at the bottom of subfigure (A) and (B), respectively. Pipe design is made in FreeCAD [47], mesh is generated in Abaqus/Gmsh [19] and post-processing of data is done in GNU Octave [15].*

two situations with distinct though assumed pressure transitions through the cement sheath, both shown in figure 30, the radial deformation of the expandable pipe is investigated with a FEM-analysis in an attempt to explain the radially outward expansion. On the left side there is a quadratic pressure transition through the cement sheath, while on the right a concentrated pressure distribution. An intuitive observation is that compression of the expandable pipe will result in a radial inward deformation of the pipe (shown as a positive displacement in the figure). However, outside the compression area, an end-effect is observed where an actual expansion is

observed and a minor radial outward deformation is visible for the left- and right subfigures. In combination with the supplemental elongation of the pipe that will be limited and constraint with the top- and bottom flanges, it is believed that the expansion will be reinforced and measurable with strain gauges, as depicted in figure 28 and figure 29.

6

CONCLUSION AND FUTURE WORK

In the monobore downhole expansion process the structural foundation, the cement sheath, is exposed to significant compression and shear load. In this design study experimental setups have been designed to study the influence of the cement sheath parameters and the cement sheath behavior. The most important findings are presented here in their respective chronological order of report appearance.

Theory and numerical application

First to identify the possibly most relevant parameters a theoretical and numerical study was done. The resulting model can be used as a design tool.

In consideration of the one-dimensional dynamic poroelastic saturated cement sheath response it is demonstrated that the fluid in the poroelastic cement - for a compression load due to cone indentation - will move towards the area of force exertion. With the coordinate origin set at the interface of expandable pipe and cement sheath, the radial cone indentation would result in a positive defined fluid pressure gradient pointing radially outward. Darcy's law would dictate in that case, that the fluid from the pore structure of the cement sheath would move towards the interface of the expandable pipe and cement sheath, which showed to be in qualitative agreement with earlier experimental work.

In the probabilistic failure prediction model the cement sheath is investigated for a variation in the extent of radial expansion and for a different type of surrounding formation, a relative flexible one, and an opposite stiff one. For cement sheath expansion in a flexible formation, the cement sheath failed already after a minor expansion rate, while for expansion in the stiff formation the cement sheath could resist almost double of the respective rate until failure occurred. For the present non- or low permeable cement structure an intact cement sheath would be unable to allow liquid to pass through towards the formation. However, in the case where flow of fluid towards the formation is permitted - through fractures in the cement sheath - a beneficial interface depressurization will occur.

A numerical prediction tool for the expansion process was developed - the annulus model - that is aimed at investigation of the cement response during expansion and annulus growth. Among others it considers; the cone position as a function of time, accumulation of fluid at the interface of cement sheath and expandable pipe, a two-phase conditioned cement

sheath and the inherent near-impermeable characteristic of the cement sheath. The developed numerical prediction tool permitted a parametric study of the expansion process. It was shown that the hydraulic bond strength parameter, a measure for the cement adherence to metal, had a significant impact on the cement sheath stress state and evolution of the annulus channel. A firm bond will suspend longitudinal annulus expansion, and instead it will force the accumulated fluid at the interface to inflate the existing channel radially outward. The result is an increased interface stress imposed on the expandable pipe until either the annulus expands in length or alternatively the expandable pipe fails.

Methodology for experimental design

The poroelastic cement response model demonstrated that compression of the fluid saturated cement sheath will result in an escape of fluid from the pores of the interior domain. In a close to impermeable cement sheath the vulnerable area where fluid might migrate to is the interface of the expandable pipe and the cement. The parameter that allows this fluid flow towards the interface is the hydraulic bond strength of the cement sheath, where the significance of this parameter is emphasized in the parametric study of the annulus model. To investigate the adherence capacity of the cement to a metal pipe, a laboratory experiment was designed and built, the so-called hydraulic bond strength test. A total of nine different tests have been done to determine the hydraulic bond strength for a variable expandable pipe wall thickness, and a variable composition of the cement mixture by comparison with a reference clean cement sample to polluted ones.

The constitutive behavior of radially compressed concentrically confined cement beyond the yield point is to be investigated. A design is set-up for a concentric confined cement dynamic deformation test where the cement sheath structure is to be exposed to different degrees of expansion and cone displacement speed. A total of twelve different tests have been identified that constitute four different degrees of expansion rates and three different cone displacement speeds. Information obtained from the experiment will illuminate the type of modeling that is permitted to analyze the expansion process. It will determine the effect of the degree of expansion on the internal pore structure of the cement sheath or porosity. Moreover, it will determine the radial preferential flow direction of the fluid in the cement sheath.

A small-scale expansion test was designed to investigate the evolution of the annulus channel that is expected to form between the cement sheath and the expandable pipe, in the expansion process and the consequential built-up of fluid pressure at the interface. The design is aligned with former performed experimental work and the numerical annulus model. The parametric study pointed out five different parameters to be inves-

tigated in a compilation of sixteen different tests. The former hydraulic bond strength test, the cement deformation test and earlier performed experimental effort are buildingblocks giving input for the small-scale expansion test in order to identify the influence of certain parameters in the expansion process.

Experiments and evaluation

Nine hydraulic strength test measurements have been performed that varied in expandable pipe wall thickness and cement composition where either a clean cement sample was considered, an oil-mud sample or a water-mud sample. In a more rigid system the clean cement sample was able to maintain its structural integrity for a longer time, as opposed to the oil- and water-mud samples, while the opposite was true for a compliant system. In consideration of the hydraulic bond strength and permeability, the oil-mud cement composition samples seem to be approximately unaffected by an increase in expandable pipe wall thickness. Once the hydraulic bond strength is broken, the water-mud cement samples demonstrated to be most permeable.

In general, a single measurement would last - on average - for about 10-14 [hrs] where at some point a structural unstable flow path would manifest itself in the cement sheath. After evaluation of the strain gauges it appeared that the expandable pipe would get compressed at the flow path entrance *and* expanded halfway the flow path, such that the flow path through the cement sheath was obstructed. After assessment of the pipe deformation with a FEA the expansion was to occur due to local end-effects outside of the compressed area and emphasized by constraint elongation of the pipe, that resulted in unstable flow.

Future work

The potential of the annulus prediction model is thus far unexplored. The foundation of the model hinges on the principles of mass conservation, (semi-) analytical expressions and the throughout literature accepted fundamental theory of poromechanics. Dedicated experimental research will have to dictate the accuracy of the model, and validation will have to be a requirement prior to enactment of the prediction model.

An alternative to the hydraulic bond strength test is the so-called shear test. The scrutinized unstable flow path amid hydraulic bond strength measurements pointed out the problem with expandable pipe compliance. The shear test would be an alternative to overcome expandable pipe compliance. In the literature one will be able to find a correlation with the hydraulic bond strength parameter, and the shear strength parameter.

The poroelastic cement response model, and the numerical annulus model both consider continuum mechanics with linear elastic behavior of the

porous medium. However the exhibition of non-linear behavior, plastic deformation, the time effect of loading and the effect of loading on the internal porous structure could affect the outcome of the developed models with its current assumptions. For that reason it is recommended to perform the cement deformation test, prior to the small-scale expansion test and verify the constitutive behavior of the fluid saturated and concentric confined cement.

A

TEST PLAN HYDRAULIC BOND

This appendix is an extent of what is treated in section 4.1, which is a brief overview of what is given here. Additional information is dedicated towards the test plan of the hydraulic bond experiment, sample specification and sample preparation due for testing.

A.1 SCOPE OF TEST

Investigate the bonding strength of cement attached to an expandable pipe in an expandable pipe, cement sheath and host pipe configuration, for a set of different wall thicknesses of the expandable pipe, and where the configuration has;

- no pollution of the cement composition,
- pollution of the cement composition by means of water based mud,
- pollution of the cement composition by means of oil based mud.

Acknowledgement:
The framework for the bonding strength experiment [17].

A.2 MATERIAL OVERVIEW

outer pipe / test vessel / V-100 / host pipe				
material	ss s355	outer diameter	188.0	[mm]
manufacturer	Shell	inner diameter	158.0	[mm]
type	custom made	wall thickness	15.0	[mm]
design temperature	amb	length	480.0	[mm]
		design pressure	115	[barg]
inner pipe / test subject / expandable pipe				
material	ss s355	outer diameter	116.0	[mm]
inner diameter	variable	length	480.0	[mm]
wall thickness	variable			

feed fluid pump / P-010				
material	ss s355	design temperature	40.0	[°C]
manufacturer	Teledyne Isco	design pressure	695	[barg]
type	100DM	volume/capacity	30.0	[ml/min]
feed vessel / V-010 / reservoir				
material	plastic	volume/capacity	1.0	[dm^3]
type	bottle			
manufacturer	Teledyne Isco			
design temperature	amb			
design pressure	atm			
collector vessel / V-300 / leak tray				
material	transparent	volume/capacity	1.0	[dm^3]
type	bottle			
design temperature	amb			
design pressure	atm			
mold				
type	custom made	outer diameter leg	158.0	[mm]
manufacturer	Shell	inner diameter leg	116.0	[mm]
		length leg	90.0	[mm]

A.3 VISION

The expansion process in the monobore well will throughout expansion of the expandable pipe compress the cement sheath. As the cement sheath at time of expansion is in a fluid saturated state the compression of the cement will result in an escape of fluid from the pores. In a close to impermeable cement sheath the vulnerable area where fluid might mitigate to is the interface of expandable pipe and cement. The parameter that determines this escape of fluid towards the interface is the so-called hydraulic bond or *bond strength* of the expandable pipe and cement as a whole and is to be investigated here.

A.4 OBJECTIVE

1. Determine the hydraulic bond strength parameter at the interface of cement sheath and expandable (inner) pipe, the strength of cement adherence to the inner pipe.
2. Determine the friction factor, or through a porous medium inverse related porous Reynolds number.
3. Measure an approximate permeability of the system, the measured resistance of the porous cement structure for a feed pump to squeeze fluid through.

A.5 SAMPLE SET

Set of pipes in the assembly are to be sandblasted and if required prior to the experiment the cemented surface of the inner pipe is to be wetted with water/oil based mud similar to the in-field situation. The cement samples are made according to the recipe of the supplier, or cement lab technician and are to be cured and *kept saturated in a liquid filled vessel* for a period of 7 days in an oven at 80° degrees centigrades [26]. An overview of the cement mixture is provided in table 10, with the additional mass percentages for a mixture of 3 [kg].

A.5.1 *brief overview explanation*

A detailed overview of the variables to be tested and the experiments to be performed is provided below in table 9. A schematic workdrawing of the setup is given in figure 32. Herein six major relevant sections are visible;

1. An *outer pipe* that for safety issues is 15 [mm] thick that encompasses the total of the to be tested system. It is expected the overdimensionalization of the outer pipe will overestimate the bonding strength.
2. An *inner pipe* that is the test subject and that is changed every experiment to investigate the effect of the compliance of the pipe on the bonding strength of the system.
3. A *cement layer* in between the inner and outer pipe that moreover is 90 [mm] removed from either top end of the respective pipes to limit influence of the both ends when the system is pressurized.
4. A *feed pump* that will pressurize the system with a liquid feed where the volume flow is increased in intervals to increase the degree of pressurization.
5. A *collector vessel* where a continuous outflow of fluid is to be measured. An initial outflow will represent a system permeability, with the limitation of the compliance of the inner tube, and a secondary increase of fluid outflow will represent a bonding strength characteristic.
6. A *mold* that is a tool to manufacture the collective test units in an equal fashion, to prevent production errors and to allow equal comparison of result.

A workdrawing for the collective test unit, the expandable pipe, the cement sheath and the host pipe configuration with all required dimensions is presented in figure 33.

A.5.2 *sample preparation*

A stepwise procedure of sample preparation will be presented below, that is to be read parallel with the information provided of the total set of experiments in table 9;

1. The inner pipe is placed on the mold that will create a required clearance of cement on the bottom end, grease is put unto the contact area of pipe and mold to prevent a cement bond.
2. The inner pipe is pre-treated with mud spray if necessary and water or oil according to the experiment outline in table 9.
3. The outer pipe is placed on the mold that will create a void in between the inner and outer pipe, again grease is put unto the contact area of pipe and mold, mark outer pipe according to table 9.
4. A cement mixture is made according to the recipe, see table 10, or the cement lab technician, and is poured inside the created void of step (3.) up to the design level pointed out in figure 33, both top ends need to have a clearance of 90 [mm] without cement, the sample is consequently closed off with the top-mold.
5. The made sample is to be put in an heated oven of approximately 80^{o} degrees centigrade for a period of 7 days, solidification of the cement structure will occur in the first 24 hours. After cement is cured the molds can be removed, but is to be kept fluid saturated.
6. The process is repeated for the total of 9 tests and is to be stored in a liquid filled container for the time being until the experiment is performed.

A.5.3 *single experiment methodology*

The test methodology is explained below in a stepwise procedure that is to be honored for all individual test samples. A prepared sample is a host pipe, with an expandable pipe that is equipped with strain gauges on the inside, while the outside of the expandable is either a clean or a polluted cement sheath see table 9. After the former is embedded the following procedure below is adopted;

1. A cured, fluid saturated and marked sample is to be assembled for the experimental run, the length of the cement sheath is to be verified and measured.
2. close off the test sample with top and bottom flange,
3. the feed pump system, strain gauges and data acquisition equipment is to be connected and mounted on the test sample,
4. feed fluid into the top clearance area of the test sample until no more air is present in the clearance area, close off the release-air nozzle,

5. the experiment is initiated with a pressurization of the system of 1 [barg], which will additionally be set as a pressure increment,

6. time, pressure, strain and fluid inflow is to be recorded throughout execution of the experiment, after the inflow of fluid is stabilized the pressure increment is added,

7. the increment increase explained in item (5.) is to be repeated until a sudden increase in outflow is measured or a strain energy release is observed as shown in figure 31, at that time the bonding strength is broken. At this point it is best to attain 4 or 5 more data points before abortion of the experiment. If a new test sample is available the above process is repeated from item (1.).

test	number of samples	inner pipe OD [mm]	ID [mm]	WT [mm]	outer pipe OD [mm]	ID [mm]	WT [mm]	length [mm]	description	strain gauges
#1	1	116	112	2	188	158	15	480	water-mud	
#2	1	116	112	2	188	158	15	480	clean	yes
#3	1	116	112	2	188	158	15	480	oil-mud	yes
#4	1	116	110	3	188	158	15	480	water-mud	
#5	1	116	110	3	188	158	15	480	clean	
#6	1	116	110	3	188	158	15	480	oil-mud	
#7	1	116	108	4	188	158	15	480	water-mud	
#8	1	116	108	4	188	158	15	480	clean	yes
#9	1	116	108	4	188	158	15	480	oil-mud	yes

Table 9: *Test overview of a total of 9 experiments. In test #2, #3, #8 and #9 strain gauges are present to estimate the deformation imposed on the inner pipe due to the presence of a fluid filled annulus in the cement layer. Variation in the different tests are related to the wall thickness of the expandable pipe, and the state of the cement where it is clean, polluted with water based mud, or polluted with oil based mud. The total length of the specimen is constant at* 480[mm] *and the length of the cement sheath is constant at* 300[mm].

Name	Composition	Purpose	Mass percentage [%]
TXI lightweight	portland cement, crystalline silica quartz	cement	100
Field fresh water	water	hydrate activation	49
EZ flo II	acetic acid, ethylene glycol	flow enhancer	0.21
D-air 5000	calcium sulfate, gypsum, calcium carbonate, crystalline silica quartz	defoamer	0.4
KCl	barium sulfate, potassium chloride, polyalkylene glycol, crystalline silica quartz	water based drilling fluid	2.0
Halad 344exp	hydrotreated light petroleum distillate	fluid loss additive	0.9
SA 640L	paraffin based petroleum oil	suspending agent	0.17
SCR 100L	no hazardous substances	retarder	1.7
oil-mud	water, oil, emulsifier, bentonite	pollution	
water-mud	water, bentonite	pollution	

Table 10: *Halliburton cement recipe for application in the Gulf of Mexico, Broussard [26]. Provided mass percentages are corrected and applicable for specified cement only and a total cement quantity of 3 [kg]* (= 100%).

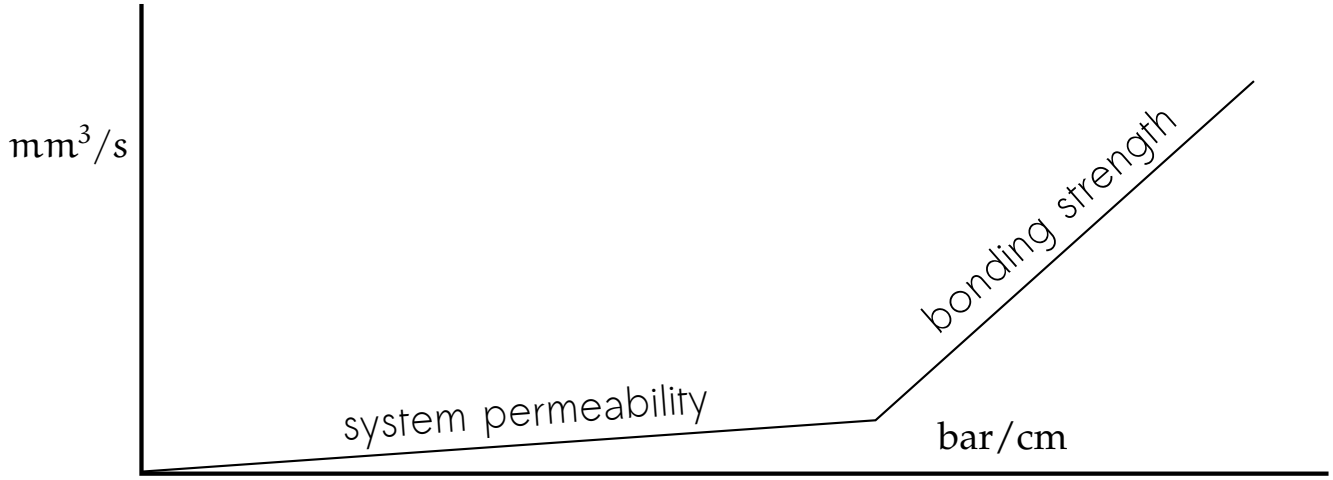

Figure 31: *The pump will feed the system continuously with a fluid, due to the porous structure a continuous outflow of fluid will be measured that represents a system permeability. Due to an interval pressure increase, at some point the pressure present in the fluid will exceed the bonding strength of the system and an increased rate of outflow of fluid will be measured where the asymptot represents the bonding strength of the system.*

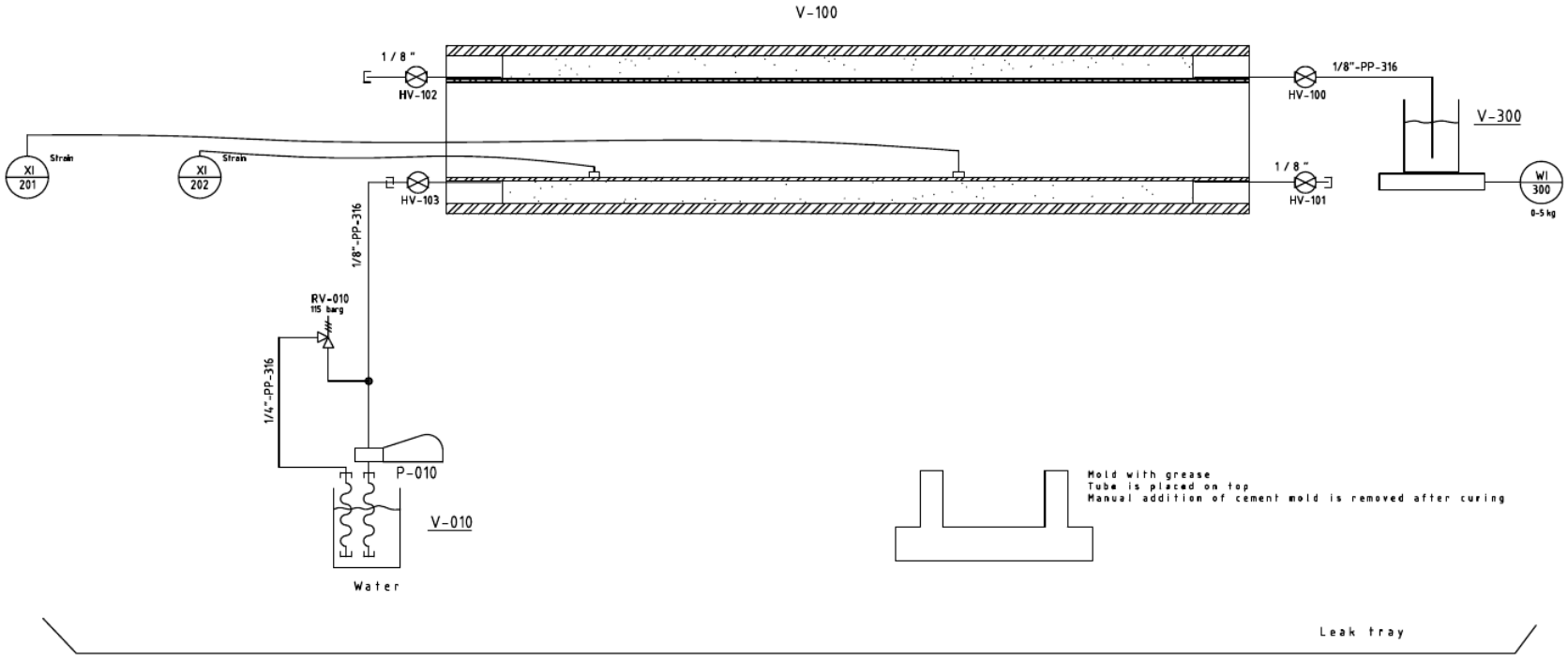

Figure 32: *A downscaled work drawing that provides an overview of the bonding strength experimental setup. Shown is an expandablePipe/cementSheath/hostPipe configuration with a feed pump on one side, and a collector vessel on the other side. The feed pump pressurizes the system with liquid and with the collector vessel an outflow of liquid is measured that represent the permeability and bonding strength of the system.*

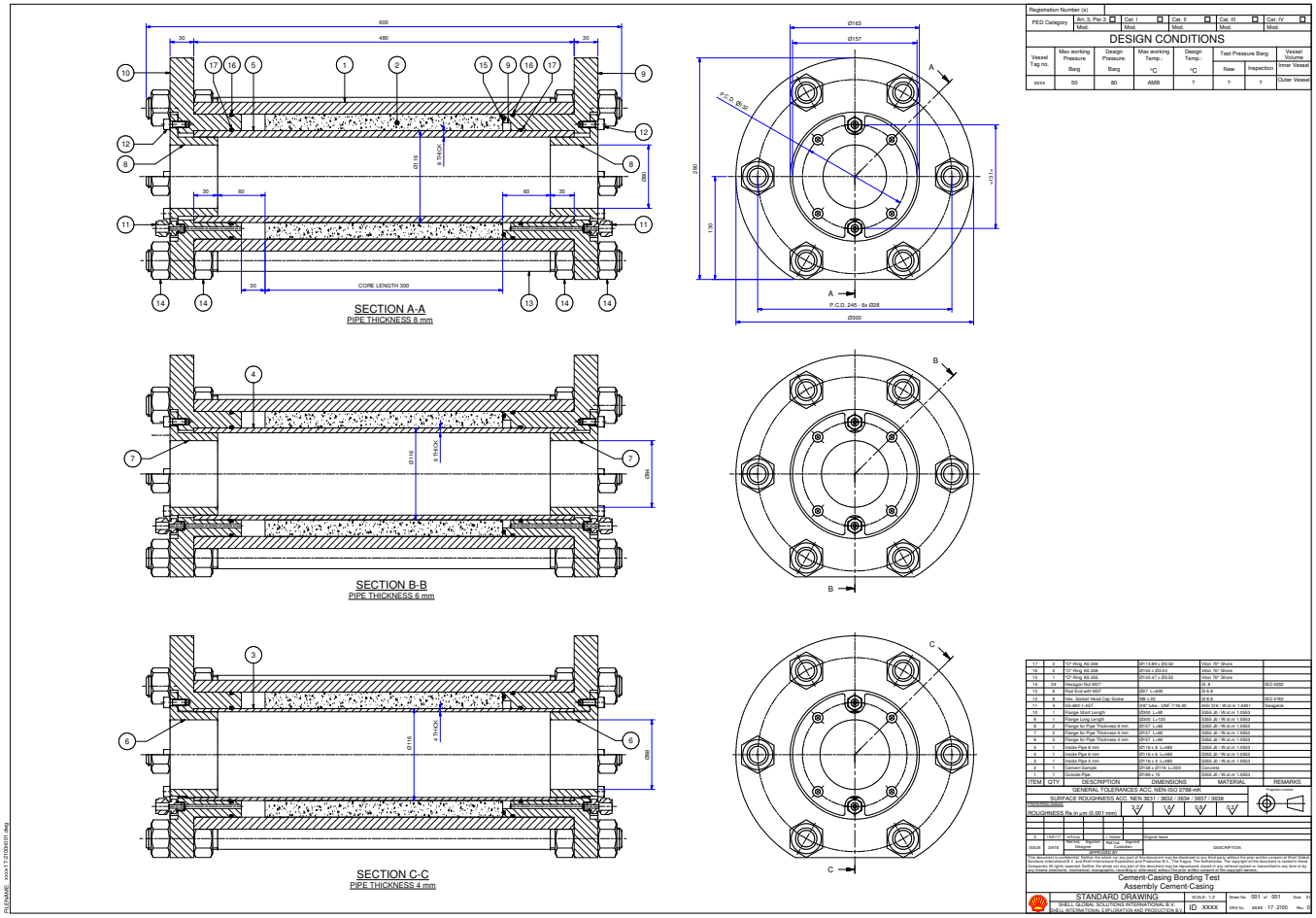

Figure 33: *A work drawing that provides an overview of the collective test unit and the required dimensions of the experimental setup. Shown is an expandablePipe/cementSheath/hostPipe configuration with the set of equipment that is to be applied in the assembly.*

B

TEST PLAN CEMENT DEFORMATON

This appendix is an extent of what is treated in section 4.2, which is a brief overview of what is given here. Additional information is dedicated towards the test plan of the cement deformation experiment, sample specification and sample preparation due for testing.

B.1 SCOPE OF TEST

To investigate the constitutive behavior of fluid saturated cement in between an expandable- and host pipe configuration that is expanded in pure radial direction. A cut-up slab of confined cement from the hydraulic bond strength test is considered that,

- is expanded in four independent stages of magnitude,
- is expanded with three independent cone displacement speeds.

B.2 MATERIAL OVERVIEW

outer pipe / host pipe				
material	ss s355	outer diameter	188.0	[mm]
manufacturer	custom made, Shell	inner diameter	158.0	[mm]
		wall thickness	15.0	[mm]
		length	50.0	[mm]
inner pipe / expandable pipe				
material	ss s355	outer diameter	116.0	[mm]
lubricant	RPSLF	inner diameter	112.0	[mm]
		wall thickness	2.0	[mm]
		length	480.0	[mm]
top flange				
material	s355 Jo	outer diameter	290.0	[mm]
wire tap holes	6xM16	inner diameter	112.0	[mm]
drain holes	2xM5	wall thickness	20.0	[mm]
bottom flange				
material	s355 Jo	outer diameter	290.0	[mm]
wire tap holes	6xM16	inner diameter	90.0	[mm]
		wall thickness	70.0	[mm]

cone				
material	st52	max diameter	70.0	[mm]
lubricant	RPSLF	min diameter	45.0	[mm]
		contact length	114.0	[mm]

B.3 VISION

The investigation of a strict radial confined saturated cement sheath and the dynamical outward expansion has thus far not been recorded in a scientific experiment. The consequence is that the constitutive behavior of the cement in the present framework is a rather unknown appearance. The constitutive behavior is associated with the capacity of the cement sheath to remain intact amid expansion, the characteristics of the porous medium, as porosity and permeability, the preferential flow direction of fluid dissolved in the cement and the application of (non-) continuum mechanics and linear elastic theory. The experiment will provide the required information to consider and embed the essential behavior of the cement throughout a radial outward expansion.

B.4 OBJECTIVE

1. Evaluation of the state of structural integrity of the cement sheath for different types of radial expansion. Fischer *et al.* [18] concluded in his research that the increase of the load rate duration would deteriorate the cement paste strength. The different types of imposed expansion is therefore dedicated to the degree of radial outward expansion, and the additional rate or speed of expansion. Darwin *et al.* [12] furthermore pointed out in his research the methodology of evaluation of the micro-fractures present in the cement sheath that have a surface density of 0.04 to 0.14 mm/mm^2 and can be observed with an optical microscope at magnifications below 50x, that is to be adopted for the present investigation.

2. The total fluid porosity of the cement sheath before and after expansion. One is able to determine the total fluid porosity by consideration of a fluid saturated yet arbitrary volume chunk of the cement sheath, weigh it and vacuum oven dry the specimen in intervals until a constant weight is obtained [20]. The result would indicate that the prior fluid saturated chunk of the cement sheath no longer holds any fluid in its internal structure, as all fluid is evaporated.

3. Determination of the preference direction of cement paste, fluid slurry or fluid expulsion amid expansion and consequently quantify the expulsion. In the numerical analysis performed in section 3.1 it got concluded that the fluid pressure gradient over the radial thickness of the cement sheath is defined positive. In consideration of Darcy's law

(26), the consequence was fluid to move towards the interior frontier of the domain, i.e., the expandable pipe and is to be confirmed in the cement deformation test and is to be quantified as a result.

B.5 SAMPLE SET

Prepared cement samples from the hydraulic bond strength test, from appendix A, are recommended for the cement deformation test, as these are ready for utilization. If new cement samples are to be made, the procedure described in the hydraulic bond strength test appendix are to be respected. A single sample from the hydraulic bond strength test is 480 [mm] long of which approximately 300 [mm] is covered with cement. A single sample for the cement deformation test is considered 50 [mm], thus a potential of approximately 5-6 cement deformation test samples per hydraulic strength test sample.

B.5.1 *single experiment methodology*

The test methodology is explained below in a stepwise procedure that is to be honored for all individual test samples, as depicted in table 12. A prepared sample is a host pipe, with an expandable pipe and fluid saturated cement in between. After the former is embedded the following procedure below is adopted;

1. The bottom flange is to be centered and positioned on a rigid test bed. The thickness of the bottom flange is designed to withstand the axial displacement for the desired radial expansion of the cement sheath.

2. A labeled cement test sample with length 50 [mm] is to be mounted on top of the bottom flange.

3. Prior- and post the labeled cement test sample is put in place, a (new) gasket is to be positioned to limit uncontrollable leakage.

4. The top flange is to close off the cement test sample, and the six rods and bolts are to hold together and seal off the system together with the gaskets in between.

5. Through the top flange the wedges and cone are to be put in place on top of the circumferential of the inner diameter of the bottom flange.

6. Data acquisition for expansion force, and axial displacement are to be connected.

7. On top of the drain holes a dedicated and separate sponge for each hole is positioned to drain fluid outflow amid expansion. The sponge prior to the measurement is nulled and contains a reference value with respect to the mass of the sponge, a sealed off - from the bottom

plastic canister - is to be adopted for each drain hole, that from the top can not pull vacuum.

8. If a new test sample is available the above process is repeated from item (2.) where the specific details are elucidated in table 12.

test	inner pipe ID [mm]	cement sheath WT [mm]	outer pipe OD [mm]	WT [mm]	cone axial disp. [mm]	cone radial indent [mm]	expansion force [kN]	expansion ratio [%]	cone axial speed [mm/min]
#1	112	21	188	15	22.95	2	119	3.57	70
#2	112	21	188	15	45.90	4	170	7.14	70
#3	112	21	188	15	68.86	6	220	10.71	70
#4	112	21	188	15	22.95	2	119	3.57	140
#5	112	21	188	15	45.90	4	170	7.14	140
#6	112	21	188	15	22.95	2	119	3.57	70
#7	112	21	188	15	45.90	4	170	7.14	70
#8	112	21	188	15	22.95	2	119	3.57	140
#9	112	21	188	15	45.90	4	170	7.14	140
#10	112	21	188	15	68.86	6	220	10.71	140
#11	112	21	188	15	22.95	2	119	3.57	70
#12	112	21	188	15	45.90	4	170	7.14	70
#13	112	21	188	15	22.95	2	119	3.57	210
#14	112	21	188	15	45.90	4	170	7.14	210
#15	112	21	188	15	68.86	6	220	10.71	210

Table 12: *Test overview for the concentric cement deformation test. Three subdivisions are dedicated to clean cement, oil-mud polluted cement and water-mud polluted cement, respectively. Estimation of the expansion force is done by evaluation of section D.5. The test samples are manufactured from the aforementioned hydraulic bond strength test* #1, #2 *and* #3 *of table 4. System parameters; host pipe yield pressure* $= 58[\mathrm{MPa}]$, *host pipe diameter/WT ratio* $= 12.5[-]$, *cement paste compressive strength* $= 25[\mathrm{MPa}]$.

C

TEST PLAN SMALL-SCALE EXPANSION

This appendix is an extent of what is treated in section 4.3, which is a brief overview of what is given here. Additional information is dedicated towards the test plan of the small-scale expansion experiment, sample specification and sample preparation due for testing.

C.1 SCOPE OF TEST

Investigate the evolution of the *annulus channel* or formation of the *traveled pressure wave* that will manifest itself in-between the cement sheath and the expandable pipe - for;

1. different wall thicknesses of host pipe (wt_{hos}), and,
2. different artificial permeability (k_{fla}) settings of top flange, and,
3. different expansion ratios (α_{cone}) by virtue of variable cone size, and,
4. different cement mixtures or compositions (`pure` or `impure`), and finally,
5. different cement sheath thicknesses (wt_{cem}).

host pipe				
tube grade/weight	s355	outer diameter	99.0	[mm]
manufacturer	železiarne pod.	inner diameter	90	[mm]
internal coating	RPSLF	wall thickness	4.5	[mm]
YS/UTS [MPa]	355/560 (0.63)	min length	2000	[mm]
(D/t)	22.0	yield pressure	32	[MPa]

expandable pipe				
tube grade/weight	st52	outer diameter	60.3	[mm]
manufacturer	rohrwerk max.	inner diameter	54.5	[mm]
internal coating	gearkote	wall thickness	2.9	[mm]
YS/UTS [MPa]	503/621 (0.81)	min length	2000	[mm]
(D/t)	20.8	expansion ratio	16.5	[%]

cone assembly				
cone code	sverker 21	max diameter	63.5	[mm]
cone/stab/mand	smooth	length cone	80	[mm]

cement, see figure 35				
type cement	lafarge	compr. strength	25	[MPa]
		comp. ratio sheath	31	[%]

tools and equipment				
sensor type #1	fluid pressure	mechanical press	400	[kN]
sensor type #2	expansion force	expansion speed	70 [1]	[mm/min]
sensor type #3	radial disp.	sensor type #4	strain gauges	

C.2 VISION

Evolution of the annulus channel in the cement sheath ahead of the cone is an important feature inherently present in the expansion process and is not well investigated in a laboratory setting thus far. Finding out the development of this feature for different input parameters[2] in the expansion process will provide essential information that is to be used to set up a strategy where accumulated fluid pressure in the cement sheath is to be mitigated, and by that preventing a potential pipe collapse.

C.3 OBJECTIVE

1. For the duration of the expansion process measure the fluid pressure in the cement sheath and radial displacement of host pipe, such that the variables mentioned in *Scope of Test* and specified in table 14 can be correlated to the evolution of the annulus [3] ahead of the cone in the cement sheath.
2. Investigate the effect of a permeable/cracked formation, or incomplete cement job by means of a variable set of drain holes in the top flange.
3. Investigate the effect of the cement unconfined compressive strength (UCS) - that is a uniaxial cement characteristic - to the radial displacement of the host pipe.
4. Validate the numerical annulus model of section 3.3, wherein the expansion process is simulated, this is done by measurement of fluid pressure in the cement layer and radial displacement of the host pipe.
5. Perform a permeability test to extract cement characteristics (porosity, permeability) before and after expansion and to additionally val-

1 Consider two/multiple expansion speed options.
2 i.e., the host pipe wall thickness, artificial permeability, expansion ratio, the composition of the cement and cement sheath thickness.
3 annulus formation, or likewise the traveled pressure wave length ahead of the cone

idate an optic microscopical characterization method. And furthermore, after sample extraction perform an unconfined compressive strength test to correlate objective point (3.) and (5.).

C.4 SAMPLE SET

Set of pipes in the assembly are to be sandblasted and prior to expansion the expansion surface of the expandable pipe is to be wetted with water/oil based mud similar to the in-field situation. The cement samples are made according to the recipe of the supplier, or cement lab technician and is specified in appendix A. A detailed overview of the variables to be tested and the experiments to be performed is provided below in table 14. Furthermore, a schematic overview of the setup is given in figure 37. Herein three relevant sections are visible;

1. Initial expansion for a pipe-only expansion, to stabilize cone into single pipe.
2. Initial expansion into the cement, to stabilize the cone into the system and to set *fixed-fixed conditions*.
3. Steady state expansion with a preferable 2 [m] total stroke, see analysis section 3.3.2, of the annulus model.

In step (2.) above an additional flange is welded to the bottom to mimic a fixed-fixed condition, that is similar to the bottom-hole anchor. To make sure the cement will not bleed away in excessive amounts, the top annulus section in figure 37 will be closed off with a perforated flange that will control outflow of liquid/cement/slurry. Three configurations for the top flange will be proposed that have a percentile permeability of $\{1.6, 5.1, 13\}$[%] that are shown in figure 34.

Figure 34: *Top flange permeability configuration.*

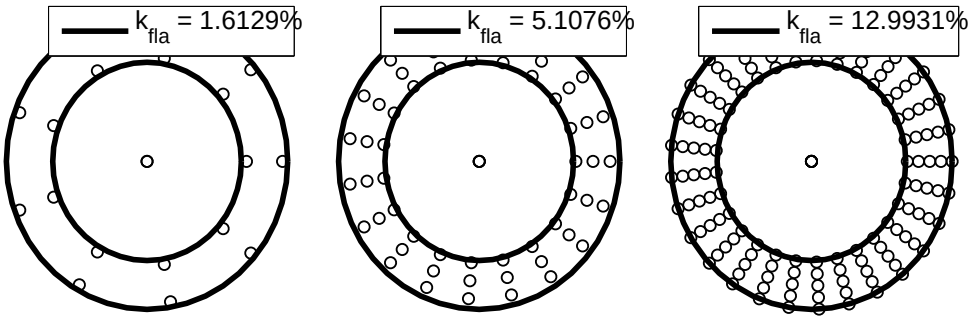

C.5 LIST OF FIGURES

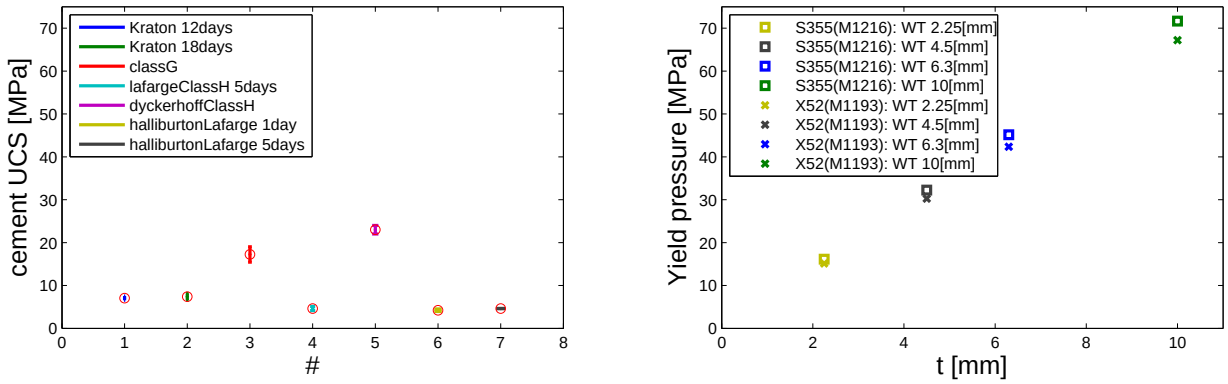

Figure 35: *The uniaxial compressive strength for cement on the left side, and the yield pressure for the host pipe on the right for the relevant pipe dimensions. The two subfigures are part of the material overview table, that is part of the design of the experimental setup.*

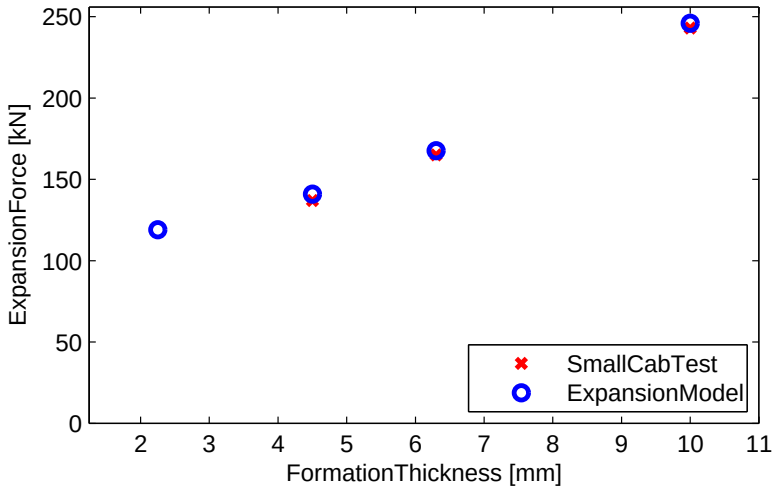

Figure 36: *The expansion force for different thicknesses of the host pipe. In red is the former gathered result from the SmallCabTest [24], and in blue is the numerical computed approximated expansion force.*

C.6 ANALYTICAL EXPRESSIONS

compression ratio of cement;

$$\texttt{compression ratio} = 1 - \frac{\texttt{deformed wall thickness cement}}{\texttt{undeformed wall thickness cement}}. \quad (42)$$

expansion ratio of expandable pipe;

$$\texttt{expansion ratio} = \frac{\texttt{cone diameter} - \texttt{inner diameter exandable}}{\texttt{inner diameter exandable}}. \quad (43)$$

yield pressure host pipe [2];

$$\texttt{yield pressure} = 0.875 \cdot \texttt{yield strength material} \cdot \left(\frac{\texttt{wall thickness pipe}}{\texttt{outer radius pipe}} \right). \quad (44)$$

test	ID_{hos}[mm]	OD_{hos}[mm]	wt_{hos} [mm]	$(D/t)_{hos}$	wt_{cem}[mm]	OD_{cone}[mm]	α_{cone} [%]	k_{fla} [%]	sample	F [kN] 36
#1	90	94.5	2.25	42.0	14.85	63.5	16.5	1.6	pure	135[kN]
#2	90	99.0	4.5	22.0	14.85	63.5	16.5	1.6	pure	149[kN]
#3	90	102.6	6.3	16.3	14.85	63.5	16.5	1.6	pure	162[kN]
#4	90	110.0	10	11.0	14.85	63.5	16.5	1.6	pure	188[kN]
#5	90	94.5	2.25	42.0	14.85	63.5	16.5	1.6	impure	122[kN]
#6	90	99.0	4.5	22.0	14.85	63.5	16.5	1.6	impure	135[kN]
#7	90	102.6	6.3	16.3	14.85	63.5	16.5	1.6	impure	147[kN]
#8	90	110.0	10	11.0	14.85	63.5	16.5	1.6	impure	171[kN]
#9	90	99.0	4.5	22.0	14.85	63.5	16.5	5.1	pure	NA
#10	90	99.0	4.5	22.0	14.85	63.5	16.5	13.0	pure	NA
#11	90	99.0	4.5	22.0	14.85	64.5	18.3	1.6	pure	157[kN]
#12	90	99.0	4.5	22.0	14.85	65.5	20.2	1.6	pure	164[kN]
#13	98	107	4.5	23.8	18.85	63.5	16.5	1.6	pure	126[kN]
#14	106	115	4.5	25.6	22.85	63.5	16.5	1.6	pure	108[kN]
#15	90	99	4.5	22.0	14.85	63.5	0	1.6	pre-perm	NA
#16	90	99	4.5	22.0	10.35	63.5	0	1.6	post-perm	NA
number	host pipe	host pipe	host pipe	ratio	cement layer	cone	cone	flange	cement	force

Table 14: *Test overview of the experiments. The diameter/thickness ratio (D/t) of the host pipe in the full scale setup is* 22.1*, the aim is to get similar conditions in the downscaled setup. Assumed is constant expandable pipe dimensions, given in the material overview table in the introduction. Presented in red is the variable that is to be investigated in the experiment. The expansion force is estimated with a numerical computation according to appendix section D.5. The experiment in purple, experiment #2 is the reference case.*

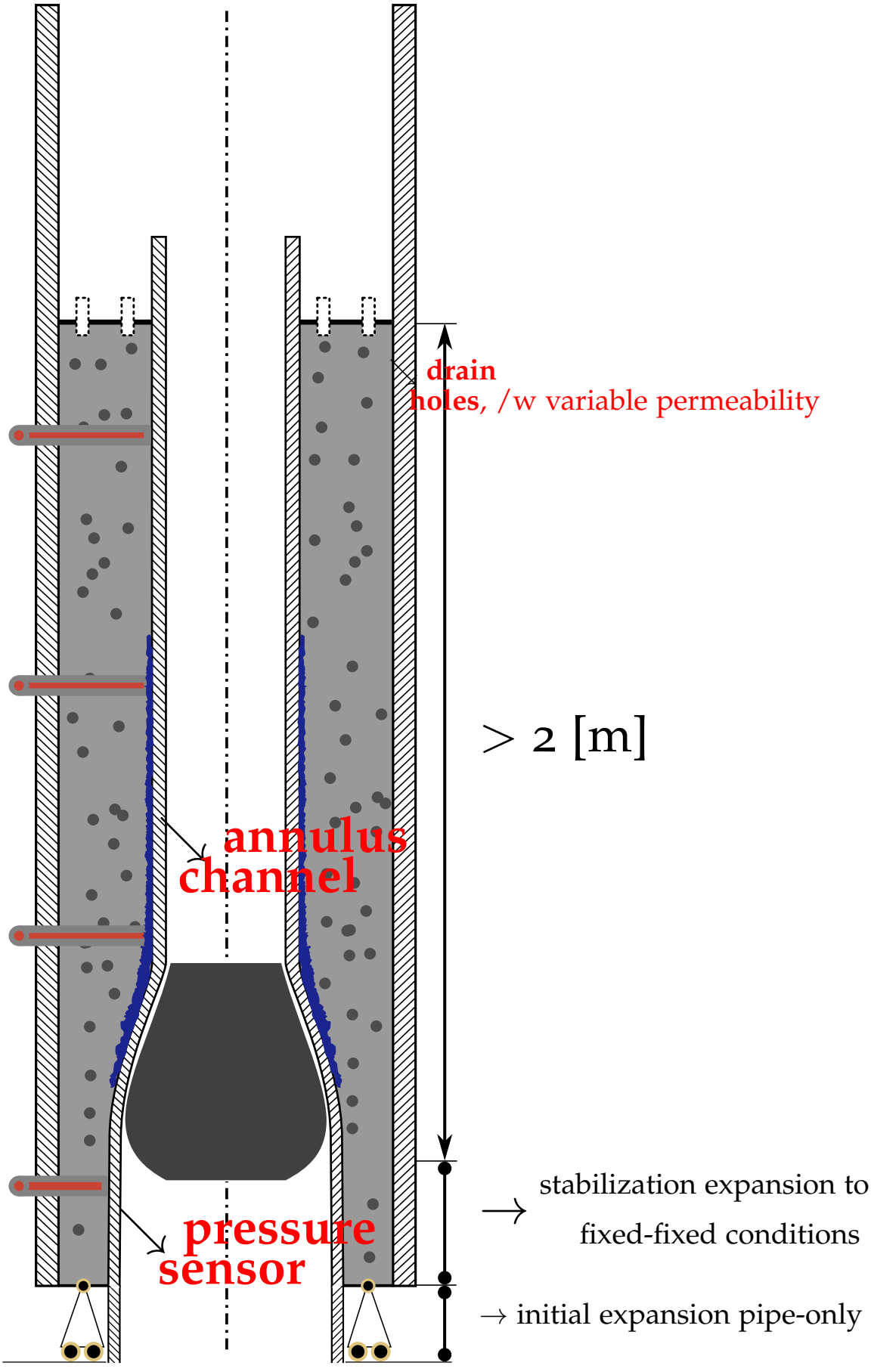

Figure 37: *A schematic of the small-scale expansion test. Shown is the core of the setup that constitutes an expandable pipe, host pipe and cement sheath in-between.*

quantity	name	ID[mm]	OD[mm]	*w*t [mm]	comment
2x	host pipe	90.0	94.5	2.25	
8x	host pipe	90.0	99.0	4.50	
2x	host pipe	90.0	102.6	6.30	
2x	host pipe	90.0	110.0	10.0	
1x	host pipe	98.0	107.6	4.50	
1x	host pipe	106.0	115.0	4.50	
16x	expandable pipe	54.5	60.3	2.9	
10x	fluid pressure sensor				50-900 [bar]
1x	expansion force sensor				50-400 [kN]
10x	radial displacement sensor				1-20 [mm]
48x	strain gauges				
1x	cone/stabilizer/mandrel		63.5		
1x	cone/stabilizer/mandrel		64.5		
1x	cone/stabilizer/mandrel		65.5		
1x	cement mixture				0.075 [m3/mtrLength]
12x	flange perm 1	60.3	90		$k_{fla} = 1.6$[%]
1x	flange perm 1	60.3	98		$k_{fla} = 1.6$[%]
1x	flange perm 1	60.3	106		$k_{fla} = 1.6$[%]
1x	flange perm 2	60.3	90		$k_{fla} = 5.1$[%]
1x	flange perm 3	60.3	90		$k_{fla} = 13.0$[%]
16x	solid bottom flange	63.3	90		$k_{fla} = 0$[%]

Table 15: *Indication of the required equipment in the small-scale expansion test.*

D

DETAILS OF THE IMPLEMENTED NUMERICAL MODELS

D.1 CEMENT RESPONSE IN POROELASTIC MATERIAL

D.1.1 *Implementation details of the numerical dynamic poroelastic model*

In section 3.1.1 Biot's poroelastic wave equations have been introduced. In this section it is desirable to find a numerical solution for these equations. The set of equations (3) - (6) form a coupled system and are rewritten into a form that will allow a finite difference assessment. It can be shown that the former mentioned equations can be written in the following form,

$$\left[1+\tau\left\{1+\frac{n\rho_f}{(1-n)\rho_s}\right\}\right]\frac{\partial u}{\partial t} = \ldots$$
$$\ldots-\frac{1}{\rho_f}\frac{\partial p}{\partial x}-\frac{ng}{k}(u-s)-\frac{\tau}{(1-n)\rho_s}\left\{\frac{\partial \sigma'}{\partial x}+\alpha\frac{\partial p}{\partial x}\right\}, \quad (45)$$

$$\frac{\partial s}{\partial t}+\frac{n\rho_f}{(1-n)\rho_s}\frac{\partial u}{\partial t} = -\frac{1}{(1-n)\rho_s}\left\{\frac{\partial \sigma'}{\partial x}+\alpha\frac{\partial p}{\partial x}\right\}, \quad (46)$$

$$\frac{\partial p}{\partial t} = -\frac{n}{S_p}\frac{\partial u}{\partial x}-\frac{\alpha-n}{S_p}\frac{\partial s}{\partial x}, \quad (47)$$

$$\frac{\partial \sigma'}{\partial t} = -\frac{1}{m_v}\frac{\partial s}{\partial x}, \quad (48)$$

where the permeability κ is replaced with the hydraulic conductivity $k = \kappa\rho_f g/\mu$. Furthermore use is made of equation (4) with respect to $\partial s/\partial t$ to come up with the rewritten form of the conservation of fluid momentum now given in equation (45). The remainder equations (46) - (48) are the conservation of whole momentum, the storage equation and the constitutive soil skeleton equation, respectively.
The set of scalar equations are written into a system of equations having the following form [1],

$$\frac{\partial \mathbf{Q}}{\partial t}+\frac{\partial \mathbf{f}(\mathbf{Q})}{\partial x}+\mathbf{G} = \mathbf{0}, \quad (49)$$

where $\mathbf{Q}$, $\mathbf{f}(\mathbf{Q})$ and $\mathbf{G}$ are used to denote,

$$\mathbf{Q} = \begin{bmatrix} \left(1+\tau\left\{1+\frac{n\rho_f}{(1-n)\rho_s}\right\}\right)u \\ s+\left(\frac{n\rho_f}{(1-n)\rho_s}\right)u \\ p \\ \sigma' \end{bmatrix}, \quad \mathbf{G} = \begin{bmatrix} \left(\frac{ng}{k}\right)(u-s) \\ 0 \\ 0 \\ 0 \end{bmatrix}, \quad (50)$$

1 The values of these constants are given in the appendix, table 16.

$$\mathbf{f}(\mathbf{Q}) = \begin{bmatrix} \left(\frac{1}{\rho_f} + \frac{\alpha\tau}{(1-n)\rho_s}\right) p + \left(\frac{\tau}{(1-n)\rho_s}\right) \sigma' \\ \left(\frac{1}{(1-n)\rho_s}\right) (\sigma' + \alpha p) \\ \left(\frac{n}{S_p}\right) u + \left(\frac{\alpha - n}{S_p}\right) s \\ \left(\frac{1}{m_v}\right) s \end{bmatrix}. \tag{51}$$

The system given in (49) is one of a hyperbolic kind [2], the physical relevance is these kind of systems have a preferential direction of propagation. The vector $\mathbf{f}(\mathbf{Q})$ is written in a decoupled form by means of the Jacobian, that will bring it to the following standard form,

$$\mathbf{Q}_t + A\mathbf{Q}_x + \mathbf{G} = \mathbf{0}, \tag{52}$$

where $AQ = \mathbf{f}(\mathbf{Q})_x = \mathbf{f}'(\mathbf{Q})\mathbf{Q}_x$, $A = \mathbf{f}'(\mathbf{Q})$, $q \in \mathbb{R}$ and $A \in [m, m]$.

Space discretization

In this section the set of equations of (52) is to be discretized in space. For space discretization the nonlinear limiter upwind scheme is adopted [58]. The key motivation for consideration of a nonlinear higher resolution scheme is the second order accuracy with a monotonicity characteristic, due to the nonlinear *limiter* $\vec{\phi}(\vec{r})$ that will prevent the appearance of oscillations [27]. A discretization in space with an upwind scheme requires evaluation of the flux $\vec{f}$ at the interfaces of an element i and its neighbors $[i-1, i+1]$, as illustrated in figure 38.

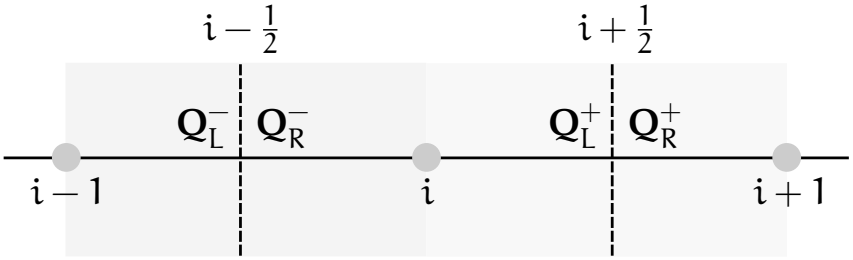

Figure 38: *A schematic of the uniform grid that is considered in the computation. The main element* i *and its neighbors* $[i-1, i+1]$. *The flux* $\mathbf{f}$ *is interpolated at the interfaces* $[i - \frac{1}{2}, i + \frac{1}{2}]$.

For a uniform spaced grid $x_i = i\Delta x$, $i \in \mathbb{Z}$, the semi-discretization of the set of equations (52) reads,

$$\mathbf{Q}_t + \frac{1}{\Delta x}\left(\vec{f}_{i+\frac{1}{2}} - \vec{f}_{i-\frac{1}{2}}\right) + \mathbf{G} = \mathbf{0}. \tag{53}$$

The numerical flux is, as mentioned, evaluated at both the interfaces of element i on the left and right side of each interface,

$$\mathbf{f}_{i+1/2} = \frac{A}{2}\left(\mathbf{Q}_R^+ + \mathbf{Q}_L^+\right) - \frac{|A|}{2}\left(\mathbf{Q}_R^+ - \mathbf{Q}_L^+\right), \tag{54}$$

2 For a system to be hyperbolic, the system matrix A that decouples the system of (49) will aggregate real eigenvalues $\Re(\lambda)$.

$$\mathbf{f}_{i-1/2} = \frac{A}{2}\left(\mathbf{Q}_R^- + \mathbf{Q}_L^-\right) - \frac{|A|}{2}\left(\mathbf{Q}_R^- - \mathbf{Q}_L^-\right). \tag{55}$$

Next is to evaluate each flux on the left- and right side, separately. The following nonlinear reconstructions that involve the neighboring elements are considered for *forward differences*, at vertex $i+1/2$,

$$\mathbf{Q}_L^+ = \mathbf{Q}_i^n + \vec{\phi}(\vec{r}_i)/2\left(\mathbf{Q}_{i+1}^n - \mathbf{Q}_i^n\right), \tag{56}$$

$$\mathbf{Q}_R^+ = \mathbf{Q}_{i+1}^n - \vec{\phi}(\vec{r}_{i+1})/2\left(\mathbf{Q}_{i+2}^n - \mathbf{Q}_{i+1}^n\right), \tag{57}$$

On the other side of the element the same procedure is repeated, and for vertex $i-1/2$ the following can be written,

$$\mathbf{Q}_L^- = \mathbf{Q}_{i-1}^n + \vec{\phi}(\vec{r}_{i-1})/2\left(\mathbf{Q}_i^n - \mathbf{Q}_{i-1}^n\right), \tag{58}$$

$$\mathbf{Q}_R^- = \mathbf{Q}_i^n - \vec{\phi}(\vec{r}_i)/2\left(\mathbf{Q}_{i+1}^n - \mathbf{Q}_i^n\right), \tag{59}$$

where $\vec{\phi}$ is a limiter function and $\vec{r}_i$ is the ratio of the forward differences, given by [58],

$$\vec{r}_{i-1} = \frac{\mathbf{Q}_{i-1}^n - \mathbf{Q}_{i-2}^n}{\mathbf{Q}_i^n - \mathbf{Q}_{i-1}^n}, \quad \vec{r}_i = \frac{\mathbf{Q}_i^n - \mathbf{Q}_{i-1}^n}{\mathbf{Q}_{i+1}^n - \mathbf{Q}_i^n}, \quad \vec{r}_{i+1} = \frac{\mathbf{Q}_{i+1}^n - \mathbf{Q}_i^n}{\mathbf{Q}_{i+2}^n - \mathbf{Q}_{i+1}^n}. \tag{60}$$

The limiter function defines the nonlinear upwind scheme, for the present work the MinMod limiter function is adopted [27],

$$\vec{\phi}(\vec{r}) = max[0, min(1, \vec{r})]. \tag{61}$$

The product of $\vec{\phi}(\vec{r})\Delta\mathbf{Q}$ is performed elementwise, i.e., $\vec{\phi}(\vec{r})\Delta\mathbf{Q} = [\phi_{1,1}\Delta Q_{1,1}; ...; \phi_{4,1}\Delta Q_{4,1}]$.

Time discretization

For time integration, the Runge-Kutta IV algorithm is considered that is third order accurate in time. The algorithm evaluates the state at the present time interval $\mathbf{k}_1$, the proceeding time interval $\mathbf{k}_4$ and two predictions half way the interval $\mathbf{k}_{2,3}$. The expressions are given in equation (62) and the correction is given in equation (63).

$$\begin{cases} \mathbf{k}_1 = & \Delta t L\left(\mathbf{Q}_n, t_n\right), \\ \mathbf{k}_2 = & \Delta t L\left(\mathbf{Q}_n - 0.5\mathbf{k}_1, t_n + 0.5\Delta t\right), \\ \mathbf{k}_3 = & \Delta t L\left(\mathbf{Q}_n - 0.5\mathbf{k}_2, t_n + 0.5\Delta t\right), \\ \mathbf{k}_4 = & \Delta t L\left(\mathbf{Q}_n - \mathbf{k}_3, t_n + \Delta t\right), \end{cases} \tag{62}$$

$$\mathbf{Q}_{n+1} = \mathbf{Q}_n - \frac{1}{6}\left(\mathbf{k}_1 + 2\mathbf{k}_2 + 2\mathbf{k}_3 + \mathbf{k}_4\right) \tag{63}$$

symbol	property	unit	value
α	biot coefficient	[-]	1.000
C_f	compressibility fluid	$[m^2/N]$	5e-10
C_s	compressibility solid	$[m^2/N]$	0.000
m_v	compressibility soil	$[m^2/N]$	2e-10
ρ_f	density fluid	$[kg/m^3]$	1000
ρ_s	density solid	$[kg/m^3]$	2650
k	permeability	$[m/s]$	0.001
n	porosity	[-]	0.400
τ	turtuosity	[-]	0.000
q	load	$[N/m^2]$	1.000
M	velocity cone	$[mm/min]$	500
L	length domain	$[m]$	1

Table 16: *Property values for the fluid and solid phase that are used in the computation. Example values are from a sandbed and have been adopted from [54].*

D.1.2 *Boundary conditions*

The cone moving with a velocity v_c is expanding an overlap part. In the one-dimensional case, the expansion will impose a deformation of the cement sheath in radial direction only. The solid deformation at the interface, given by $f(t)$ is imposed by the cone and is modeled as a sine function,

$$f(0,t) = \frac{L}{2}\left(1 - \cos(\pi t/T)\right), \tag{64}$$

where $T = L_c/v_c$ and t is the time vector $[0, T]$. The set of equations given in (52) do not constitute a solid deformation. A solid particle velocity of the matrix is implemented instead [3] and can easily be obtained by differentiation,

$$s(0,t) = \frac{df(0,t)}{dt} = \frac{\pi L}{2T}\sin(\pi t/T). \tag{65}$$

The boundary condition imposed at $x = 0$ is shown in equation (64) - (65) and is pointed out in figure 39 on the left- and rightside, respectively. The boundary conditions are summarized as follows,

$$\begin{aligned}
&t > 0,\ x = 0: && s = s(t) \rightarrow \textit{eq:}\ (65),\\
&t > 0,\ x = L: && s = 0\\
&t > 0,\ x = L: && \sigma' = 0,\\
&t = 0,\ x = \{0, L\}: && p = \sigma' = u = s = 0,
\end{aligned} \tag{66}$$

whereas the remainder are homogeneous Neumann boundary conditions $(d/dn = 0)$.

3 Intentionally done to prevent second order differential terms.

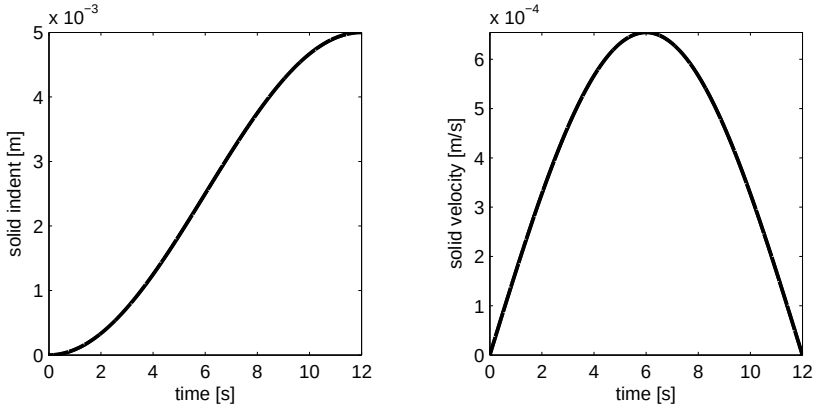

Figure 39: *The boundary condition for the solid matrix invoked by the moving cone. Due to the geometry of the cone the cement matrix will be gradually indented* $5[\mathrm{mm}]$. *The prescribed indent* $\mathtt{f}(0,\mathtt{t})$ *in x-direction is given on the left, and the implemented solid particle velocity* $\mathtt{s}(0,\mathtt{t})$ *is given on the right.*

D.1.3 *Strength and weakness of the model*

The numerical model in its current state can simulate the evolution of system parameters that constitute a porous matrix while a load is imposed due to cone migration.
In the derivation of the governing equations it is assumed that interaction for solid matrix deformation is proportional to the effective stress and by that assuming linear elastic theory, disregarding stress history or plastic deformation. Furthermore, an isothermal system is adopted, disregarding the temperature effect and with that assuming only a pressure dependency. Although the model shows a consistent result on grid-refinement (omitted from the text), a quantitative validation is up to this point, lacking.
Classical consolidation theory that in particularly is of interest to the field of civil engineering is the study of porous media where the fluid and solid both are incompressible and is typically governed by large characteristic time scales. The result is the elimination of higher order time derivatives (acceleration terms) in the set of governing equations of (49). While many commercial software packages describe the classical consolidation problem [21], it is evident that for the present situation of dynamical pipe expansion, time dependency in particular is becoming paramount. The classical consolidation theory for that reason is often considered to be the predecessor of the poroelastic set of wave equations by Biot [54].

D.2 CEMENT FAILURE PREDICTION DUE TO THE EXPANSION PROCESS

D.2.1 *Boundary conditions*

When shear stress is neglected, an axi-symmetrical system is taken into account and moreover a plane strain analysis is assumed, then the governing equations can be expressed as,

$$\frac{\partial}{\partial r}\left(\frac{k}{\gamma}\frac{\partial p}{\partial r}\right)+\frac{1}{r}\frac{k}{\gamma}\frac{\partial p}{\partial r}+\frac{1}{r^2}\frac{\partial}{\partial \theta}\left(\frac{k}{\gamma}\frac{\partial p}{\partial \theta}\right)=0, \tag{67}$$

$$\frac{\partial \sigma'_R}{\partial r}+\frac{\sigma'_R-\sigma'_\theta}{r}=0, \tag{68}$$

$$\frac{1}{r}\frac{\partial \sigma'_\theta}{\partial \theta}=0, \tag{69}$$

where k is the anisotropic permeability of the cement sheath and γ the volumetric weight of the fluid. A numerical solution is sought for the fluid pore pressure to incorporate the anisotropic permeability of the cement sheath. While for the given assumptions, an analytical solution can be obtained for the effective stress equilibrium of the cement sheath. The set of equations are defined by the following boundary conditions,

$$\begin{aligned} &0<\theta<\pi/2, \quad p(r=R_I)=\rho_w g y_c, \quad p(r=R_O)=\rho_s g y_s, \\ &0<\theta<\pi/2, \quad u_r(r=R_I)=u_I, \qquad u_r(r=R_O)=u_o. \end{aligned} \tag{70}$$

The fluid pore pressure at $p(r=R_I)$ is the hydrostatic pressure due to the weight of the fluid inside the cement while the pore pressure at $p(r=R_O)$ is a hydrostatic pressure within the stone formation. The evaluation height for the hydrostatic pressure y_c and y_s is kept equal and the boundary conditions at $\theta=0$ and $\theta=\pi/2$ are symmetry conditions.

D.2.2 *Fluid pore pressure in cement sheath*

A central differences approach is adopted to approximate the fluid pore pressure. It is confirmed [4] that the nature of the partial differential equation given in (67) is in fact of a Poisson nature that will permit the following discretization of the problem. Considering a two dimensional cylindrical coordinate system such that an approximate solution for the fluid pore pressure $\tilde{p}$ is given in the discrete domain $\tilde{p}\in\mathbb{R}^{\Omega}$, where $\Omega=\{r,\theta\}|R_I<r_i<R_O,\ 0<\theta_j<\pi/2$ and $i=1,2...N_r$ and $j=1,2...N_\theta$. The approximation for the pore pressure $\tilde{p}$ is written in the form of,

$$L[\tilde{p}]\tilde{p}=f_{\tilde{p}}, \tag{71}$$

4 If the determinant of the system matrix is a Laplace operator the nature of the equation is said to be a Poisson related one.

where $f_{\tilde{p}} = 0$ and $L[\tilde{p}]\tilde{p}$,

$$L[\tilde{p}]\tilde{p} = \left[\frac{P_{i+1,j}\frac{k}{\gamma}\big|_{i+1/2,j} - P_{i,j}\left[\frac{k}{\gamma}\big|_{i+1/2,j} + \frac{k}{\gamma}\big|_{i-1/2,j}\right] + P_{i-1,j}\frac{k}{\gamma}\big|_{i-1/2,j}}{h_r^2}\right] + \frac{1}{r}\frac{k}{\gamma}\Big|_{i,j}\left[\frac{P_{i,j} - P_{i-1,j}}{h_r}\right] + \frac{1}{r^2}\left[\frac{P_{i,j+1}\frac{k}{\gamma}\big|_{i,j+1/2} - P_{i,j}\left[\frac{k}{\gamma}\big|_{i,j+1/2} + \frac{k}{\gamma}\big|_{i,j-1/2}\right] + P_{i,j-1}\frac{k}{\gamma}\big|_{i,j-1/2}}{h_\theta^2}\right],$$

where a central differences scheme is adopted to have a second order accurate approximation for the fluid pore pressure. A Gauss-Seidel iterative solver is adopted where the residual $\tilde{r}$ is obtained by calculation of the following,

$$\tilde{r}^k = f_{\tilde{p}}^k - L[\tilde{p}^k]\tilde{p}^k, \tag{72}$$

where k is the iteration level. Having obtained the residual one can update the approximation to level $(k+1)$ by means of,

$$\tilde{p}^{k+1} = \tilde{p}^k + \omega\delta_{\tilde{p}}, \quad \textit{where} \quad \delta_{\tilde{p}} = \tilde{r}^k / \left[\frac{\partial L[\tilde{p}^k]\tilde{p}^k}{\partial \tilde{p}_{i,j}^k}\right] \tag{73}$$

where ω is a relaxation coefficient and $\tilde{p}_{i,j}^k$ is the central node of the considered set of elements. When (72) is to have passed a threshold value a numerical solution for the fluid pore pressure is obtained.

D.2.3 *Effective stress in cement sheath*

For effective stress equilibrium and the given assumptions it is possible to obtain an analytical solution. Considering radial stress equilibrium (68) in a plane strain analysis, one can integrate the equation with respect to r and it can be shown that the following holds,

$$u_r(r) = \frac{R}{R_I}\left(\frac{u_I - u_o\left(\frac{R_O}{R_I}\right)}{1 - \left(\frac{R_O}{R_I}\right)^2}\right)\cdot\left(1 - \left(\frac{R_O}{R}\right)^2\right) - u_o\left(\frac{R_O}{R}\right), \tag{74}$$

$$\sigma'_R(r) = \frac{E}{(1+\nu)(1-2\nu)}\left[\frac{1}{R_I}\left(\frac{u_I - u_o\left(\frac{R_O}{R_I}\right)}{1 - \left(\frac{R_O}{R_I}\right)^2}\right)\ldots \ldots\cdot\left(1 + \left(\frac{R_O}{R}\right)^2\cdot(1-2\nu)\right) - \left(\frac{u_o R_O}{R^2}\right)(1-2\nu)\right], \tag{75}$$

$$\sigma'_\theta(r) = \frac{E}{(1+\nu)(1-2\nu)}\left[\frac{1}{R_I}\left(\frac{u_I - u_o\left(\frac{R_O}{R_I}\right)}{1 - \left(\frac{R_O}{R_I}\right)^2}\right)\ldots \ldots\cdot\left(1 - \left(\frac{R_O}{R}\right)^2\cdot(1-2\nu)\right) + \left(\frac{u_o R_O}{R^2}\right)(1-2\nu)\right], \tag{76}$$

where u_r, E, and ν are the radial deformation, elastic modulus and Poisson ratio of the cement matrix, respectively.

D.2.4 *Parametric voids*

Little is known about the mechanical properties of the specific cement material under investigation. Halliburton [31] provided two relevant parameters, an ultimate compression strength σ_{uc} and a unit weight γ_w parameter. It is possible to relate the compression strength parameter to the tensile strength σ_t of a brittle material by means of an empirical relation [8]. For a given ultimate compression strength, the tensile strength of cement can be estimated by - among others - one of the following relations,

$$\sigma_t = 0.3 \cdot \sigma_{uc}^{2/3}, \quad \sigma_t = 0.2 \cdot \sigma_{uc}^{0.7}, \quad \sigma_t = 0.12 \cdot \sigma_{uc}^{0.7}, \tag{77}$$

that respectively are suggested by Raphael *et al.*, Oluokun *et al.* and the British code of practice *BS 8007:1987*.
The elastic modulus of cement sheath E is another parameter that is to be estimated. Typical well operation conditions are at 80[°C] and 800[bar] formation pressure. Odelson *et al.* [42] showed that the elastic modulus at elevated temperatures is reduced significant with respect to the initial elastic modulus. For elevated temperatures at 80[°C], i.e., the operating condition [31], an averaged reduction of 10 to 20[%] of elastic capacity was obtained for the different tested species in the laboratory. Noguchi *et al.* [41] provided a practical relation for the the elastic modulus of cement as a function of the compressive strength, unit weight, coarse aggregate and cement admixtures,

$$E = 3.35 \cdot 10^4 k_1 k_2 \left(\frac{\gamma_w}{2400}\right)^2 \left(\frac{\sigma_{uc}}{60}\right)^{1/3}, \tag{78}$$

where k_1 and k_2, both $O(1)$, are determined by the cement aggregates and admixtures, respectively, given in [41]. It is furthermore mentioned that (78) can provide an estimation of the elastic modulus within 90[%] certainty of the real value. Together with the temperature effect, there is approximately a 75[%] certainty for the elastic modulus. It is pointed out that the approximation does not include an estimation of the time to cure the cement. The aforementioned empirical relations are given in SI-units, where the stress is in [MPa] and the unit weight in [kg/m^3].

D.2.5 *Crack propagation algorithm*

To break an atomic bond within the cement sheath, the following procedure is adopted;

- a crack is defined, current crack position placed at $r = R_I$ and $\theta =$ pi/4,
- expansion load is initiated, this is the result of the deformation of the cone,
- the elastic stress equilibrium and fluid pore pressure is calculated within the cement sheath, and as a result the total stress is determined,

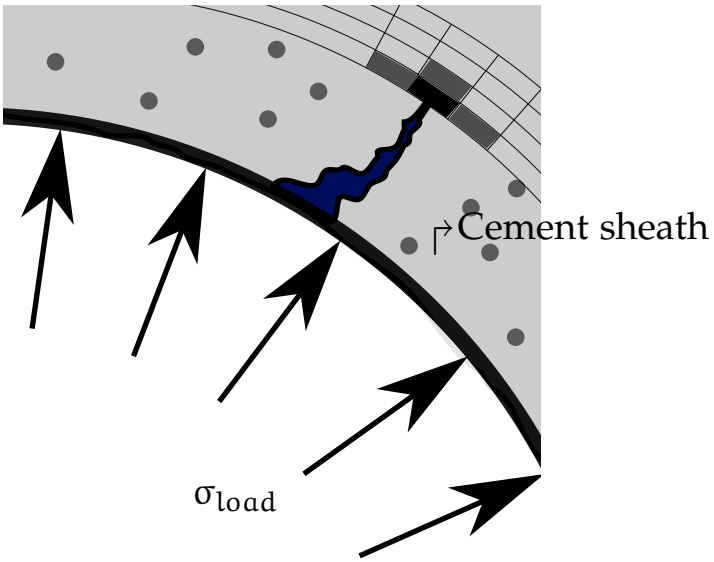

Figure 40: *Four elements are considered in the vicinity of the crack tip. For a crack tip present in the black element* $[i, j]$*, the vicinity elements would be* $[i, j-1]$*,* $[i, j+1]$ *and* $[i+1, j]$.

Evaluation of vicinity crack tip, see figure 40.

1. the stress intensity factor is determined in the vicinity of the crack tip (19),
2. the strain energy is determined in the vicinity of the crack tip (21),
3. the bond energy is determined in the vicinity of the crack tip (22),
4. A residual stress for every element is determined in the vicinity of the crack tip,
$$E_{res} = E_s - E_b(1-n), \tag{79}$$
5. Evaluate the maximum residual stress in the vicinity and either stagnate or propagate,

```
if E_res > 0
    - Crack propagation to new position;
    - Go back to step 1;
else
    - break;
end
```

The porosity n is incorporated in the *fourth* step to deal explicitly with the solid material present in the element. The residual stress is an introduced parameter to deal with a potential fracture of a multitude of cells and originates itself from the energy principle of Griffith [38]. When the *fifth* step is rejected an equilibrium between the strain and atomic bond energy is obtained and crack propagation is put to a stop.

D.2.6 *Grid Convergence*

A grid convergence analysis is performed on a quasi-solid cylinder. A quasi-solid cylinder is believed to be less sensitive for boundary effects. For an identical deformation of the inner side of the cylinder nineteen simulations were performed, each for a different grid level. The elements in the circumferential direction are set up with respect to the number of radial elements, such that the ratio of the length and width of the elements are of $O(1)$. The grid convergence is given in figure 41 and numerical values are given in table 17.

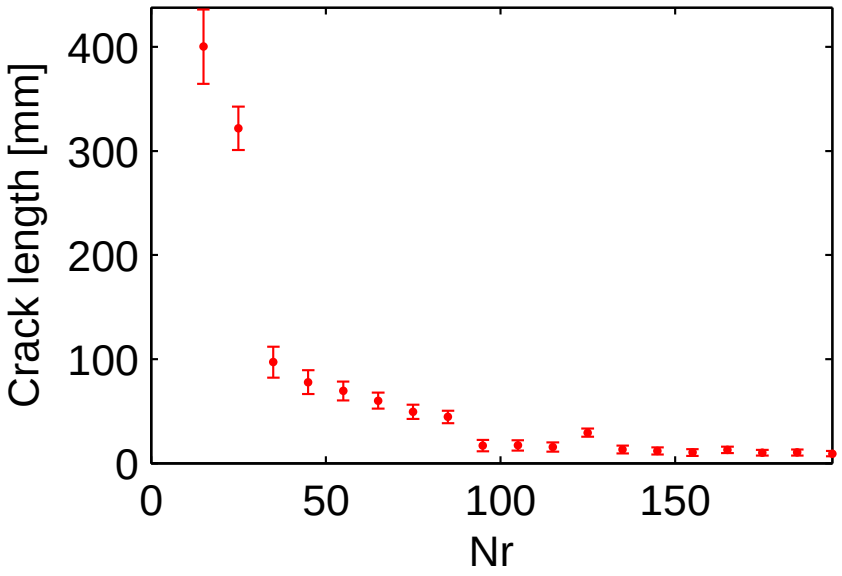

Figure 41: *The crack length for identical model settings except for the number of elements. Nineteen different simulations have been performed up to* $Nr = 195$ *elements in the radial direction.*

D.2.7 *Table for material and system properties*

The values adopted for the cement failure prediction model are presented in table 18.

D.2.8 *Discussion of the crack propagation model*

The propagation of a crack in the algorithm is aligned with the element mesh size, which is a limitation of the model with regards to actual crack growth and questionable at best. Perhaps more suitable terminology would be probabilistic energy propagation through brittle material.
Extension of the model by a more advanced simulation of the formation. Currently a linear elastic model is adopted, having the limitation that it cannot simulate the situation where $E_f \nleq E_c$. In literature provided by Shell [23] an experiment is performed where the cement in its partially

N_r x N_θ	Crack length [mm]	h_r [mm]	ΔL [mm]
15 x 136	0.4002	0.0179	[–]
25 x 232	0.3217	0.0104	0.0785
35 x 329	0.0971	0.0074	0.2246
45 x 426	0.0779	0.0057	0.0192
55 x 523	0.0694	0.0046	0.0085
65 x 620	0.0601	0.0039	0.0093
75 x 717	0.0495	0.0034	0.0106
85 x 814	0.0445	0.0030	0.0050
95 x 911	0.0169	0.0027	0.0276
105 x 1007	0.0171	0.0024	0.0002
115 x 1104	0.0156	0.0022	0.0015
125 x 1201	0.0293	0.0020	0.0137
135 x 1298	0.0132	0.0019	0.0161
145 x 1395	0.0117	0.0017	0.0015
155 x 1492	0.0103	0.0016	0.0014
165 x 1589	0.0128	0.0015	0.0025
175 x 1685	0.0101	0.0014	0.0027
185 x 1782	0.0103	0.0014	0.0002
195 x 1897	0.0091	0.0013	0.0012

Table 17: *The crack length for identical model settings except for the number of elements. Nineteen different simulations have been performed up to* $N_r = 195$ *elements in the radial direction.*

cured state had a compression strength that surpassed the strength of the formation. A next step would be to explore the latter with the present model.

Multiple stress intensity factors are found in the literature, a small collection are documented in the following papers [33][38][59]. One of these included the radius of the pore size, that is not present in the current state of the model, but could potentially relax or amplify the stress intensity factor and change the outcome of the presented results up to this point. A stress *concentration* factor according to Griffith [22] that included the pore radius is expressed as,

$$K_c = 1 + 2\sqrt{\frac{c}{\rho}}, \tag{80}$$

where c, ρ are a hole radius and hole curvature radius. The stress concentration factor is to be coupled to a stress intensity factor.

A single crack is modeled, however in fact a multitude of cracks will be present in the cement sheath. As a form of relaxation is considered that is quadratic proportional to the cracklength in the definition of the

symbol	property	unit	value
σ_{uc}	Compression strength*	[MPa]	4.6
ν	Poisson ratio cement	[-]	0.15
ρ_w	Density water	[kg/m^3]	1000
ρ_s	Density formation	[kg/m^3]	2400
g	Gravity acceleration	[m^2/s]	10
α	Biot coefficient	[-]	1
R_I	Inner radius	[m]	0.28
R_O	Outer radius	[m]	0.35

Table 18: *Numerical values for the material properties utilized in the model. * Adopted from Halliburton [31].*

atomic bond energy, a multitude of cracks will potentially relax the cement sheath more, and thus the published results are to some degree an over-estimation of the real physical problem.

D.3 EVOLUTION OF THE ANNULUS CHANNEL

D.3.1 *The compressed cement sheath*

The compressed cement sheath is developed to quantify a fluid discharge from the domain due to the cone indentation. The compressed cement sheath is connected to the **2:** porous cement sheath and **3:** the annulus channel, that both will consume the discharged fluid. If the fluid in the domain is incompressible, the fluid porosity n is assumed, then according to the cone geometry one will be able to determine the quantity of discharged fluid, clarified in figure 42. The total undeformed surface S_o over

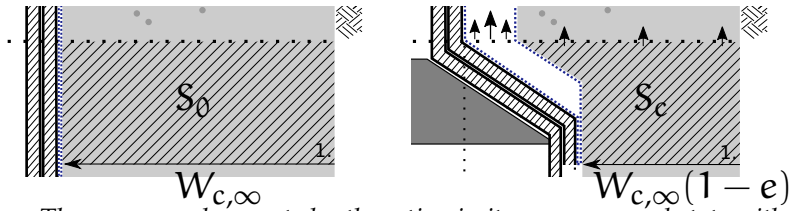

Figure 42: *The compressed cement sheath section in its uncompressed state with area S_0 (left) and compressed or deformed state with area S_c (right). As the cement sheath is considered saturated with fluid, compression of the sheath will discharge fluid from the interior domain.*

time is given by,

$$S_o(t) = W_{c,\infty} v_c t, \tag{81}$$

where $W_{c,\infty}$ is the original cement sheath thickness or *width*. As the cone is migrating upwards with a velocity v_c the total compressed surface S_c is determined by,

$$S_c(t) = S_o(1-e), \tag{82}$$

where e is the compression ratio of the cement. The compression ratio of the cement is related to the undeformed and deformed cement sheath thickness,

$$e = 1 - \frac{W_c}{W_{c,\infty}}, \tag{83}$$

where W_c is the deformed cement sheath thickness. The deformed cement thickness is a function of the type of formation and is to be estimated accordingly, an example of how to determine this deformation is given in appendix D.5. Having determined a compression ratio one can calculate the resulting fluid expulsion that will escape from the compressed domain and can be expressed according to the following expression,

$$\dot{m}_{tot} = \rho_f S_c n \cdot \left(1 - \frac{S_c}{S_o}\right) \quad [kg/s/m]. \tag{84}$$

If it is assumed that the majority of the fluid will be expelled towards the path of least resistance than the massflow of fluid towards the annulus channel and respectively the cement sheath is expressed by,

$$\dot{m}_a = r_\alpha \dot{m}_{tot}, \quad \dot{m}_c = (1 - r_\alpha)\dot{m}_{tot}, \tag{85}$$

where $\varinjlim r_\alpha \to 1$ and is the amount of fluid that is to proceed to the annulus channel.

D.3.2 *The porous cement sheath*

The porous cement sheath is positioned upstream of the cone, arranged parallel to the annulus channel. The porous sheath is premeditated to permit interaction from the annulus channel through the porous cement sheath towards the formation. As the porous cement sheath is fluid saturated, it will constitute a fluid and a solid phase. The significance is that the total stress in the sheath is associated with an effective stress in the solid phase, and a fluid pressure in the fluid pore space. The interaction that will take place in the porous cement sheath is appointed by the accumulated fluid pressure from the annulus channel, and the discharge of fluid from the compressed cement sheath, the situation is depicted in figure 43.

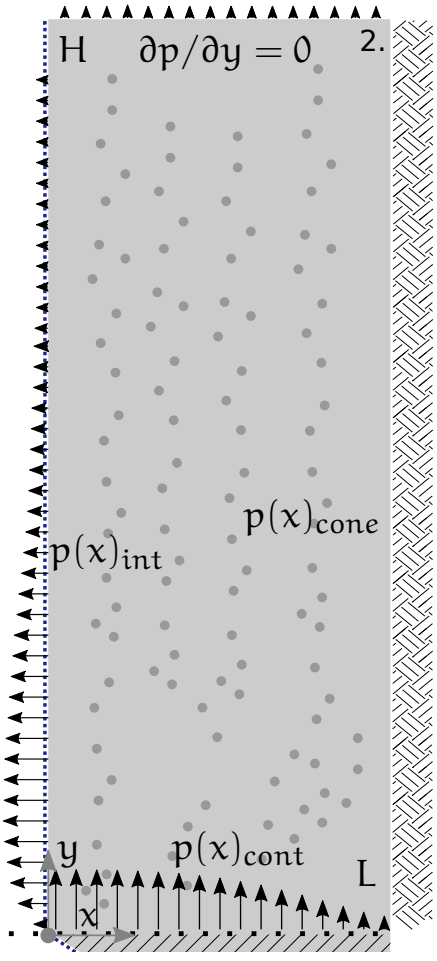

Figure 43: *Diffusion of fluid into the porous domain is done with a quadratic velocity inlet profile* $V_c(x)$*, a cubic velocity expulsion profile* $U_w(y)$ *and a zero outflow at the northern interface due to the impermeable nature of the porous medium.*

If a velocity field in the cement sheath is estimated with an analytical expression as shown in appendix D.3.3, than the total stress can be calculated correspondingly. The effective stress will be calculated with a plane

strain analysis, as done earlier in (68). Then what remains is the estimation of the pore pressure that will be explained in the following section.

For a strict incompressible and smooth fluid particle traveling from one point to another the energy conservation theorem of Bernoulli dictates,

$$\frac{1}{\rho_f}\left(p-\rho_f\vec{g}y+\frac{\rho_f V^2}{2}\right)=\texttt{constant}, \tag{86}$$

along a streamline. Here p/ρ_f is the enthalpy per unit mass, $\vec{g}y$ is the gravitational energy per unit mass, $V^2/2$ is the *absolute* kinetic energy $V=\sqrt{u^2+v^2}$ and $\vec{g}=[0,-g]$. At this point it is desired to couple this to describe viscous flow in a porous material. A common way to achieve that is by application of a Darcy flux. Here it is recognized that the complexity of fluid flow through porous material and the former two assumptions of a Bernoulli flow and the combination with a Darcy flux may be considered a rather bold one. The application throughout the literature is therefore known as an approximate justification of Darcy's law [32]. For a Darcy's flux the following Bernoulli relation is adopted [61],

$$q=-\frac{k}{\mu}\frac{d}{dn}\left(p-\rho_f\vec{g}y+\frac{\rho_f V^2}{2}\right), \tag{87}$$

where q is a volumetric flow per cross-sectional area $[m/s]$, k is a permeability $[m^2]$ and μ is a fluid viscosity $[Pa\cdot s]$. A fluid mass conservation principle across the surface of figure 43 can be shown to yield,

$$-\left(\frac{\partial\rho_f q_x}{\partial x}+\frac{\partial\rho_f q_y}{\partial y}\right)=\frac{\partial\rho_f n}{\partial t}. \tag{88}$$

The horizontal and vertical Darcy flux, given in (87) can be shown to be equal to,

$$q_x=-\frac{k}{\mu}\frac{\partial}{\partial x}\left(p+\frac{\rho_f V^2}{2}\right),\quad q_y=-\frac{k}{\mu}\frac{\partial}{\partial y}\left(p-\rho_f gy+\frac{\rho_f V^2}{2}\right). \tag{89}$$

Performing an individual chain rule for differentiation on each term of (27) and substituting (88) it can be shown to yield after some calculus,

$$\begin{aligned}\underbrace{\rho_f n\left(C_n+C_f\right)\frac{\partial p}{\partial t}}_{\texttt{Compressibility}}=\frac{\rho_f k}{\mu}\Bigg[C_f\Bigg\{&\underbrace{\left(\frac{\partial p}{\partial x}\right)^2+\left(\frac{\partial p}{\partial y}\right)^2}_{\texttt{Enthalpy energy}}\ldots\\&\ldots+\underbrace{\frac{\partial p}{\partial x}\frac{\partial k_E}{\partial x}+\frac{\partial p}{\partial y}\frac{\partial k_E}{\partial y}}_{\texttt{Kinetic energy}}+\underbrace{\frac{\partial p}{\partial y}\frac{\partial}{\partial y}(-\rho_f gy)}_{\texttt{Gravitational energy}}\Bigg\}\ldots\\&\ldots+\underbrace{\frac{\partial^2 p}{\partial x^2}+\frac{\partial^2 p}{\partial y^2}}_{\texttt{Enthalpy energy}}+\underbrace{\frac{\partial^2 k_E}{\partial x^2}+\frac{\partial^2 k_E}{\partial y^2}}_{\texttt{Kinetic energy}}+\underbrace{\frac{\partial^2}{\partial y^2}(-\rho_f gy)}_{\texttt{Gravitational energy}}\Bigg],\end{aligned} \tag{90}$$

where $k_E = 1/2\rho_f V^2$. The factors C_n and C_f represent a compressibility of the solid and fluid, respectively and are defined by,

$$C_n = \frac{1}{n}\frac{\partial n}{\partial p}, \quad C_f = \frac{1}{\rho_f}\frac{\partial \rho_f}{\partial p}. \tag{91}$$

The expression given in (28) is the governing equation that describes transient physical flow of fluid through porous cement. There are two unknown variables in the equation i.e., the pore fluid pressure p and the fluid velocity V. If an analytical solution is sought for the velocity distribution throughout the porous cement given in appendix section D.3.3, than (90) for the pore pressure can be adopted to compute the resulting pressure field.

The pore pressure is defined by a set of boundary conditions, where the porous sheath is to be coupled to the annulus domain. Furthermore, empirical evidence points out that the pore pressure will incorporate (by part) the behavior imposed by the cone in the expansion process [24][57]. The latter is a suggestion that emphasizes that the cement sheath is in a saturated state in the course of the expansion process. To that end, the pressure active in the fluid filled annulus channel will be transmitted as the sum of the effective stress and fluid pore pressure across the boundary of the cement sheath. The resulting boundary conditions for the porous cement sheath are the following,

$$\begin{array}{llll} x = 0, & 0 < y < H, & p = \sigma_{tot} - \sigma_{eff}, & \\ x = W_{c,\infty}, & 0 < y < H, & p = p(y)_{cone}, & \textit{see eq: (126)} \\ 0 < x < W_{c,\infty}, & y = 0, & p = p(x)_{cont}, & \textit{see eq: (93)} \\ 0 < x < W_{c,\infty}, & y = H, & \partial p/\partial y = 0, & \end{array} \tag{92}$$

where the total stress σ_{tot} will follow from the fluid pressure of the annulus channel (domain #3) and σ_{eff} will follow from the a plane strain solution of the cement sheath (domain #2) shown in (36). The boundary condition at $y = 0$ will make sure there is a smooth transition of fluid pore pressure along the interface of the annulus and the interaction effect of the growing annulus. The continuity pressure is estimated with a third order polynomial function and can be shown to appear like,

$$p(x)_{cont} = \left(p(x = 0, y = 0) + 3\Delta p\,(x/W_{c,\infty})^2 - 2\Delta p\,(x/W_{c,\infty})^3\right), \\ \Delta p = p(x = W_{c,\infty}, y = 0) - p(x = 0, y = 0). \tag{93}$$

The boundary condition at $y = H$ will for a Darcy flux claim there is no fluid flux across that interface.

D.3.3 *Velocity field in cement sheath*

The present section is an extension of section 3.3.1.2 and will present an assumption and derivation of a velocity field in the cement sheath. The physical transport of fluid through porous media is analyzed analytically.

In consideration of continuum theory, the porous medium is modeled as an interconnected resistance throughout the computational domain. The consequence is a relative slow moving fluid $Re \sim O(1)$, that will allow one to adopt a linear and homogeneous two-dimensional Laplace equation to prescribe steady state fluid flow and yields,

$$\frac{\partial^2 V}{\partial x^2} + \frac{\partial^2 V}{\partial y^2} = 0, \tag{94}$$

where $V = f(x, y)$, $x \in \{0, W_{c,\infty}\}$ and $y \in \{0, H\}$. The porous medium is depicted in figure 44 with the required boundary conditions applicable to the porous domain. The problem given in (94) is defined by a set of

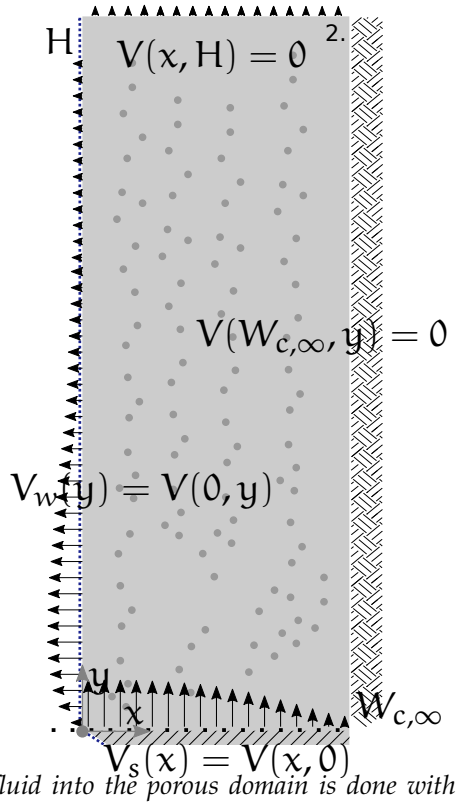

Figure 44: *Diffusion of fluid into the porous domain is done with a quadratic velocity inlet profile V_s at the south interface and a cubic velocity expulsion profile V_w at the west interface.*

non-homogeneous boundary conditions,

$$\begin{aligned}
x = 0,\ y: &\qquad V(0, y) = V_w(y),\\
x = W_{c,\infty},\ y: &\qquad V(W_{c,\infty}, y) = 0,\\
x,\ y = 0: &\qquad V(x, 0) = V_s(x),\\
x,\ y = H: &\qquad V(x, H) = 0.
\end{aligned} \tag{95}$$

A common solution method for the partial differential equation in (94) is the separation of variables technique. The solution method however, requires homogeneous boundary conditions creating a problem since three out of the four boundary conditions are non-homogeneous. To circumvent the problem a superposition principle is adopted where the analysis is split up into three separate subproblems, where in each part all boundaries are homogeneous with the exception of one non-homogeneous boundary. The solution for $V(x,y)$ of (94) eventually is the summation of all non-homogeneous subproblems,

$$V(x,y) = V_1(x,y) + V_2(x,y). \tag{96}$$

What follows is the application of the separation of variables method to each subproblem. In the end the former superposition principle is adopted and the velocity field is presented.

Two subproblems are defined, 1 : the velocity field due to the influx at the southern wall and 2 : the velocity field due to the expulsion of fluid at the western wall.

Velocity field BC through southern border

The problem formulation of (94) is adopted where $V(x,y)$ is replaced by V_1 and for the present case is defined by the following boundary conditions,

$$\begin{aligned} x = 0,\ y: &\qquad V_1(0,y) = 0,\\ x = W_{c,\infty},\ y: &\qquad V_1(W_{c,\infty},y) = 0,\\ x,\ y = 0: &\qquad V_1(x,0) = V_s(x),\\ x,\ y = H: &\qquad V_1(x,H) = 0. \end{aligned} \tag{97}$$

The velocity $V_1(x,y)$ is split up into the following separate form $V_1(x,y) = X(x)Y(y)$. Substitution into (94) will lead to,

$$\begin{aligned} X(x)'' - \lambda X(x) = 0 &\qquad Y(y)'' + \lambda Y(y) = 0,\\ X(0) = X(W_{c,\infty}) = 0 &\qquad Y(H) = 0. \end{aligned} \tag{98}$$

The above formulation is incomplete and the sign of λ is of yet undetermined. Considering $X(x)$ it can be shown that $\lambda \leqslant 0$ will lead to a zero solution, and as such the eigenvalue $\lambda > 0$ and the corresponding general solution is given by,

$$X(x) = A\sin\left(\sqrt{\lambda}x\right) + B\cos\left(\sqrt{\lambda}x\right). \tag{99}$$

Substitution of the boundary conditions will show that there are an infinite amount of solutions $\{1,2,...\infty\}$ in the following form,

$$X(x) = \sin\left(\frac{\pi n x}{W_{c,\infty}}\right), \quad \lambda = \left(\frac{\pi n}{W_{c,\infty}}\right)^2, \quad n \in \{1,2,...\infty\}. \tag{100}$$

Now the eigenvalue λ is determined, one can substitute the expression into (98) to end up with,

$$\begin{aligned} &Y(y)'' + (\pi n/W_{c,\infty})^2 Y = 0, \\ &Y(H) = 0. \end{aligned} \tag{101}$$

As the eigenvalue is known and the only boundary condition is given at $y = H$ the following general solution is adopted,

$$Y(y) = A\cosh\left(\frac{n\pi(y-H)}{W_{c,\infty}}\right) + B\sinh\left(\frac{n\pi(y-H)}{W_{c,\infty}}\right). \tag{102}$$

It can be shown that substitution of the boundary condition will lead to the following half solution,

$$Y(y) = B\sinh\left(\frac{n\pi(y-H)}{W_{c,\infty}}\right). \tag{103}$$

The separation of variables technique can get one up to this point. The derived solution to the partial differential equation (94) for $V_1(x,y)$ that takes into account the three homogeneous boundary conditions is given by,

$$V_1(x,y) = X(x)Y(y) = \sum_{n=1}^{\infty} B_{1,n}\sin\left(\frac{\pi n x}{W_{c,\infty}}\right)\sinh\left(\frac{n\pi(y-H)}{W_{c,\infty}}\right), \tag{104}$$

where the variable $B_{1,n}$ will incorporate the final non-homogeneous boundary condition. Substitution of the final boundary condition $V_1(x,0) = V_c(x)$ into (104) will lead to,

$$V_1(x,0) = V_s(x) = \sum_{n=1}^{\infty} \underbrace{B_{1,n}\sinh\left(\frac{n\pi(-H)}{W_{c,\infty}}\right)}_{\texttt{Fourrier sine coefficient}} \sin\left(\frac{\pi n x}{W_{c,\infty}}\right). \tag{105}$$

To adopt the boundary condition and calculate the value for $B_{1,n}$ a Fourrier series theory is applied [13], where the former expression is written as,

$$B_{1,n}\sinh\left(\frac{n\pi(-H)}{W_{c,\infty}}\right) = \frac{2}{W_{c,\infty}}\int_0^{W_{c,\infty}} V_s(x)\sin\left(\frac{\pi n x}{W_{c,\infty}}\right) dx. \tag{106}$$

It turns out that (94) is honored by (97) when the value of B_n is equal to,

$$B_{1,n} = -\frac{2}{W_{c,\infty}\sinh\left(\frac{n\pi H}{W_{c,\infty}}\right)}\int_0^{W_{c,\infty}} V_s(x)\sin\left(\frac{\pi n x}{W_{c,\infty}}\right) dx. \tag{107}$$

Velocity field BC through western border

The problem formulation of (94) is adopted where V is replaced by V_2 and for the present case is defined by the following boundary conditions,

$$\begin{aligned} x = 0,\ y: &\qquad V_2(0,y) = V_w(y), \\ x = W_{c,\infty},\ y: &\qquad V_2(W_{c,\infty},y) = 0, \\ x,\ y = 0: &\qquad V_2(x,0) = 0, \\ x,\ y = H: &\qquad V_2(x,H) = 0. \end{aligned} \tag{108}$$

The velocity $V_2(x,y)$ is split up into the following separate form $V_2(x,y) = X(x)Y(y)$. Substitution into (94) will lead to,

$$\begin{aligned} &X(x)'' - \lambda X(x) = 0 \qquad && Y(y)'' + \lambda Y(y) = 0, \\ &X(W_{c,\infty}) = 0 && Y(0) = Y(H) = 0. \end{aligned} \tag{109}$$

The above formulation is incomplete and the sign of λ is of yet undetermined. Considering $Y(y)$ it can be shown that $\lambda \leqslant 0$ will lead to a zero solution, and as such the eigenvalue $\lambda > 0$ and the corresponding general solution is given by,

$$Y(y) = A\sin\left(\sqrt{\lambda}y\right) + B\cos\left(\sqrt{\lambda}y\right). \tag{110}$$

Substitution of the boundary conditions will show that there are an infinite amount of solutions $\{1, 2, ...\infty\}$ in the following form,

$$Y(y) = \sin\left(\frac{\pi n y}{H}\right), \quad \lambda = \left(\frac{\pi n}{H}\right)^2, \quad n \in \{1, 2, ...\infty\}. \tag{111}$$

Now the eigenvalue λ is determined, one can substitute the expression into (109) to end up with,

$$\begin{aligned} &X(x)'' - (\pi n/H)^2 X = 0, \\ &X(W_{c,\infty}) = 0. \end{aligned} \tag{112}$$

As the eigenvalue is known and the only boundary condition is given at $x = W_{c,\infty}$ the following general solution is adopted,

$$X(x) = A\cosh\left(\frac{n\pi(x - W_{c,\infty})}{H}\right) + B\sinh\left(\frac{n\pi(x - W_{c,\infty})}{H}\right). \tag{113}$$

It can be shown that substitution of the boundary condition will lead to the following half solution,

$$X(x) = B\sinh\left(\frac{n\pi(x - W_{c,\infty})}{H}\right). \tag{114}$$

The separation of variables technique can get one up to this point. The derived solution to the partial differential equation (94) for $V_2(x,y)$ that takes into account the three homogeneous boundary conditions is given by,

$$V_2(x,y) = X(x)Y(y) = \sum_{n=1}^{\infty} B_{2,n} \sinh\left(\frac{n\pi(x - W_{c,\infty})}{H}\right) \sin\left(\frac{\pi n y}{H}\right), \quad (115)$$

where the variable $B_{2,n}$ will incorporate the final non-homogeneous boundary condition. Substitution of the final boundary condition $V_1(x,0) = V_c(x)$ into (115) will lead to,

$$V_2(0,y) = V_w(y) = \sum_{n=1} \underbrace{B_{2,n} \sinh\left(\frac{n\pi(-W_{c,\infty})}{H}\right)}_{\texttt{Fourrier sine coefficient}} \sin\left(\frac{\pi n y}{H}\right). \quad (116)$$

To adopt the boundary condition and calculate the value for $B_{2,n}$ a Fourrier series theory is applied [13], where the former expression is written as,

$$B_{2,n} \sinh\left(\frac{n\pi(-W_{c,\infty})}{H}\right) = \frac{2}{H}\int_0^H V_w(y) \sin\left(\frac{\pi n y}{H}\right) dy. \quad (117)$$

It turns out that (94) is honored by (108) when the value of B_n is equal to,

$$B_{2,n} = -\frac{2}{H \sinh\left(\frac{n\pi W_{c,\infty}}{H}\right)} \int_0^H V_w(y) \sin\left(\frac{\pi n y}{H}\right) dy. \quad (118)$$

Velocity field solution

The velocity profile through the porous medium is a combination of the subproblems treated so far. As mentioned before, one can adopt a superposition principle where one simple performs a summation of the subproblems (96),

$$V(x,y) = \sum_{n=1}^{\infty} \left\{ B_{1,n} \sin\left(\frac{\pi n x}{W_{c,\infty}}\right) \sinh\left(\frac{n\pi(y - H)}{W_{c,\infty}}\right) \ldots \right.$$
$$\left. \ldots + B_{2,n} \sinh\left(\frac{n\pi(x - W_{c,\infty})}{H}\right) \sin\left(\frac{\pi n y}{H}\right) \right\} \quad (119)$$

$$B_{1,n} = -2/(W_{c,\infty} \sinh(n\pi H/W_{c,\infty})) \int_0^{W_{c,\infty}} V_s(x) \sin(\pi n x/W_{c,\infty})\, dx,$$

$$B_{2,n} = -2/(H \sinh(n\pi W_{c,\infty}/H)) \int_0^H V_w(y) \sin(\pi n y/H)\, dy, \quad (120)$$

Note that (119) is defined in terms of $V_s(x)$ and $V_w(y)$. Additionally note that this will create the flexibility necessary for a transient process e.g., cone migration. Although a steady state solution is sought to simulate fluid flow, the expression in (119) is to be computed every time step due to the transient behavior of the system. The flexible boundary conditions

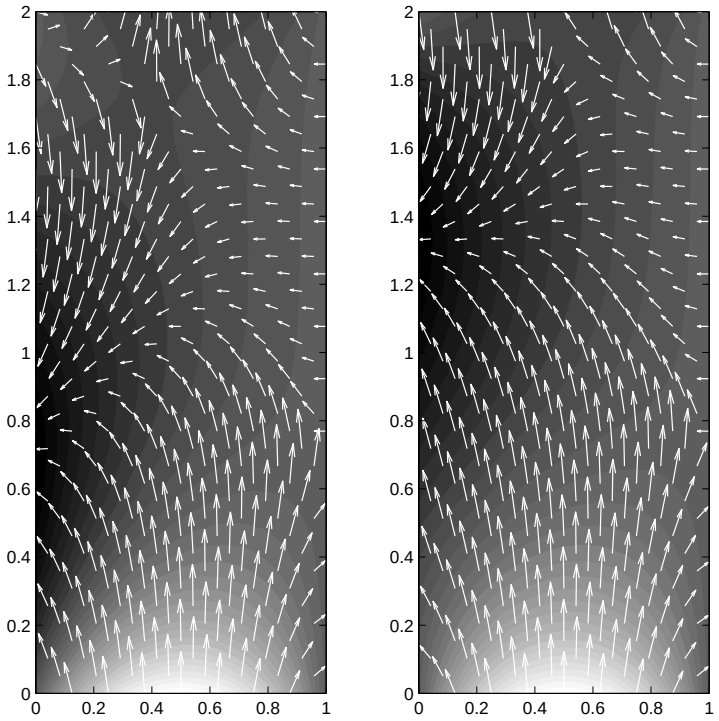

Figure 45: *The velocity field for a given* $V_s(x)$ *and* $V_w(y)$ *in an early (left) and further on (right) developed state of the velocity field. The state of the velocity field is determined by the pressure built-up in the annulus.*

will allow an evaluation of the velocity according to the state of the entire system. A typical result for two different developed states have been given in 45.

D.3.4 *Western BC velocity profile in cement sheath*

The velocity profile at the Western interface of the cement sheath is imposed. Figure 13 indicates a cubical velocity profile. A cubic velocity profile will provide the necessary flexibility to deal with the pressure gradient in the annulus, adjacent to the Western boundary of the cement sheath. The velocity profile imposed is written in terms of the incoming massflux $\dot{m}_c$ along the height H of the column,

$$V_w(y) = \frac{\dot{m}_c}{\rho_f H\left(\frac{A}{2}+\frac{B}{3}+\frac{C}{4}\right)}\left(A\left(\frac{y}{H}\right)+B\left(\frac{y}{H}\right)^2+C\left(\frac{y}{H}\right)^3\right) \tag{121}$$

where $\dot{m}_c$ is given in (24) and A, B and C are constants given by,

$$A = \left(\frac{2H-3\delta}{\delta}\right)\left(\frac{H}{H-\delta}\right)^2,$$
$$B = -\left(\frac{2H^2-3\delta^2}{\delta^2}\right)\left(\frac{H}{H-\delta}\right)^2,$$
$$C = H\left(\frac{H-2\delta}{\delta^2}\right)\left(\frac{H}{H-\delta}\right)^2, \tag{122}$$

where $\{0 < \delta < H\}$ is the position of the extremity along the $y-$axis. For $\delta = \{1/2\}$ the velocity profile $V_w(y)$ reduces to a quadratic profile and values $\delta < \{1/3\}$ and $\delta > \{2/3\}$ will allow *backflow* into the porous sheath. For $\dot{m}_c = 0$, no flow of fluid will occur in the cement sheath and the kinetic energy of (28) is reduced to a zero value.

D.3.5 *Eastern BC pressure profile in cement sheath*

In this section an approximation of the pressure magnitude of the Eastern interface of the cement sheath, depicted in figure 13 is established and the pressure profile is determined that is to be adopted as a boundary condition in the model of section 3.3.1.2. The pressure profile that is adopted here has taken form after an analysis of former experimental performed work [24], also treated in appendix section D.4.

An estimate of the pressure profile for prescription of the Eastern interface of the cement layer is started with conservation of fluid momentum, derived earlier in (45),

$$\left[1+\tau\left\{1+\frac{n\rho_f}{(1-n)\rho_s}\right\}\right]\frac{\partial v}{\partial t} = \ldots$$
$$\ldots -\frac{1}{\rho_f}\frac{\partial p}{\partial x}-\frac{ng}{k}(v-s)-\frac{\tau}{(1-n)\rho_s}\left\{\frac{\partial \sigma'}{\partial x}+\alpha\frac{\partial p}{\partial x}\right\}. \tag{123}$$

It is required to obtain an estimate for the pore pressure adjacent to the cone, though accros the cement layer at $x = W_{c,\infty}$. For that the following scaling parameters are adopted,

$$\Delta v \sim \frac{\dot{m}_c}{\rho_f W_{c,\infty} e}, \quad \Delta t \sim \frac{W_{c,\infty}}{v_c}, \quad \Delta x \sim W_{c,\infty} \ldots$$
$$\ldots \quad \Delta s \sim \frac{W_{c,\infty} e}{\Delta t}, \quad \Delta \sigma' \sim (\sigma_r(x = W_{c,\infty}) - \sigma_r(x = 0)), \quad (124)$$

where $\dot{m}_c$ is the massflow through the cement layer, ρ_f is the density of fluid in the cement layer, $W_{c,\infty}$ is the undeformed cement thickness, e is the compression ratio, v_c is the migration speed of the cone and σ_r is the radial effective stress obtained in radial equilibrium. Equation (45) is rewritten with respect to the pressure and scaled down according to the parameters provided above in (124),

$$\frac{\Delta p}{W_{c,\infty}} \sim -\left(\frac{1}{1/\rho_f + \tau/\tilde{\rho}_s}\right)\left[\left(1 + \tau\left\{1 + \frac{n\rho_f}{\tilde{\rho}_s}\right\}\right)\frac{\Delta v}{W_{c,\infty}} + \ldots\right.$$
$$\left.\ldots \frac{ng}{k}(\Delta v - \Delta s) + \frac{\tau}{\tilde{\rho}_s}\frac{\Delta \sigma'}{W_{c,\infty}}\right], \quad (125)$$

where $\tilde{\rho}_s = (1-n)\rho_s$. The pore pressure drop (increase) over the cement thickness will determine the magnitude of the pore pressure at $x = W_{c,\infty}$. A result is given in figure 46 for four different lengths of the annulus. Two curves are distinguished, a small *constant* curve determined by the cone geometry and a larger *variable* curve determined by the annulus length. The presented pore pressure profile is a result of an attempt to mimic the experimental behavior of the pore pressure recorded in the *SmallCabTest* [11]. The pressure profile that is to be imposed on the Eastern interface provided in the SmallCabTest can be simulated according to a set of sequences. For a given total annulus length `totalAnnulusLength`;

$$p_{cone}(y) = \begin{cases} f_{cone}, & \textit{for: } y \leqslant L_c \\ \\ f_{annulus}, & \textit{for: } y > L_c \end{cases}, \quad (126)$$

where,

$$f_{cone} = cM\left[1 - sine\left(\frac{\pi y}{2L_c}\right)^2\right],$$
$$f_{annulus} = aM\left[1 - sine\left(\frac{\pi y}{2L_{ff}}\right)^2\right]. \quad (127)$$

Here cM describes the fraction of the magnitude imposed by the cone, aM is the remaining fraction of the pressure drop magnitude determined earlier in (125), L_c is the length of the cone and L_{ff} is the developed annulus length determined by $L_{ff} = \texttt{totalAnnulusLength} - L_c$. The boundary condition is to be updated every time step, to include the continuous changing annulus length and the pressure drop due to the accumulation of fluid at the interface of expandable pipe and cement.

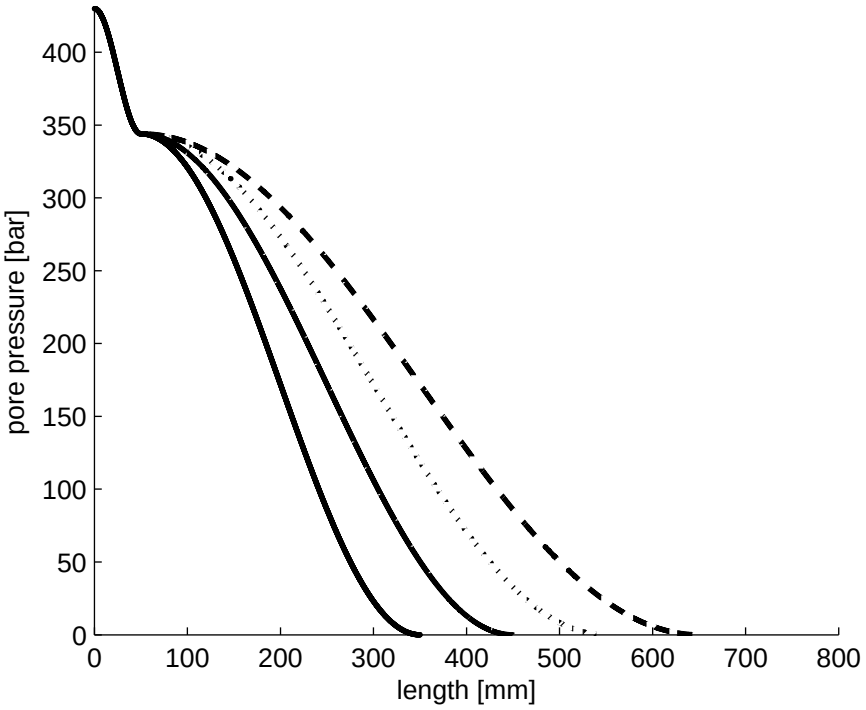

Figure 46: *The pore pressure boundary condition on the Western interface of the cement sheath. The pore pressure profile is given for an annulus length of* $[0.35, 0.45, 0.55, 0.65]$ *mtr., respectively. Note the increase of pressure that is induced within the first* $40[\mathrm{mm}]$ *of the frame due to the cone indent.*

D.3.6 *The fluid filled annulus channel*

The fluid filled annulus channel is located upstream of the cone, in-between the porous cement sheath and the expandable pipe. Development of the annulus channel section will allow determination of the pressure state throughout the channel, hence assessment of the load imposed on the expandable pipe. The annulus channel will drain fluid from the **1:** compressed cement sheath, and a portion from the **2:** porous cement sheath, visualized in figure 14. The annulus channel will be able to expand in size in radial (x-coordinate) and longitudinal (y-coordinate) direction. Expansion in radial direction is determined by the fluid pressure in the annulus channel, while expansion in longitudinal direction is determined by the evaluation of the hydraulic bond strength and interface stress in the cement sheath, discussed in section 3.3.1.4.

For a given annulus geometry $\Omega \in \{0 < x < w(y)\}|\{0 < y < H(t, p_e)\}$ [5] a general form of the Reynolds equation can be derived to approximate the fluid pressure in the channel. Here it is assumed that the initial width/height (w/H) of the channel is in a similar order $\sim O(1)$, and an additional creeping flow is considered $Re \sim O(1)$. The traditional Reynolds

5 The annulus height is determined by evaluation of p_e, a pressure evaluation point that will be covered below in section 3.3.1.5.

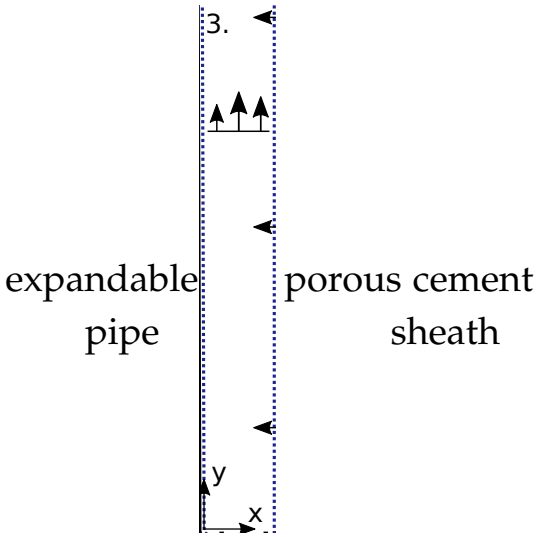

Figure 47: *A pre-existing fluid filled annulus channel between the interface of expandable pipe and* **2:** *porous cement sheath.*

equation requires a solution for the velocity field $\vec{v} = \{u, v\}$, wherein the present case the flow direction is denoted by v (the longitudinal direction), whereas the velocity component perpendicular to the flow direction is denoted by u (the radial direction),

$$\frac{\partial u}{\partial x} + \frac{\partial v}{\partial y} = 0. \tag{128}$$

For the given assumptions it can be shown that the velocity field $\vec{v}$ can be approximated by Poisseulle flow approximations,

$$\frac{\partial p}{\partial x} = \mu \frac{\partial}{\partial x}\left(\frac{\partial u}{\partial x}\right), \quad \frac{\partial p}{\partial y} = \mu \frac{\partial}{\partial x}\left(\frac{\partial v}{\partial x}\right), \tag{129}$$

and is defined by,

$$\begin{aligned} &x = 0, && y: \quad u = u_b, && v = v_b, \\ &x = w(y), && y: \quad u = u_t(y), && v = v_t, \end{aligned} \tag{130}$$

where $u_t(y)$ is given in (122) and u_b, v_b and v_t are constants defined according to the compliance of the tube and migration speed of the cone, respectively. Solution of these velocity components for u and v, can be written as,

$$u(x,y) = \frac{1}{\mu}\left[\int_0^x p(x,y)dx - \left(\frac{x}{w}\right)\int_0^w p(x,y)dx\right] + \left[1 - \left(\frac{x}{w}\right)\right] u_b + \left(\frac{x}{w}\right) u_t(y), \tag{131}$$

$$v(x,y) = \frac{1}{\mu}\left[\int_0^x f_{p_y}(x,y)dx - \left(\frac{x}{w}\right)\int_0^w f^w_{p_y}(x,y)dx\right] + \left[1 - \left(\frac{x}{w}\right)\right] v_b + \left(\frac{x}{w}\right) v_t, \tag{132}$$

where $f_{p_y}(x,y) = \int_0^x \left(\frac{\partial p}{\partial y}\right) dx$ and $f^w_{p_y}(x,y) = \int_0^w \left(\frac{\partial p}{\partial y}\right) dx$. Substitution of the velocity field into the continuity equation of (128) will lead to the general Reynolds equation,

$$\begin{aligned} 0 = \frac{1}{\mu}\Bigg[& p(x,y) - \frac{1}{w}\int_0^w p(x,y)dx \\ & -\frac{1}{w}\int_0^w f^w_{p_y}(x,y)dx \cdot \frac{\partial x}{\partial y} - x\int_0^w f^w_{p_y}(x,y)dx \cdot \frac{\partial}{\partial y}\frac{1}{w} \\ & -\frac{x}{w}\frac{\partial}{\partial y}\int_0^w f^w_{p_y}(x,y)dx + \frac{\partial}{\partial y}\int_0^x f_{p_y}(x,y)dx\Bigg] \\ & + \left(\frac{1}{w}\frac{\partial x}{\partial y} + x\frac{\partial}{\partial y}\frac{1}{w}\right)(\nu_t - \nu_b) + \left(\frac{U_e(y) - u_b}{w}\right). \end{aligned} \tag{133}$$

The Reynolds equation is essentially an assembly of the velocity field to determine the pressure distribution through a narrow channel. The Reynolds equation will be solved with a numerical solver to determine the approximate pressure field. That would allow a semi-analytical determination of the flow field with the equations (131) and (132). The Reynolds equation (133) is defined with the mass conservation principle,

$$\begin{aligned} y = 0,\ x: \quad & \partial p/\partial y\big|_{y=0} && = f(\dot{m}_a), \\ y = H(t, p_e),\ x: \quad & \partial p/\partial y\big|_{y=H} && = f(\dot{m}_a, \dot{m}_c), \end{aligned} \tag{134}$$

and from a Poiseuille flow approximate solution of equation (129) the inlet condition can be written according to,

$$\left.\frac{\partial p}{\partial y}\right|_{y=0} = \frac{6\mu}{w_0^2}\left[(\nu_b + \nu_t) - 2\left(\frac{\dot{m}_a}{\rho_f w_0}\right)\right],$$

$$p_{i,j=1} = \Delta y \left.\frac{\partial p}{\partial y}\right|_{i,j=1} + p_{i+1,j=1}, \tag{135}$$

where $\dot{m}_a$ is the mass flow into the annulus domain, covered in section 3.3.1.1. The outlet condition is obtained by again a mass conservation principle ($\dot{m}_{out,a} = \dot{m}_a + \dot{m}_c$),

$$\int_0^{w_L} v(y = H, x)dx = \int_0^{w_0} v(y = 0, x)dx + \int_0^H u(y, x = w)dy. \tag{136}$$

For the inlet a pressure gradient is calculated based on the massflow from (85), while for the outlet the massflow is based upon (84) that includes direct inflow from the compressed domain, and indirect lateral inflow from the cement sheath domain. It can be shown that the following holds,

$$\left.\frac{\partial p}{\partial y}\right|_{y=H} = \frac{6\mu}{w_H^2}\left[(\nu_b + \nu_t) - 2\left(\frac{\dot{m}_a + \dot{m}_c}{\rho_f w_H}\right)\right],$$

$$p_{i,j=N_y+1} = H \left.\frac{\partial p}{\partial y}\right|_{i,j=N_y+1} + p_{i,j=N_y}. \tag{137}$$

In these expressions $w_0 = w(x, y = 0)$ and $w_H = w(x, y = H)$, and thus the fluid pressure is determined by the system configuration and material properties that allow fluid to enter the annulus volume. The pressure magnitude present in the fluid filled annulus channel is thus a pre-dominant function of the deformation imposed by the cone and the interacting formation, portrayed in section 3.3.1.2 and appendix D.3.5.

D.3.7 *Annulus width due to elastic formation*

An effective stress field for the cement sheath enclosed in between R_i and R_o is calculated with a plane strain analysis. While the transmission of fluid pore pressure is referred to earlier in appendix D.3.5. The resulting stress equilibrium will give the radial displacement u_r as a function of the radius R. Even when the radial displacement at the outer interface is an unknown quantity, it is known that the cement sheath is in contact with the formation. There is a continuity that will imply at the East interface $u_r(R_o) = u_{fo}$, pointed out in figure 15. Considering the latter, the radial stress and the displacement field can be obtained with the following,

$$\sigma_r = \frac{A}{R^2} + 2C, \quad u_r = \frac{1+\nu}{E_c}\left[-\frac{A}{R} + 2(1-2\nu)CR\right], \tag{138}$$

with the boundary conditions,

$$\sigma_r(R_i) = \sigma_{r,i}, \quad u_r(R_o) = u_{fo}, \tag{139}$$

where $\sigma_{r,i}$ is the imposed radial stress due to the fluid pressure active in the annulus. The solution for the radial displacement field is given, the radial stress is omitted from the text,

$$u_r(R) = R\left(\frac{1+\nu}{E_c}\right)\left[\left(\frac{\left(\frac{E_c}{1+\nu}\right)\left(\frac{u_{fo}}{R_o}\right) + \left(\frac{R_i}{R_o}\right)^2 \sigma_{r,i}}{(1-2\nu) + \left(\frac{R_I}{R_o}\right)^2}\right) \cdot \left((1-2\nu) + \left(\frac{R_i}{R}\right)^2\right) - \left(\frac{R_i}{R}\right)^2 \sigma_{r,i}\right]. \tag{140}$$

The formation, modeled as an elastic spring-system with elastic modulus E_f (formation), will deform as a result of the imposed load emanated from the annulus domain. The deformation is proportional to the spring force of the formation,

$$F_{fo} = k_{fo} u_{fo}, \tag{141}$$

where k_{fo} is the spring stiffness of the formation. The spring stiffness is related to the dimensions of the cement sheath $k_{fo} = A_y/(R_o - R_i)E_f$ where A_y is the circumferential surface area of the *slice* of formation interacting with the cement sheath $A_y = 2\pi R_o\, dy$. Although u_{fo} is an unknown, it is possible to estimate the deformation by means of a resultant force that emanates from the annulus. Than in an iterative picard procedure an equilibrium is established between the spring force and the resultant force on

the cement sheath at R_o that will result in a radial displacement, obtained by the routine,

```
radialDisplacement = guessValue;
while displacementDifference > thresHold
 1: Determine radialStress;
 2: Determine springDisplacement;
 3: Determine displacementDifference;
 4: Determine radialDisplacement = springDisplacement;
 5: Determine counter = counter + 1;
end
```

where the `thresHold` value is set to $1e-10$. Note that the radius R will increase with channel expansion.

D.4 ANNULUS MODEL COMPARED TO "SMALLCABTEST"

Performance of the annulus model as presented in section 3.3 is tested here where it is compared to former performed experimental work, known by the SmallCabTest [24].

The SmallCabTest is an experiment performed in Rijswijk to support the development of the Cap and Pull system and to investigate the failure mechanism associated with the system. The experiment is constructed after observation of high forces in the field trial of the Cameron TX test well. In the SmallCabTest it was observed that for insufficient drainage of the cement sheath at time of expansion a potential pipe collapse may occur.

The expansion process is performed with an expandable pipe surrounded with cement, and the cement surrounded with a host pipe under so-called fixed-fixed conditions. Thereupon the top of the uniaxial system is sealed with a (drainable) flange and after an initial expansion the bottom of the system is sealed with a impermeable flange. At a certain length of the cement column H_y fluid pressure measurements have been performed in the cement sheath as depicted in figure 48. Evaluation of figure 11 and

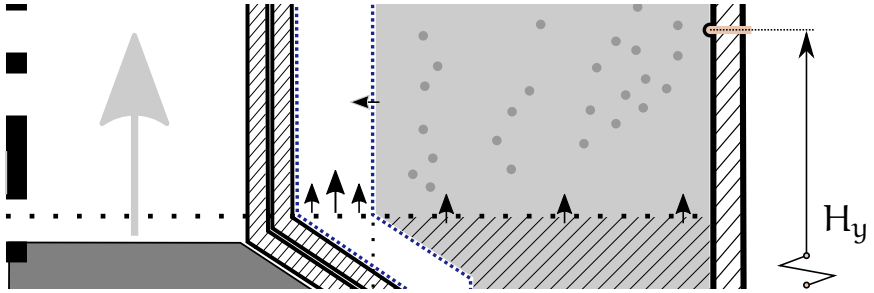

Figure 48: *In former performed experimental work the pressure is measured in the outside of the cement sheath by means of pressure gauges that were positioned at a certain length H_y of the cement column. And moreover, instead of an experiment performed in a soil formation, the experiment is performed in a host pipe as substitute for a soil formation.*

likewise figure 48 will point out that that the SmallCabTest is not an expansion test with a soil formation, but with a host pipe as substitution of a soil formation. The consequence for comparison of the SmallCabTest with the numerical annulus model of section 3.3 is a minor adjustment to incorporate a host pipe, instead of a soil formation.

The experiments eligible for comparison with the numerical annulus model were those that had a cement sheath in between expandable pipe and host pipe, contained drain holes that would allow fluid to be drained and had pressure gauges installed to measure the pressure. A numerical overview is given in table 19. Herein a radial cement strain is included that will distinguish each experiment and is obtained by the following,

$$\texttt{strain} = 1 - \left(\frac{\texttt{innerRadiusHost} - \texttt{outerRadiusPostExp}}{\texttt{undeformedCementThickness}} \right). \tag{142}$$

The corresponding graph is given in figure 49 for the four different per-

name	H_y [mm]	p exp. [bar]	p num. [bar]	Δ [%]	strain [%]
test 7	400	279	506	81	27.86
test 9a	400	475	533	12	31.86
test 9b	200	470	546	16	31.36
test 11	400	765	796	4	42.25

Table 19: *Numerical overview of the SmallCabTest for four different performed experiments wherein the position of the pressure gauge is given, the experimental and numerical response of the pressure gauge, the percentile difference of the aforementioned pressures, and the radial cement strain.*

formed experiments. An initial comparison of the SmallCabTest and the numerical model will reveal that an overestimation (varies from 4-81%) is visible for the performed experiments, although the numerical model is able to predict the trend captured in the SmallCabTest.

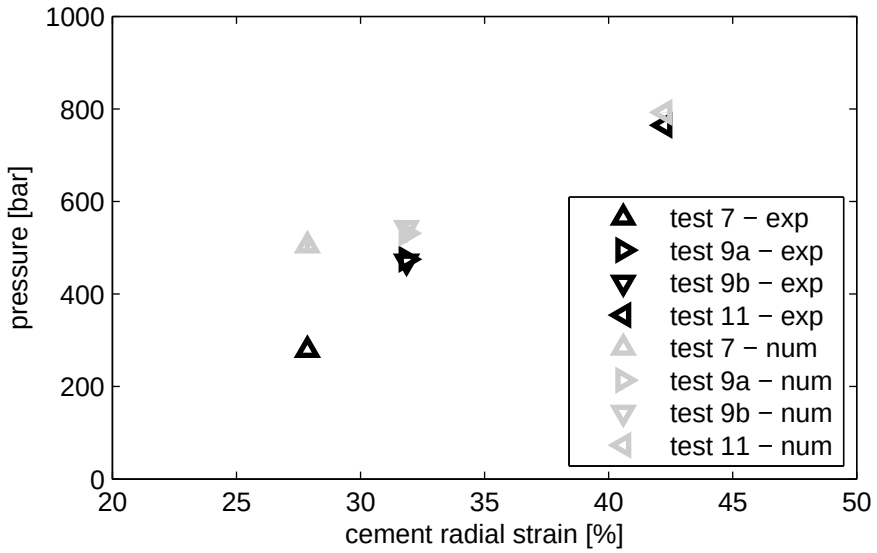

Figure 49: *Performance of the numerical annulus model compared to the former performed experimental SmallCabTest [24]. Shown is the fluid pressure measured in the cement sheath where the experimental result is marked by the darker colored symbols, and the numerical result marked by gray lighter colored symbols.*

D.5 ESTIMATION OF THE EXPANSION FORCE

It is desired to determine an estimate for the expansion force. The expansion force is related to the radial load and contact force imposed by the cone on the tube system. A situation sketch is given in figure 50. The starting point is given in equation (36), whereas in the present case the following boundary conditions are adopted,

$$\begin{aligned} u_r(R = R_1) &= x_1, \quad u_r(R = R_2) = x_2, \\ u_r(R = R_2) &= x_2, \quad u_r(R = R_3) = x_3, \\ u_r(R = R_3) &= x_3, \quad u_r(R = R_4) = x_4, \end{aligned} \tag{143}$$

where the deformation at the interface at $(R = R_1)$ of the expandable pipe will follow from the deformation imposed by the cone.
If each domain is considered separately, while for now the displacement x_1, x_2, x_3, and x_4 at this point are considered known than a stress-displacement solution for a single domain will suffice to predict the remainder. A solution in the following form is sought,

$$u_r(R) = C_1 R + \frac{C_2}{R}, \tag{144}$$

than the following solution is found, for every respective domain,

$$u_r(R) = \left(\frac{x_o R_o - x_i R_i}{R_o^2 - R_i^2}\right) R + \left(\frac{R_i}{R}\right) x_i \ldots \\ \ldots - \left(\frac{R_i^2}{R_o^2 - R_i^2}\right)\left(\frac{x_o R_o - x_i R_i}{R}\right), \tag{145}$$

$$\sigma_r(R) = \left(\frac{x_o R_o - x_i R_i}{R_o^2 - R_i^2}\right)\left(\left(\frac{E}{1-\nu}\right) + \left(\frac{E}{1+\nu}\right)\left(\frac{R_i}{R}\right)^2\right) \ldots \\ \ldots - \left(\frac{E}{1+\nu}\right)\left(\frac{x_i R_i}{R^2}\right). \tag{146}$$

Stress-deformation equilibrium given above is adopted in the expandable pipe, the cement layer and the formation pipe.
Considering each respective domain, the system is a coupled system that is simplified with respect to a mass or interface and spring system, depicted in figure 51. The mass-spring system of figure 51 can be written in the following mathmatical form,

$$\begin{bmatrix} k_1 & -k_1 & 0 & 0 \\ -k_1 & k_1 + k_2 & -k_2 & 0 \\ 0 & -k_2 & k_2 + k_3 & -k_3 \\ 0 & 0 & -k_3 & k_3 \end{bmatrix} \begin{bmatrix} x_1 \\ x_2 \\ x_3 \\ x_4 \end{bmatrix} = \begin{bmatrix} f_1 \\ f_2 \\ f_3 \\ f_4 \end{bmatrix}, \tag{147}$$

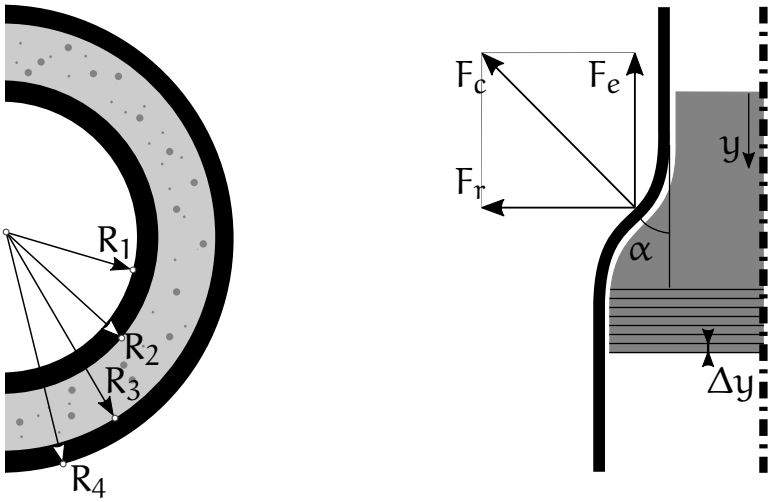

Figure 50: *Left side is shown the expandable tube surrounded by a layer of cement that is surrounded by a formation or host pipe. Right side is shown the cone moving through the expandable liner and the force components relevant in this problem.*

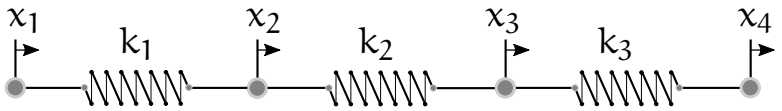

Figure 51: *The expandable pipe, cement layer and the formation pipe simplified to a mass-spring system. The variables x_1, x_2, x_3, and x_4, refer to the displacement of the inner radius expandable, outer radius expandable or inner radius cement, outer radius cement or inner formation and outer formation radius, respectively in* [m]. *The variables k_1, k_2 and k_3 refer to the stiffness of the expandable pipe, cement sheath and formation pipe, respectively in* [N/m].

where three resistances (k_1, k_2, k_3) are considered that denote the expandable pipe (1), cement layer (2) and formation pipe (3). The material stiffness is estimated with regards to the elastic moduli of the respective material,

$$k_1 = 2\pi\Delta y \left(\frac{R_2 - R_1}{R_2}\right) E_e, \quad k_2 = 2\pi\Delta y \left(\frac{R_3 - R_2}{R_3}\right) E_c,$$
$$k_3 = 2\pi\Delta y \left(\frac{R_4 - R_3}{R_4}\right) E_f. \quad (148)$$

Now it is desired to determine the displacement of every interface. Consequently, the displacement variables in equation (146) are separated and written towards a matrix notation with respect to the former determined matrix (147),

$$\begin{bmatrix} f_1 \\ f_2 \\ f_3 \\ f_4 \end{bmatrix} = \begin{bmatrix} \hat{\sigma}_{1,1}A_1 & \hat{\sigma}_{1,2}A_2 & \hat{\sigma}_{1,3}A_3 & \hat{\sigma}_{1,4}A_4 \\ \hat{\sigma}_{2,1}A_1 & \hat{\sigma}_{2,2}A_2 & \hat{\sigma}_{2,3}A_3 & \hat{\sigma}_{2,4}A_4 \\ \hat{\sigma}_{3,1}A_1 & \hat{\sigma}_{3,2}A_2 & \hat{\sigma}_{3,3}A_3 & \hat{\sigma}_{3,4}A_4 \\ \hat{\sigma}_{4,1}A_1 & \hat{\sigma}_{4,2}A_2 & \hat{\sigma}_{4,3}A_3 & \hat{\sigma}_{4,4}A_4 \end{bmatrix} \begin{bmatrix} x_1 \\ x_2 \\ x_3 \\ x_4 \end{bmatrix}, \quad (149)$$

Now equation (147) and equation (149) are equal and can be solved accordingly,

$$\begin{bmatrix} k_1 - \hat{\sigma}_{1,1}A_1 & -k_1 - \hat{\sigma}_{1,2}A_2 & -\hat{\sigma}_{1,3}A_3 & -\hat{\sigma}_{1,4}A_4 \\ -k_1 - \hat{\sigma}_{2,1}A_1 & k_1 + k_2 - \hat{\sigma}_{2,2}A_2 & -k_2 - \hat{\sigma}_{2,3}A_3 & -\hat{\sigma}_{2,4}A_4 \\ -\hat{\sigma}_{3,1}A_1 & -k_2 - \hat{\sigma}_{3,2}A_2 & k_2 + k_3 - \hat{\sigma}_{3,3}A_3 & -k_3 - \hat{\sigma}_{3,4}A_4 \\ -\hat{\sigma}_{4,1}A_1 & -\hat{\sigma}_{4,2}A_2 & -k_3 - \hat{\sigma}_{4,3}A_3 & k_3 - \hat{\sigma}_{4,4}A_4 \end{bmatrix} \cdot \begin{bmatrix} x_1 \\ x_2 \\ x_3 \\ x_4 \end{bmatrix} = \vec{0}, \quad (150)$$

leading to a well defined system of equations. Once the displacement is known the total radial force contribution can be determined subsequently with a resulting force expression, given by,

$$F_r = -\frac{(R_1 + x_{1,\infty}) - (R_4 + x_{4,\infty})}{R_{exp} + R_{cem} + R_{form}} \quad (151)$$

where the resistances are given by,

$$R_{exp} = \frac{\frac{1}{2}\left([R_2 + x_2] + [R_1 + x_1]\right)}{2\pi k_1 (x_2 - x_1)\Delta y (R_1/(R_2 - R_1))^2},$$
$$R_{cem} = \frac{\frac{1}{2}\left([R_3 + x_3] + [R_2 + x_2]\right)}{2\pi k_2 (x_3 - x_2)\Delta y (R_2/(R_3 - R_2))^2},$$
$$R_{form} = \frac{\frac{1}{2}\left([R_4 + x_4] + [R_3 + x_3]\right)}{2\pi k_3 (x_4 - x_3)\Delta y (R_3/(R_4 - R_3))^2}. \quad (152)$$

Inspection of figure 50 will reveal that once the radial load (F_r) is known and where the contact force (F_c) is related to the expansion force (F_e), than an expression can be obtained for the expansion force. To compute the expansion force (F_e) the square of the considered forces will yield the contact force (F_c),

$$F_c^2 = F_r^2 + F_e^2. \quad (153)$$

The radial force follows from an expression of a resulting radial stress (151), whereas the contact force will follow from the expansion force [37],

$$\sigma_c = \frac{F_c}{A_c}, \quad \sigma_c = \frac{F_e}{A_e}, \quad \rightarrow \quad F_e = \left(\frac{A_e}{A_c}\right) F_c. \quad (154)$$

If the computation of the expansion is considered to be a discrete problem divided into N_y smaller problems and the above expression is rewritten with respect to the contact force (F_c) and substituted in (153) an expression will follow for the expansion force (F_e), where $\left(F_e = \sum_{j=1}^{N_y} F_{e,j}\right)$,

$$F_{e.j} = \sqrt{\left(\frac{F_{r,j}^2}{\left(A_{c,j}/A_{e,j}\right)^2 - 1}\right)}. \quad (155)$$

and the contact surfaces $A_c = \sum_{j=1}^{N_y} A_{c,j}$ and expansion surfaces $A_e = \sum_{j=1}^{N_y} A_{e,j}$ are defined by,

$$A_{c,j} = \pi(R_{ex,j+1} + R_{ex,j}) \cdot \sqrt{\Delta y^2 + (R_{ex,j+1} - R_{ex,j})^2},$$
$$A_{e,j} = \pi(R_{ex,j+1}^2 - R_{ex,j}^2) \cdot (1 + \mu \cot(\alpha_j)). \quad (156)$$

Note that the former indicates that the cone is divided in $L_c/\Delta y$ elements N_y, where L_c is the length of the cone. The radii $R_{ex,j}$ denotes the cone shape profile and the displacement of the expandable pipe as a result, that is approximated with a second order polynomial function,

$$R_{ex,j} = \texttt{coneProfile}(y_j) + \frac{1}{2}(x_{1,j} + x_{2,j}). \quad (157)$$

Furthermore μ is the friction coefficient set to 0.05, that originates from Kupresan [37] and is related to the adopted lubricant in the expansion process.
Approximate material property values shown in table 20 have been included that feature the *SmallCabTest*, an earlier performed experiment. For

Variable	Name	Unit	Value
E_c	elastic modulus cement	[GPa]	1.00
E_e	elastic modulus expandable	[GPa]	210.00
E_f	elastic modulus formation	[GPa]	100.00
L_c	length cone	[mm]	80.00
R_1	inner radius expandable	[mm]	30.15
R_2	outer radius expandable	[mm]	33.15
R_3	outer radius cement	[mm]	[46.30,44.50,40.80]
R_4	outer radius formation	[mm]	50.80
WT_e	wall thickness expandable	[mm]	3.00
WT_f	wall thickness formation	[mm]	[4.50,6.30,10.00]
μ	friction coefficient	[-]	0.05
ν	poisson ratio	[-]	0.15

Table 20: *Dimensions and material property values that feature the SmallCabTest performed earlier within Shell [24] that have been adopted for the present numerical model for expansion force computation.*

the preset settings of table 20 the displacement $[x_1, x_2, x_3, x_4]$ of the interfaces are obtained and are shown in figure 52. Note that the undashed lines depict the undeformed state, wheras the dashed lines depict the deformed state. With the displacements of the interfaces known, the radial force (F_r) and as a result the expansion force (F_e) can be computed with (151) and (155), respectively. Integration of the expansion force over each element Δy will give an estimation of the total expansion force, that is to be compared to the *SmallCabTest* experiment. Figure 53 presents the expansion force measured in the *SmallCabTest* experiment [24] and the comparison with the current *expansionModel*. Numerical data of figure 52 and figure 53

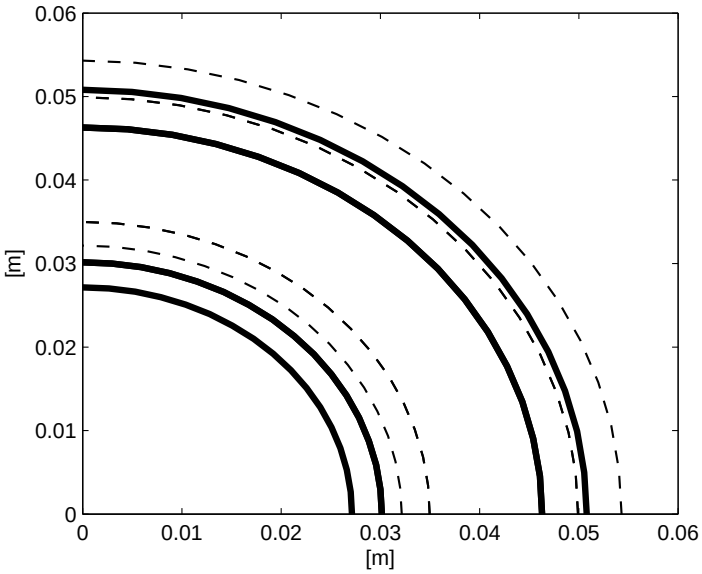

Figure 52: *A quarter of the cylindrical setup as shown earlier in figure 50. The original setup cylindrical setting i.e., the expandable pipe, the cement layer and the formation pipe is shown with the undashed black line. The maximum deformed state with a* $WT_f = 6.3[mm]$ *is shown with the dashed lines.*

is given in table 21. The table will provide additional values for the radial force neccesary to make the expansion possible.

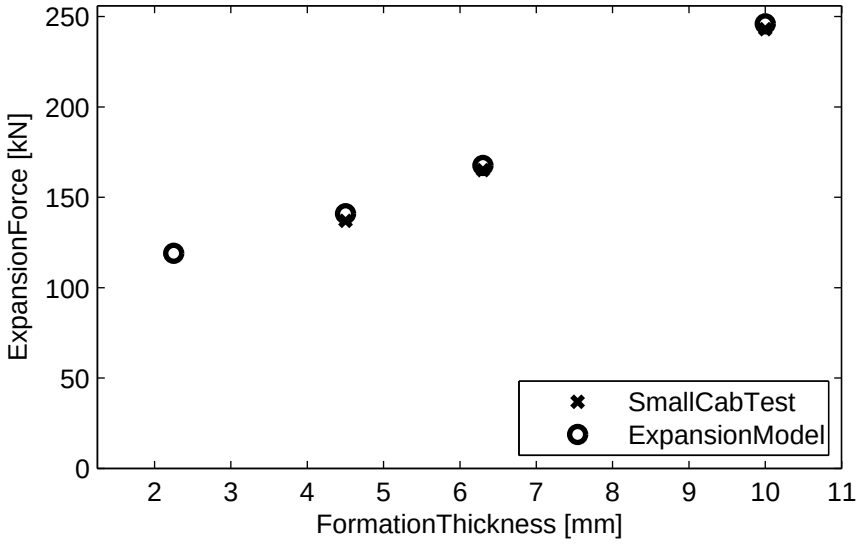

Figure 53: *The measured expansion forces from the SmallCabTest for the four applicable and relevant tests;* [test#7, test#9, test#9a, test#11]. *These measured expansion forces are compared to the computed expansion forces of the expansionModel. Corresponding numerical data is provided below in table format.*

Variable	Unit	test #7	test #9	test #9a	test #11
WT_c	[mm]	16.15	14.35	14.35	10.65
WT_e	[mm]	3.00	3.00	3.00	3.00
WT_f	[mm]	4.50	6.30	6.30	10.00
x_1	[mm]	5.01	5.02	5.02	5.00
x_2	[mm]	4.83	4.84	4.84	4.83
x_3	[mm]	3.62	3.38	3.38	2.83
x_4	[mm]	3.51	3.22	3.22	2.61
F_r	[kN]	652.42	777.13	777.13	1164.69
F_e	[kN]	136.78	163.48	163.48	244.92
F_e (SmallCabTest)	[kN]	137.00	165.00	165.00	243.00

Table 21: *Numerical data of figure 52 and figure 53 with additional values of the radial force* (F_r). *The variables* [$x_1..x_4$] *refer to the interface displacement, and* WT_c *is the cement layer thickness. The expansion force* (F_e) *(SmallCabTest) is the experimental result [24].*

E

PDENG PROGRAM

The following is an overview of the PDEng courses that are fulfilled as a requirement for the program. The table covers 12 different items of which item #1-#4 are obligatory courses, and the remainder are elective courses. Additionally, item #7 is a capita selecta, that is a self-defined course accredited by the PDEng supervisor and the content is an assembly of section 3.3 and section D.5 in the appendix.

N	Course	Credits	Done	Not done
#1	systems engineering	7.5	x	
#2	design methodology	7.5	x	
#3	failure mechanics and life pred.	6	x	
#4	structural health and condition	6	x	
#5	computational fluid dynamics	5	x	
#6	programming in engineering	3	x	
#7	capita selecta	13	x	
#8	analytical storytelling	0.5	x	
#9	presenting	1.0	x	
#10	spanish one + two	2.0	x	
#11	discrete particle interaction	1.0	x	
#12	professional effectiveness	2.0	x	
		54.5	54.5	0.0
	PDEng project	68	x	
		122.5	122.5	0.0

Table 22: *An overview of courses in the PDEng program.*

BIBLIOGRAPHY

[1] Construction. A1 Ultrabuilders. "Importance of good foundation in construction building." In: *Central Park Subd.* (2016), pp. 1–2.

[2] Hodgson T Adams AJ. "Minimum internal yield pressure, Calibration of Casing/Tubing Design Criteria by Use of Structural Reliability Techniques." In: (2017). http://petrowiki.org/Strength_of_casing_and_tubing, p. 1.

[3] M. Arafa. "Mechanical Properties of Ultra High Performance Concrete Produced in the Gaza Strip." In: *Asian Journal of Materials Science* (2010). http://scialert.net/fulltext/?doi=ajmskr.2010.1.12.

[4] Z. Bazant. "Probabilistic modeling of quasibrittle fracture and size effect." In: *Structural safety and reliability SWETS AND ZEITINGER* (2001). URL: http://cee.northwestern.edu/people/bazant/PDFs/Papers/S44.pdf.

[5] A. Bejan. "Convection Heat Transfer." In: *Wiley* (2013). https://www.wiley.com/en-us/Convection+Heat+Transfer%2C+4th+Edition-p-9780470900376.

[6] MW. van den Berg. "The ramification effect of the expansion process in the monobore well." In: *University Twente, Shell Expandables Rijswijk* (2018), pp. 31–49.

[7] AM. Biot. "Theory of propagation of elastic waves in a fluid-saturated porous solid." In: *Acoustical Society of America* (1956).

[8] Civil Engineering. Blogspot. "Relation between compressive and tension strength of concrete." In: *Foundation, Concrete and Earthquake Engineering* (2017). URL: https://civil-engg-world.blogspot.nl/2009/04/relation-between-compressive-and.html.

[9] L. Carter. "A study of cement pipe bonding." In: *Society of Petroleum Engineers office* (1964), p. 1.

[10] Georgios Constantinides and Franz-Josef Ulm. "The effect of two types of C-S-H on the elasticity of cement-based materials: Results from nanoindentation and micromechanical modeling." In: *Cement and Concrete Research* 34.1 (2004), pp. 67 –80. ISSN: 0008-8846. DOI: https://doi.org/10.1016/S0008-8846(03)00230-8. URL: http://www.sciencedirect.com/science/article/pii/S0008884603002308.

[11] D. Crescenzo. "Cement and pull system, small scale testing and failure investigation." In: *Shell Internal* (2012), pp. 75–76.

[12] D. Darwin. "Submicroscopic deformation in cement paste and mortar at high load rates." In: *Air Force Office of Scientific Research* (1988). URL: https://kuscholarworks.ku.edu/handle/1808/20401.

[13] P. Dawkins. "Laplace equation." In: *Lamar University Lecture Notes* (2016). http://tutorial.math.lamar.edu/.

[14] J. Dean. "Fracture, Toughness, Fatigue, and Creep Materials Science." In: *West Virginia Lecture Notes* (2016). URL: http://slideplayer.com/slide/8455413/.

[15] J. Eaton. "GNU Octave: version 4.0.0 manual, a high-level interactive language for numerical computations." In: *GNU Octave website* (2017). http://www.gnu.org/software/octave/doc/interpreter.

[16] Svetlana A. Epshtein, Feodor M. Borodich, and Steve J. Bull. "Evaluation of elastic modulus and hardness of highly inhomogeneous materials by nanoindentation." In: *Applied Physics A* 119.1 (2015), pp. 325–335. ISSN: 1432-0630. DOI: 10.1007/s00339-014-8971-5. URL: https://doi.org/10.1007/s00339-014-8971-5.

[17] S. Euving. *Fluid flow in the cement layer of Mono-Diameter wells during casing expansion*. Enschede, The Netherlands: University Twente, 2017.

[18] I. Fischer. "Compressive strength of cement paste as a function of loading rate, experiments and engineering mechanics analysis." In: *Cement and Concrete Research* (2014). URL: http://www.sciencedirect.com/science/article/pii/S0008884614000222?via\%3Dihub.

[19] C. Geuzaine. "Gmsh: a three-dimensional finite element mesh generator with built-in pre- and post-processing facilities." In: *International journal for numerical methods in engineering* (2009). http://gmsh.info/doc/preprints/gmsh_paper_preprint.pdf.

[20] S. Ghabezloo. "Poromechanical behavior of hardened cement paste under isotropic loading." In: *Cement and Concrete Research* (2008). URL: https://www.researchgate.net/publication/1772335_Poromechanical_Behaviour_of_Hardened_Cement_Paste_Under_Isotropic_Loading.

[21] J. Grabe. "Numerical simulation of wave propagation in fully saturated soil modeled as a two-phase medium." In: *International conference on structural dynamics* (2014), pp. 1–3.

[22] A. Griffith. "The phenomena of Rupture and Flow in Solids." In: *Royal Society of Publishing* (1920). URL: http://rsta.royalsocietypublishing.org/content/roypta/221/582-593/163.full.pdf.

[23] Expandable Technology Group. "Worst case overlap test including cement and OHA." In: *Shell Exploration and Production, Rijswijk* (2015).

[24] Expandables Technology Group. "Test Report Cap Small-scale Test." In: *Shell Internal* (2009), pp. 15–16.

[25] Shell Expandable Group. "TAap worst case overlap test including cement and OHA." In: *Shell Internal, RP: PTI-20/11* (2011), pp. 15–16.

[26] Halliburton. "Primary Lab results." In: *Shell Internal* (2015), pp. 1–4.

[27] C. Hirsch. *Numerical Computation of Internal and External Flows*. 2007, pp. 580–582.

[28] IEA. "Oil Market Reports." In: *International Energy Agency* (2017). URL: https://www.iea.org/oilmarketreport/omrpublic/charts/.

[29] CE. Inglis. "Stresses in a Plate due to the Presence of Cracks and Sharp Corners." In: *Institution of Naval Architects* (1913).

[30] GR. Irwin. "Analysis of stresses and strains near the end of a crack traversing in a plate." In: *Journal of Applied Mechanics* (1957).

[31] B. Johnson. "Shell cement lab results - Primary." In: *Lab report* (2016).

[32] W. Kalma. *An Introduction to the Environmental Physics of Soil, Water and Watersheds*. 2004, p. 334.

[33] D. Kendall. "A Simple Fracture Mechanics Based Method for Fatigue Life Prediction in Thick Walled Cylinders." In: *Research and Development, US Army Armament Center* (1986). URL: http://pressurevesseltech.asmedigitalcollection.asme.org/article.aspx?articleid=1455831.

[34] M. Khamsi. "A Picard iteration." In: *SOS-math* (2017). URL: http://www.sosmath.com/diffeq/first/picard/picard.html.

[35] M. Khanam. "Technological Advancement in Oil Industry." In: *YoungPetro* (2013). URL: http://youngpetro.org/2013/10/29/technological-advancement-in-oil-industry/.

[36] S. Kopits. "Hard Core Peak Oil Forecast." In: *Econbrowser* (2010). URL: http://econbrowser.com/archives/2010/06/eia_hard_core_p.

[37] D. Kupresan. "Experimental Assesment of Expandable Casing Technology as a Solution for Microannular Gas Flow." In: *Shell Internal* (2014), pp. 4–20.

[38] B. McGinty. "Griffith's Energy Release Rate." In: *Fracture Mechanics.org* (2017). URL: http://www.fracturemechanics.org/index.html.

[39] T. Nakajima. "Assesment of Well Integrity at Nagaoka CO2 Injection site using Ultrasonic logging and cement bond log data." In: *Energy Procedia* (2013), pp. 1–8.

[40] JC. Newman. "Fracture Analysis of Surface and Through Cracks in Cylindrical Pressure Vessels." In: *National Aeronautics and Space Administration* (1976). URL: https://ntrs.nasa.gov/archive/nasa/casi.ntrs.nasa.gov/19770007577.pdf.

[41] T. Noguchi T. Fuminori. "A practical equation for elastic modulus of concrete." In: *ACI Structural Journal* (2009). URL: http://faculty.washington.edu/nemati/aci_str1.pdf.

[42] E. Odelson J. Kerr. "Young's modulus of cement paste at elevated temperatures." In: *Elsevier Cement and Concrete Research* (2005). URL: http://www.sciencedirect.com/science/article/pii/S0008884606002730.

[43] N. Opedal. "Experimental study on the cement formation bonding." In: *SPE International* (2014). https://www.onepetro.org/conference-paper/SPE-168138-MS.

[44] PA. Parcevaux. "Cement Shrinkage and Elasticity: A new approach for a Good Zonal Isolation." In: *Society of Petroleum Engineers of AIME* (1984). URL: https://www.researchgate.net/publication/254513456_Cement_Shrinkage_and_Elasticity_A_New_Approach_for_a_Good_Zonal_Isolation.

[45] A. Parker. "Stress Intensity and Fatigue Crack Growth in a Pressurized, Autofrettaged Thick Cylinder." In: *Research and Development, US Army Armament Center* (1982). URL: http://www.dtic.mil/dtic/tr/fulltext/u2/a120789.pdf.

[46] Zeleziarne Podbrezova. "Standard expandable pipe units." In: *Zeleziarne-Products* (2017), pp. 0–1. URL: http://www.zelpo.eu/.

[47] J. Riegel. "FreeCAD 0.17: A parametric 3D modeler for design of real-life objects." In: *FreeCADweb website* (2017). http://www.freecadweb.org.

[48] M. Rocha. "Prediction of Fatigue life of Reinforced Concrete Bridges Using Fracture Mechanics." In: *Taylor and Francis Group* (2012). URL: https://infoscience.epfl.ch/record/180270/files/CH513.pdf.

[49] Royal Dutch Shell. "Website Reference." In: *ShellNederland* (2017). URL: http://www.shell.nl/.

[50] L. Struble. "A review of the cement-aggregate bond." In: *Cement and Concrete Research* (1980). URL: https://www.sciencedirect.com/science/article/pii/0008884680900848.

[51] X. Tang. "Study on the Heterogenety of Concrete and its Failure Behavior Using the Equivalent Probabilistic model." In: *Journal of materials in civil engineering* (2011). URL: http://ascelibrary.org/doi/abs/10.1061/(ASCE)MT.1943-5533.0000179.

[52] K. Terzaghi, R.B. Peck, and G. Mesri. *Soil Mechanics in Engineering Practice*. Wiley-Interscience publication. Wiley, 1996. ISBN: 9780471086581. URL: https://books.google.nl/books?id=bAwVvO71FXoC.

[53] Shell in USA. "Stones Deep-water project." In: *Energy and Innovation* (2016). https://www.shell.us/energy-and-innovation/energy-from-deepwater/shell-deep-water-portfolio-in-the-gulf-of-mexico/stones.html.

[54] A. Verruijt. *An introduction to Soil Dynamics*. Delft, The Netherlands: Springer, 2010.

[55] A. Verruijt. "Introduction to soil mechanics." In: *Springer* (2010). URL: http://geo.verruijt.net/.

[56] A. Verruijt. *Theory and Problems of poroelasticity*. Delft, The Netherlands: Delft University of Technology, 2013.

[57] S. Vries. "Cone on a stick, Lab tests cement and pull system." In: *Shell Internal* (2009), p. 2.

[58] E. van der Weide. *Discretization schemes for hyperbolic partial differential equations*. UTwente, 2016.

[59] N. Yazdani. "Probabilistic fracture mechanics application to highway bridges." In: *Engineering Fracture Mechanics* (1990). URL: http://www.sciencedirect.com/science/article/pii/0013794490900218.

[60] M. Zhang. "Micromechanical modelling of deformation and fracture of hydrating cement paste using X-ray computed tomography chacterisation." In: *Composites part B* (2015). URL: https://www.sciencedirect.com/science/article/pii/S1359836815006757.

[61] W. Zimmerman. *Diffusion equation for fluid flow in porous rocks.* 2003, pp. 1–2.